Shear Localization Modeling of Friction Stir Welding and Applications in Process Window Estimation

by

Xianjun Pei

A dissertation submitted in partial fulfillment
of the requirements for the degree of
Doctor of Philosophy
(Naval Architecture and Marine Engineering)
in The University of Michigan
2017

Doctoral Committee:

Professor Pingsha Dong, Chair
Associate Professor Dale G. Karr
Professor Wei Lu
Professor Jing Sun

Xianjun Pei
xpei@umich.edu
ORCID id: 0000-0001-5282-0607

Acknowledgement

First and foremost, I would like to express my sincere gratitude to my advisor Prof. Pingsha Dong for the continuous support of my Ph.D. study and related research, for his patience, motivation, and immense knowledge. His guidance helped me in all the time of research and writing of this thesis. I could not have imagined having a better advisor and mentor for my Ph.D. study.

Besides my advisor, I would like to thank the rest of my thesis committee: Prof Dale Karr, Prof. Wei Lu, and Prof. Jing Sun, for their insightful comments and encouragement.

My sincere thanks also go to my colleagues in our group Dr. Shaopin Song, Dr. Shizhu Xing, Dr. Jifa Mei, Hanqing Lu, Wenqing Zhou and Sandipp Krishnan Alina Shrestha Dr. Ping Wang, Prof. Wei Zhang, Prof. Xiangwei Li, Prof. Wenjing Wang, Prof. Wei Wang, Prof. Yuedong Wang, Prof. Hongliang Qian, and Prof. Tao Zhu for their support, encouragement, stimulating discussions and giving me the feeling at home.

I would also like to thank my friends during my Ph.D. study, from New Orleans: He , Yi, Xiaoke, Tingting, Li, Ting, Rui, Gong, Zhao and Jian; from Ann Arbor: Lulu, Xiaoze, Shiyang, Yan, Yuxi, Chenyang, Hao, Sicheng, Dayin, Lan, Weiran, Zhenzhong, Xiwei, Tiezhi, Zhaojian, Xiang, Cao, Chuliang and Yutong and from Boston: Yucun, Qin, Tianxiang, Hua and Meng for their company support and encouragement.

Last but not the least, I would like to dedicate this work to my parents. They are

always there supporting me, giving me the confidence to face challenges as well as providing me advices for fighting through difficulties in life and works over the years. I also heartfully thank my girlfriend, Wang, for her love, support and continuing encouraging me to finish my thesis and defense as early as possible.

Table of Contents

List of Figures

List of Tables

Abstract

Friction stir welding (FSW) has numerous advantages over conventional fusion welding processes, particular for metals or dissimilar metals that are difficult to weld with conventional welding method, which has been viewed as a key enabler for achieving structural lightweighting. However, FSW process development for a given application, i.e., establishing a process window in terms of welding travel speed and pin rotation speed, relies largely on empirical process, typically requiring detailed Design of Experiments (DoE) which can be rather time-consuming and costly.

In this work, a shear localization model is presented to study the joint formation and defect generation mechanism during FSW by focusing the band structure development which is the unique feature associated with FSW process.

A simplified shear localization model is first conducted to demonstrate its application in studying FSW process of different metals. With this model, some fundamental questions such as why titanium alloys are more difficult to weld than aluminum alloys or steels, can be more quantitatively addressed. Different material constitutive equations are also compared and Sellars Tegart material model is identified to be more suitable for the proposed shear localization model.

A three dimensional analytical based heat transport model is further developed to provide the thermal environment within which shear localization phenomenon happens. Pin/workpiece

interaction during FSW is studied in detail by introducing a contact mechanics model. The shear localization model is then refined by coupling the heat transport model and contact model. The refined shear model can provide a good estimation of peak temperature and torque information during FSW which is examined by published experimental data.

Some of the major weld defect formation mechanisms (e.g. “lack of fusion”, “abnormal stirring”, “surface gilling” and “excess flash”) have been elucidated in details based on the refined shear localization model by further enforcing both mass conservation and plastic flow continuity conditions. A set of algorithms are also developed to theoretically estimate process window of FSW based on the proposed model. To demonstrate this capability, the model is exercised for three types of aluminum alloys on which process windows were determined through DoE and published by various investigators. The theoretically estimated process windows are in good agreement with experimental results.

Chapter 1

Introduction

Research Background

There is an increasing need to design lightweight structures such as those in aircraft panels and vehicle body shells. Advanced joining technology is an integral part of the manufacturing processes of lightweight structures. Considerable effort has been expended to develop various joining processes and assess their suitability for use in lightweight structures. Friction stir welding (FSW) has been proven to be ideal for lightweight structure construction which creates high quality welds in a number of materials, including those which are extremely difficult to weld by conventional fusion processes [1,2].

Friction stir welding, which was first developed by The Welding Institute (TWI) in 1991 [3], shows its superiority as a solid-state, hot-shear joining process [4]. As compared to the conventional welding methods, FSW consumes considerably less energy. No cover gas or flux is used, thereby making the process environmentally friendly. The joining does not involve any use of filler metal and therefore base metal can be joined without concern for the compatibility of composition, which is an issue in fusion welding.

The basic idea of FSW is remarkably simple. A non-consumable rotating tool

with a specially designed pin and shoulder is inserted into the abutting edges of sheets or plates to be joined and travel along the line of joint. (Figure 1.1). The tool serves as a heat source to soften the base metal and also stirs the material to produce the joint. The heating is accomplished by friction between the tool and the workpiece and plastic dissipation of the workpiece. The localized heating softens the material around the pin and combination of tool rotation and translation leads to movement of material from the front of the pin to the back of the pin. During the FSW process, the material undergoes intense shear plastic deformation [5] at elevated temperature, resulting in the generation of fine and equiaxed recrystallized grains [6,7]. The fine microstructure in friction stir welds produces good mechanical properties. As a result of this process a joint is produced in 'solid state' compared with traditional fusion welding.

The two major movements in FSW are the rotation of the pin and the translation of the tool along the weld line, thus it is obvious that the most important process parameters of FSW are the rotational speed and travel speed of the tool. However, for a given application, i.e., establishing a process window of FSW in terms of welding travel speed and pin rotational speed (Figure 1.2), relies largely on empirical process, typically requiring detailed Design of Experiments (DoE) which can be rather time-consuming and costly [8]. Once developed, it may not be transferrable to conditions where there may be only some minor changes in joint configuration, material selection, plate or sheet thickness. Although plenty of numerical models for friction stir welding have been proposed or attempted over the last two decades, only few efforts were made in the development of effective computational modeling procedures which can be used to establish an approximate description of process window and associated key process

parameters [9]. This kind of model with the capability to estimate process windows based on unique physics associated with FSW is highly desired. Then, selected welding trials can be used to confirm and finalize the process window for final adoption for an actual application.

Noted Research Efforts on Experimental and Numerical Study of Friction Stir Welding

Due to its energy efficiency, environment friendliness, versatility and all the other metallurgical and mechanical benefits, FSW has been a subject of a considerable amount of experimental and numerical study. This section will provide a brief literature review of both experimental and numerical works relevant to current study.

1.1.1 Literature review of experimental work on FSW

The joint formation process of FSW highly relies on material flow during the welding procedure [4,5], thus lots of published works are devoted to visualize material flow patterns in FSW experimentally and to correlate weld quality, mechanical properties and microstructures to material flow behavior. Colligan [10] followed material flow in 6061 and 7075 aluminum by imbedding small steel balls as tracers into grooves cut into the workpiece parallel to the weld direction. Grooves were at various distances from the weld centerline and at various depths. After welding, the distribution of steel balls was revealed by radiography in both the plan and the cross-sectional views. The results shows that not all material influenced by the pin is actually “stirred” in the welding process, while much of the material movement take place by simple extrusion. Argebast [11] confirmed this observation and drew relationships between pin tool geometry, operating

parameters and material flow stress by modeling metal flow of extrusion zone using mass balance principle. Since then, using tracer and “stop action” has been a popular way to experimentally study material flow behavior during FSW. Guerra [12], studied the flow of metal during FSW through faying surface tracer and nib frozen technique. Two distinct zones, i.e. rotation zone and transition zone in front of the pin are identified (Figure 1.3). The size of rotation zone is about three times thicker than the distance that the nib moves in one revolution, and material within this zone rotates with the same velocity of the pin. It is believed that material in the transitional zone also rotates but its velocity decreases from the rotational velocity of the pin at the inner edge of the transition zone to zero at its outer edge. Schmidt et al. [13], confirmed this observation by investigating material flow using traditional metallography as well as X-ray and computer tomography (CT). The authors affirmed the existence of rotation zone and transition zone and gave the first attempt to estimate flow velocities in FSW based on thorough experimental investigations. Fonda et al [14] engaged a FSW machine emergency stop function to perform “stop action” and furthermore, they were the first researchers pouring water onto workpiece immediately after machine was stopped to quench the metal and let the microstructure “frozen” as weld conditions. By doing this, clear band structure can be found in front and behand the pin. This kind of plastic flow phenomena in form of band structures has already been reported by Schneider and Nunes [15] and, Yang et al.[16], for high strength aluminum alloys, by Knipling and Fonda[17] and Pilchak et al.[18] for titanium alloys. These experimental observations, that is, nearly all of the defect free FSW joints have this kind of neatly looked band structures, suggests that formation of band structures may directly relate to the overall quality of the FSW joint. Numerous

scholars have made great progress on understanding band structure formation mechanism experimentally. Chen et al. [19] broke the pin suddenly during FSW and let it embedded in the workpiece. This technique is referred as pin-breaking technique which enables a better examination of the material that detaches from the pin during FSW experiments. By carefully examine the pin-workpiece couple, the authors pointed out that the band formation is due to the material is forged and spread by the flank of pin into the space left by the advance of the tool. Krishnan [20] studied different cross section under different welding condition. He postulated that the tool appears to wait for a short time to produce frictional heat and extrude a cylindrical shaped band around the pin within each revolution. Nunes [21] compared the band formation process in FSW with metal cutting and argued that because of the unique character of metal deformation in terms of banded structure, a velocity "discontinuity" occurs in FSW and determines much of the character of the welding mechanism. Xu and Deng [22] studied texture patterns of AA6061 FSW welds both experimentally and numerically. They confirmed the spacing between the bands on the longitudinal and horizontal cross-sections equals the distance traveled by the welding tool in one revolution. Furthermore, the texture patterns are found to correlate well with equivalent plastic strain contours from simulations of the corresponding FSW process, suggesting that the texture patterns may be formed because periodically spaced material regions experience very different levels of plastic deformation during the FSW process. Schmidt and Nunes [23] further applied an orientation image mapping (OIM) technique to study joint cross-section of FSW, and proposed that the material flow in FSW may decomposed into 3 component: rigid body rotation, uniform translation, and ring vortex. They also pointed out bands may correspond, respectively, to a "straight-

through" current of metal bypassing the pin tool in a single rotation or less and a " maelstrom" current rotating a number of times around the pin tool.

Efforts are also made by numerous researchers to correlate the band structure with mechanical properties and weld quality of FSW joint. Yang and Sutton [16] carefully investigate the banded microstructure observed on horizontal transverse cross-sections in all AA2024-T351 and AA2524-T351 aluminum. The examination of band structure indicates the presence of periodic variations in the size of equiaxed grains, micro-hardness, and concentration of base metal impurity particles. They further performed series of micro-mechanical experiments quantify how FSW process affects the material response within the periodic bands [24]. Sectioning of small samples were employed and micro-tensile testing using digital image correlation (DIC) were performed to quantify the local stress–strain variations in the banded region. They found that they have different hardening rates with the particle-rich bands having the higher strain hardening exponent exhibit a periodic variation in micro-hardness across the bands while individual bands in each material have the same initial yield stress.

None regular formation of band structure can also lead to defects of FSW joint. Kim et al [25] used different sets of weld parameters to conduct FSW. 3 types of defect were found, i.e. (1) A large mass of flash due to the excess heat input; (2) cavity or groove-like defects caused by insufficient heat input; and (3) cavity caused by the abnormal stirring. The author also experimentally illustrated the shape of FSW process window of ADC12 aluminum alloy. Lakshminarayanan [26] developed the process window of AA2219 by method of Design of Experiment, and examining the tensile properties, microstructures of the joint. Constructions of FSW process windows through

experimental results are also performed by Zhang [27], Gadakh [28] and Commin [29].

In summary, numerous researcher did tremendous work on study material flow behavior during FSW, one of the most important finding is that it seems the plastic flow of metal in terms of band structure govern the overall joint quality (Figure 1.1). Inappropriate weld parameters will lead to irregularity of band structure and cause defects in FSW joint. Appropriate combination of FSW parameters in terms of process window are usually determined by Design of Experiment.

1.1.2 Literature review of numerical work on FSW

The behavior of the FSW joints is not only influenced by the geometry of the tools and the joints but also by different process parameters, also highly complex process comprises several highly coupled (and non-linear) physical phenomena. These phenomena include large plastic deformation, material flow, mechanical stirring, surface interaction between the tool and the workpiece, dynamic structural evolution and heat generation resulting from friction and plastic deformation. Multiple parameters greatly influence the quality of the FSW joints. Due to the complexity of the FSW process, it is very difficult to gain insight into the joint during the actual forming process. Furthermore, studying all these phenomena through experiment are often too time consuming and costly. Consequently, numerical analysis has frequently been used since the 2000. However the complex geometry of some kinds of joints and their three dimensional nature make it difficult to develop an overall system of governing equations for predicting the behavior of the FSW joints. In addition, material non-linearity due to plastic behavior is difficult to incorporate because the analysis becomes very complex in

the mathematical formulation. Due to the complexity mentioned above, simulation of FSW is not an easy task. However, since it involves the interaction of thermal and mechanical phenomena. Some established numerical modeling techniques have been developed that can explain and predict one or a few important features of the process physics involved in the FSW. The FSW models cover a broad range of complexity, from the simple conduction heat transfer models [e.g. 30,31], to the metal flow models [e.g. 32], to the fully coupled thermal mechanical material flow models [e.g. 33] .

1.1.2.1 Thermal model

Thermal effect is a very important issue for every kind of welding, since the temperature history can significant affect mechanical property of workpiece. Consequently, researchers have put a lot of efforts on prediction of temperature profile during FSW. Among which Jerry and Feng [30] first provide analytical approach to estimate heat flow of aluminum during FSW. They started with well-known Rosenthal equation which describes quasi-steady state temperature field due to a moving point heat source, thus temperature singularity on the heat line are inherited in the model. They also calibrate the fraction coefficient using experimental data. Due to the limitation of their simplification, temperature difference in advancing side and retreating side of FSW cannot be captured. To address this issue, Vilaca et al [31] improve the analytical solution by providing a correction term to include asymmetric effect due to rotating and translation velocities. One of the deficiencies of their work is that a tuning coefficient is introduced to calibrate the temperature field. Schmidt [34] proposed an analytical model to capture heat generation model for FSW including sliding condition, sticking condition

and partial sliding/sticking condition. They did not solve the heat equation in this work. Later on, the same author published another work [35] incorporate this heat generation model in a heat transfer model to study heat flow around tool probe in FSW numerically using a commercial FE software package FEMLAB. Schmidt and Hattel summarized their thermal model in Ref. [36] and extended their model to include the temperature-dependent yield stress effect. Beyond Schmidt's work, by using a welding simulation code WELDSIM, Chao [37] study heat transfer phenomena of FSW numerically and also verified their results with experimental results. Here the heat transfer was not only considered into workpiece but also into the tool. They concluded that the majority of the heat is generated from friction and larger amount of heat is transferred into workpiece than into tool. The temperature field gained from thermal modeling can be followed by a sequential coupled thermal mechanical model to study residual stress generation of FSW. Zhu and Chao [38] using the same software code (WELDSIM) and similar approach to calculate the temperature profile and imported into a mechanical model to compute residual stress distribution during FSW. Song and Kovacevic [39] introduced a moving coordinate to reduce the difficulty of modeling the moving tool. Then a three-dimensional heat transfer model is presented and solved by a finite difference method. Comparison between numerical result and experimental data was made to verify their procedure and they further found out preheat to the workpiece is beneficial to FSW. The models discussed above estimate heat generation during FSW mainly through contact friction due to forging force. On the other hand, Khandkar et al [40] provide an input torque based model to predict temperature distribution and thermal history. In their model, the moving heat source engendered by the rotation and linear traverse of the pin

tool has been correlated with the actual machine power input. This power, obtained from experimental investigation, has been distributed to the different interfaces formed between the tool and the workpiece based on the torques generated at different tool surfaces. They also investigated effects of various heat transfer conditions at the bottom surface of the workpiece, thermal contact conductance at the interface between the workpiece and backing plate and different backing plate materials on the thermal profile in the weld material.

1.1.2.2 Material flow model

Beyond thermal behavior, material flow phenomena seems to be equally or more important in FSW. Schmidt and Hattel [41] presented a simple model to prescribe a 2D velocity field for material flow in the shear layer around the probe in FSW. They addressed the importance of balance of mass in deriving the flow field. They further incorporated their material model with the experimental result [13] and identify 2 distinct zones around the pin. Arbegast [11] further emphases this mass balance principle and perform analogy between FSW and extrusion process. By doing this, he got a rather insightful result and draw relationship between pin tool geometry, operating parameters and flow stress of material to be joined. Based on these observations, he gave a viewpoint paper [42] and further proposed a flow partitioned deformation zone model to describe defect formation during FSW. Equations of motion for a multi-body dynamic system are innovatively used. Nunes [43] pointed out the shear flow around FSW tool is analogous to metal cutting procedure. Combining “rotating plug” flow field model and “wiping” model of tool interaction with weld metal, the FSW joint formation mechanism is

explained and critical parameters of FSW process are made clear. Using this model, the effect of tool geometry on FSW shear surface are also related to published torque measurements. Reynolds [44] gave a high level summary and discussion of material flow in FSW. In his work, 3 primary questions are proposed: (1) by what mechanism is material transported in the pin-rounding flow field; (2) what is responsible for the periodicity observed in FSW microstructure and in FSW process responses and (3) how are (1) and (2) related.

1.1.2.3 Fully coupled model

In reality, thermal behavior and material flow are highly coupled in FSW. The metal is moveable only when it is soften by the high temperature, thus the thermal behavior has significance influence on material flow. On the other hand, the plastic dissipation caused by metal flow contributes a lot on heat generation and will impact the temperature field greatly. Consequently, a fully coupled thermal mechanical model is highly desired. Recent fully coupled thermal mechanical model can be mainly classified into 3 groups: computational fluid dynamics (CFD) based, finite element analysis (FEA) based and particle method (including smooth particle hydrodynamics (SPH) and discrete element method (DEM)) based.

Along this line Seidel and Reynolds [45] performed a fully coupled model based on computational fluid dynamics (CFD). The solid state material transport during welding is handled as a laminar, viscous flow of a non-Newtonian fluid past a rotating circular cylinder. The heat necessary for the material softening is generated by plastic deformation of the material. Comparison was made between metal flow visualization

experiment and predicted flow field. The model also predicts a deviation from normal material flow for certain combinations of welding parameters suggesting a possible mechanism for the occurrence of some typical FSW defects. Colegrove and Shercliff [46] also applied a commercial CFD code FLUENT to study the 2D material flow and optimized the shape of FSW tool by change the cylindrical tool into 6 tools with different shape. Based on their simulation, a trivex shape tool was finally chosen. They further extend their model to three dimensional [47]. Using this 3D model, they were able to capture not only transverse force but also the downward force. They also improve the convectional Triflute tool into Trivex tool based on the numerical result. In addition, this model was applied to size the pin features reducing the need of experiments. With this technique, material flow around a threaded tool was also study by the same author [48]. Even though the model is helpful to gain a better understanding of material flow around a complex FSW tool and can demonstrate the effect of the tool feature and welding parameter, it gave pool predictions of welding forces and overestimates the heat generation and led to a large over-prediction in weld temperature. The author owed this to not enough softening effect was considered near the solidus in their model. As a further improvement of 3D CFD simulation of FSW, Nandan et al [49] treated material transfer in FSW as non-Newtonian viscosity flow. In their model, material constitutive model proposed by Sheppard and Wright is used, and the model is refined by considering temperature dependent thermal mechanical properties. The coupled governing equations were solved by SIMPLE algorithm which is capable of calculating three-dimensional heat transfer and fluid flow with a stationary or moving heat source, with a free or flat surface, and has been well tested by their previously work reported for the calculations of

heat transfer and fluid flow in several fusion welding processes. Based on their results, the heat and mass flow during welding was found to be strongly three dimensional. Also significant asymmetry of heat and mass flow which increased with welding speed and rotational speed was observed. Their model revealed that convective transport of heat is an important mechanism of heat transfer near the tool surface. They also compared the numerically simulated temperature fields, cooling rates, and the geometry of the thermomechanically affected zone (TMAZ) with independently determined experimental values, and they were in good agreement. Using the approach documented in Ref. [49], Nandan et al. further performed simulation for FSW of mild steel [50] and stainless steel [51]. They confirmed that convection was the primary mechanism of heat transfer around the pin and three-dimensional nature of transport of heat and mass. They also found that the non-Newtonian viscosity for FSW of stainless steel was found to be of same order of magnitude as that for the FSW of aluminum, and the viscosity was a strong function of both strain rate and temperature, while strain rate seemed to be most dominant factor. The calculated stream lines indicated that the material was transported mainly around the pin in the retreating side. On the bases of CFD computation of FSW, Cho et al. [52] proposed a viscoplastic self-consistent approach for simulating texture of polycrystal metal. They simulated the texture development in FSWed ferritic stainless steel from the velocity gradients along the streamlines in the material flow field. The simulation results showed that the shear deformation texture is significantly developed in the FSWed region. The experimental measured temperatures and microstructural characteristic agree fairly well with their predicted data.

Besides CFD approach, finite element analysis (FEA) is also a popular method to

solve the fully coupled problem in FSW. Deng and Xu [53] performed a two-dimensional finite element simulation to study the material flow in FSW. The author used commercial FEA code ABAQUS to implement the numerical model and applied arbitrary Largrangian Eulerian (ALE) approach to overcome the large element distortion under FSW condition. 2 schemes of interaction between pin and workpiece are proposed, i.e. slipping interface scheme and frictional contact scheme. The first schemes is similar as CFD based approach (as that documented in Ref. [45]), that is the plate material particles at the interface rotate with an angular velocity (say ω_f) that is equal (on sticking condition) or smaller than the rotating speed of the pin (sliding condition). The disadvantage of this scheme is that the angular velocity ω_f is not known in advance, which must be determined indirectly through comparisons with experimental results. On the other hand, the second scheme modeled frictional contact described by modified Coulomb friction law with a friction coefficient of μ. Because the frictional contact model treats contact and friction along the tool-workpiece interface explicitly, this scheme is believed to be more realistic than the first scheme and is one of the mainly advantage of FEA over CFD. The second difference between FEA approach and CFD approach the 2 approach treats material mechanical behavior differently. In FEA, elasto-viscoplastic material is used material is modeled by Young's modulus Poisson ratio and various plastic model including temperature softening effect and strain or strain rate hardening effect. For CFD approach, mechanical behavior is mainly modeled through material viscosity which is calculated based on the flow stress σ_e. Thus material elastic effect is not included. Figure out that friction contact scheme is the better approach for modeling interaction between pin and workpiece, the same author further presented

another work [54] to apply their method to simulate material flow of AA6061 FSW. Their results compared favorably with experimental observations and revealed that the material tend to pass and move behind the rotating pin from retreating side rather than both sides. Ulysse [55] developed a 3D FE model to simulate FSW of aluminum alloy by taking advantage of commercial software FIDAP. In his model, the tool with pin was explicitly modeled thus the forces acting on the tool can be calculated. According their model, the pin forces increase with increasing welding speed while opposite effect was observed for increasing rotational speeds. Zhang [56,57] present a FE model to simulate FSW of AA606l also using ABAQUS and ALE mesh. Through their simulation, they found that equivalent plastic strain correlates well with the distribution of the microstructure zones in the joint, which agrees with Xu's observation [22]. A swirl was also found on the advancing side. Parametric study of their work revealed a qusi-linear relation between the change of the axial load on the shoulder and the variation of equivalent plastic strain. Due to the 3D nature of their approach, their model has the ability to predict the difference of material flow in different thickness. They also point out that the effect of shoulder on the material behavior on the top surface is significant. Chen and Kovacevic [58] developed a 3D FE model to study the thermal history and thermo-mechanical phenomena in the butt-welding of AA6061-T6 using commercial FE code ANASYS. Their model also incorporated the mechanical reaction between the tool and weld material. Experiments were conducted and X-ray diffraction technique used to measure residual stress in the welded plate. The relationship between the calculated residual stress of the weld and process parameters was presented. The prediction of residual stress is the novelty compared with previous studies. Buffa et al [59] developed a

continuum based FE model for simulation of FSW of AA7075. Instead of using Arbitrary Lagrangian Eulerian (ALE) mesh, a pure Largrangian implicit scheme was used to solve the governing equation. By taking advantage of the re-mesh capability of the commercial FEA software DEFORM-3D, the element distortion issue was easily overcome. In their simulation, a regid-viscoplastic temperature and strain rate dependent material model is employed. According their results, the effective strain distribution is non-symmetric about the weld line while the temperature profile is almost symmetric in the weld zone. This observation agrees with Zhang's results [57]. The FE study mentioned above are all based on implicit approach and usually gives more accurate results, however there exists some convergence issue and usually be computationally expensive. It is because in nonlinear implicit analysis, solution of each step requires a series of trial solutions (iterations) to establish equilibrium within a certain tolerance. On the other hand, for explicit analysis, no iteration is required as the nodal accelerations are solved directly. Implicit analysis requires a numerical solver to invert the stiffness matrix once or even several times over the course of a load/time step. This matrix inversion is an expensive operation, especially for large models. Explicit doesn't require this step. Explicit analysis handles nonlinearities with relative ease as compared to implicit analysis. Bearing this in mind, Schmidt and Hattel's work [60] should be reviewed since their FE model was developed using explicit formulation. In their model, ALE mesh was also applied to overcome large distortion issue. To capture the temperature, strain and strain rate dependent material behavior, material law of Johnson-Cook was used. The also modeled contact force through Coulomb's Law of friction, and separation between the workpiece and the tool was allowed, which was often neglected in previous models. Thanks to these

treatments, their model has the capability to simulate void formation during FSW. Thus their model can be used to examine weld parameters prior to experiment.

For better describing temperature softening, strain hardening and strain rate hardening effect on material mechanical behavior, various material constitutive equation was used by different researchers, such as Johnson-Cook model in Schmidt's work [60], rigid-viscoplastic material model in Buffa's work [59], traditional strain hardening material model in Zhang's work [56], Sellar-Tegart model in Colegrove's work [48] and Seidel's work [45] and Sheppard-Wright model in Nandan work [50]. Each material constitutive equation has its own advantage and limitation. Kuykendall and Nelson [61] gave a thorough review on thermal mechanical behavior of constitutive law for FSW and provided numerical examples for each material model. Tello et al. [62] summarized and presented constants for the Sellars-Tegart constitutive model for hot metalworking. The materials considered are aluminum alloys 2024, 5083, 6061, 7050, 7075 and 356, carbon steel 1018, stainless steel 304, titanium alloy 6Al–4V, and magnesium alloys AZ31 and AZ61.

Compared with CFD method and FEA model, Lagrangian particle methods is newly developed method to deal with sever deformation in FSW. Two kinds of particle method can be found in current literature, one is based on smooth particle hydrodynamics (SPH) and the other is based on discrete element method (DEM). Unlike traditional grid based methods, Lagrangian particle methods can simulate the dynamics of interfaces, large material deformations and the material's strain and temperature history without employing complex tracking schemes. Pan et al [63] developed a three dimensional SPH model for FSW of AZ31 Mg alloy. In their model, temperature history and distribution,

grain size, microhardness as well as texture evolution are presented. Their numerical results are found to be in good agreement with experimental observations. Other than SPH method, Mitsufuji [64] conducted a DEM method to study FSW. This method treats the model of elastic plastic deformation with spring-damper system. Therefor plastic flow is calculated easily. However DEM is extremely computationally expensive and particles placement is sensitivity of the matter. In addition to DEM method, Krzyzanowski [65,66] proposed a multiscale approach which combined DEM and FEM together. The DEM approach to simulate FSW is new develop and still need some refinement until now but has a promising prospect.

In addition to modeling heat transfer, material flow and mechanical behavior of FSW, some researchers also try to predict material properties such as microstructure, grain size, hardness and texture through numerical model. These model usually based on fully coupled thermal mechanical model but adding some further relationship between material properties with state variables in fully coupled model. For example in Pan's work [63], the author related the grain size d with state variable Zener-Hollomon parameter using an empirical equation: $ln(d) = 9 - 0.27ln(Z)$, in which $Z = \dot{\epsilon}_e \exp(Q/RT)$ is the Zener-Hollomon parameter. The hardness can be estimated from grain size using the Hall-Petch equation $H_v = 40 + 72d^{-1/2}$. Cho [67] modeled strain hardening and texture evolution in friction stir welding of stainless steel. Their model began from a fully coupled heat transfer and viscoplastic flow model. The velocity field at the macroscopic scale is linked to the crystal scale by adopting the extended Taylor hypothesis. The effect of the complex response due to intense shearing is demonstrated with crystallographic texture. The texture displays a nonmonotonic strengthening and

weakening history along streamlines that pass close to the tool pin. Based on their previous fully coupled FE model, Frantini and Buffa [68] presented a continuous dynamic recrystallization phenomena (CDRX) model to study average grain size in FSW of aluminum alloys. The linkage between the evolution of grain size and macro scale FE model is achieved by the equation $D_{CDRX} = C_1 \epsilon^k \dot{\epsilon}^j D_0^h \exp(-Q/RT)$. As a consequent, the utilized model took into account the local effects of strain, strain rate and temperature. Finally an inverse identification approach, based on a linear regression procedure is utilized in order to develop the proper material characterization. Different from the model mentioned above, in which prediction of microstructure is made by drawing linkage through macro scale fully coupled model, Simar [69] successfully predicted the local microstructures and flow properties of 2 FSW joints through their novel microstructure based strain-hardening model. Rather than relying on macro scale thermal mechanical model, their work presented the advantage of describing coupled phenomena of nucleation, growth and coarsening which take place during a thermal cycle in an alloy containing a particle size distribution and is based on a finite difference formulation of the classical precipitation model. The principle and bases of their model can be referred from Ref. [70-72].

1.1.2.4 Simplified but not simple model

The numerical models mentioned in 1.2.2.3 are all full scale and fully coupled model. Even through this kind of model usually takes account most important physical mechanism within FSW together, they are usually computational expensive and involve everything together. To address these issues, a lot of researches put efforts on the

simplified model either to reduce dimension of the model or emphases on one or a few of different aspects of the FSW. These simplified methods sometimes mislead the reader into suspecting oversimplifications; however, these are not convenient shortcuts, and usually they are the result of years of intense work and community feedback. Along this line, Dong [73] provided a series decoupled models and investigated the following phenomena in a separated manner: (1) coupled friction heat generation; (2) plastic flow slip zone development; and (3) 3D heating and material flow. A simplified 3D heat and material, based on the observations from the coupled friction heat generation model, was used to establish some initial insight regarding the heat and material flow. The results, from the 3 subproblem areas were then generalized in the form of a simple parametric relationship between welding variables in terms of traveling and rotational speed and weld formation conditions. The findings from the study not only illuminate some of the important weld formation mechanisms in FSW, but also provide an effective framework for more focused investigations into some of the fundamental phenomena identified in these three areas.

Dimensional analysis is the analysis of the relationships between different physical quantities by identifying their fundamental dimensions and units of measure and tracking these dimensions as calculations or comparisons are performed which is very popular in fluid dynamics. This method usually yields several useful dimensionless numbers and is helpful to understand the physical properties of the system to be studied. Roy et al [74] developed a dimensionless correction to estimate the peak temperature during FSW based on Buckingham's π theorem. A relationship is proposed between dimensionless peak temperature and dimensionless heat input. Their model is useful for

the selection of welding conditions to prevent melting of the workpiece during FSW. The peak temperatures reported in the literature during FSW of various materials and welding conditions were found to be in fair agreement with their model.

Among these mathematically simpler approaches, scaling analysis provides an appealing balance of simplicity and accuracy. Scaling models are usually based on governing equations and proper identification of dominant terms of governing equations. A set of scaling laws for the coupled thermo-mechanical problem of FSW was introduced and compared with published data in by Tello [75]. The author then presented a novel and systematic approach to effectively perform approximation and asymptotic scaling of equations in engineering. This method in known as "order of magnitude scaling" (OMS) and the details of this method can be found in Ref. [76-78]. The proposed method permits a simple computer implementation of the scaling procedure and overcomes the limitations of the traditional scaling approach in which dominant terms are manually selected and tested for consistency. Using this approach, Tello et al. further estimate the final grain size in the stir zone of FSW and compared their prediction with published experiment data [79]. Finally Mendez et al [80] applied this method to study the coupling of heat transfer and plastic flow around the pin. An analogy between FSW and boundary layer analysis in fluid mechanics has been made, and solved by OMS, which yields a set of closed-form expressions for the maximum temperature, thickness of shear layer and the shear stress around the pin.

Other than scaling analysis, Arora et al. [81] also provided an approximate analytical estimation of peak temperatures, torque and hardness of thermomechanically affect zone by calculation of three-dimensional material flow during FSW which was

simplified as an incompressible fluid induced by a solid rotating disk.

Qian et al. [9] also set up an analytical model to optimize rotation speed and travel speed of FSW for defect-free joints through simplified approach. In their model, they evaluated the thickness of shear boundary layer in one dimensional case and enforced the mass conservation law within this layer at an optimum temperature. The final output is a closed-form formula for optimum rotational speed and travel speed.

1.1.2.5 Summary of literature review on numerical model for FSW

This section serves as a summary for the literature assessment of numerical work on FSW. The numerical model can be classified as full scale model and simplified model. The full scale model usually simulates the whole physical domain using at least two dimensional model or three dimensional model. The simplified model usually emphases on study mechanism of FSW without simulating the physical domain. Depends on the complexity of the full scale model, they can be categorized as thermal model, material flow model and fully coupled model. The simplified models are usually dealt with dimensional analysis, scaling analysis or analytical technique and yields closed-form formula to estimate one or few physical quantiles of FSW. The summary of modeling effort of FSW is illustrated in Figure 1.4.

Objectives of This Research

As mentioned in the background, FSW shows its superiority as a solid-state joining process. Two dominant welding parameters, i.e. rotational speed and traveling speed in terms of process window are determined through costly and time consuming experiment nowadays. From the review in Sec. 1.2.1, it can be seen that the band

structure is the unique feature of FSW compared to other fusion welding, and this band structure seems to govern the overall joint quality of FSW. However the survey of numerical model for FSW in Sec. 1.2.2, indicates that few models have been developed to illustrate the formation mechanism of band structure. Based on these observations from experimental study of FSW and numerical finding by previous researchers, it can be concluded that hot-shearing process is the key mechanism to form the band structure and thus the joint of FSW. The overall objective of the present work is to develop a shear localization model which can explain the band formation mechanism and relate the modeling results to joint quality of FSW. Specifically, the following tasks need to be accomplished:

- Develop a shear localization model to explain the band formation mechanism in FSW.
- Relate the modeling results to explain typical defect generation condition in FSW.
- Propose a set of algorithms to estimate processing window in terms of rotational speed and traveling speed taking account of effect of other welding parameters and material behavior of workpiece.

Outline of Present Work

The three tasks proposed in Sec. 1.3 are addressed in four chapters in this thesis. A primary illustration of shear localization model is given in Chapter 2. Here definition of shear band (SB) width, SB formation time, and SB propagation speed are first given. The SB propagation speed in this context is used as a theoretical estimate of the maximum welding speed possible for a given material and prescribed welding conditions,

such as stir pin rotation speed and torque level. Three base materials, i.e. titanium alloy Ti–6Al–4V, high strength low alloy steel 4340, and aluminum alloy 2024 are compared in terms of shear localization parameters, to demonstrate material effect on band structure formation process. The material constitutive law used here is Johnson-Cook material model.

The disadvantage of Johnson Cook material law to study the band formation in FSW is pointed out in Chapter 3. By comparison of different type of constitutive law, Sellars-Tegart material model in terms of Zenner-Hollomon parameter is identified to be more suitable for shear localization model. The peak temperature estimated by shear localization model using Sellars-Tegart law compares well with experimental measured data. With this model, some fundamental questions such as why titanium alloys are more difficult to weld than aluminum alloys or steels can be more quantitatively addressed. And consequently, potential means for mitigating some of the difficulties in FSW of some of the alloys can be theoretically examined to provide guidance for cost-effective development of welding process parameters for new applications.

In Chapter 2 and 3, the frictional stress between the tool pin and workpiece is estimated from the torque information in FSW experiment. However, this information is usually unknown prior to FSW experiment. Thus the approach provided in Chapter 2 and 3 cannot be applied as guidance before performing FSW. Furthermore, the heat effect due to friction between tool shoulder and workpiece is also not included in the model. To address these 2 issues, a novel analytical based 3D heat flow model to take account the shoulder heating effect is firstly proposed. The heat flow model has several advantages over traditional analytical based heat conduction model and can provide a temperature

environment in which shear localization happens. This heat flow model is followed by a contact mechanics based shear localization model which estimates the friction between tool pin and workpiece through a contact mechanics approach. The peak temperatures and torque level can be estimated based on this model and tested against sets of published experimental results. A algorithm to estimate the optimum combination of travel speed and rotational speed during FSW are also given based on the proposed model.

Finally in Chapter 5 an integrated shear localization model is presented for studying the weld formation mechanism in FSW. The integrated model takes account of the heat generation by shoulder, and models both sliding stage and sticking stage in FSW. The result can exactly reflect some distinguish features experimentally observed in FSW such as “rotation zone” and “transition zone”. A theory combining shear localization results and mass balance law is then developed and explains the typical defects formation mechanism in FSW such as lack of fill, abnormal stirring, surface galling and excessive flash quantitatively. A set of algorithm for estimation of FSW process window is given based on the defect formation mechanism. The predicted process windows are in good agreement with experimental results of 3 aluminum alloys.

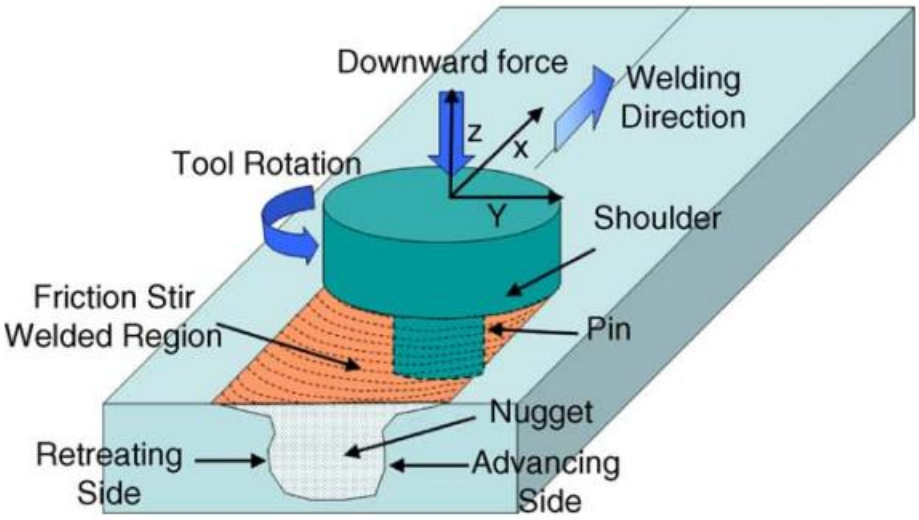

Figure 1.1: Schematic drawing of Friction stir welding (FSW) [5]

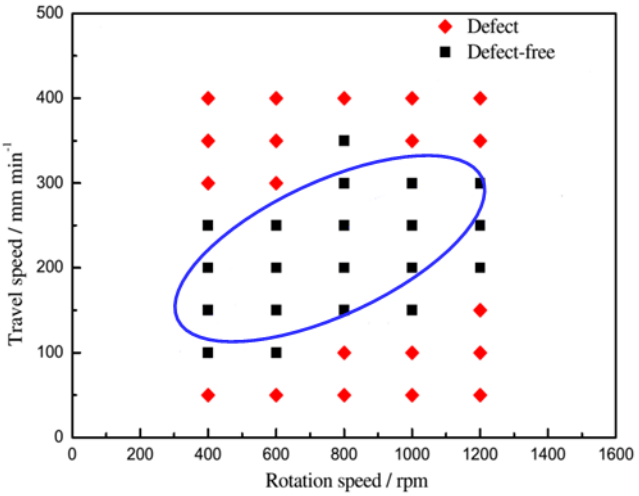

Figure 1.2: Typical processing window of FSW in terms of rotation speed and travel speed.

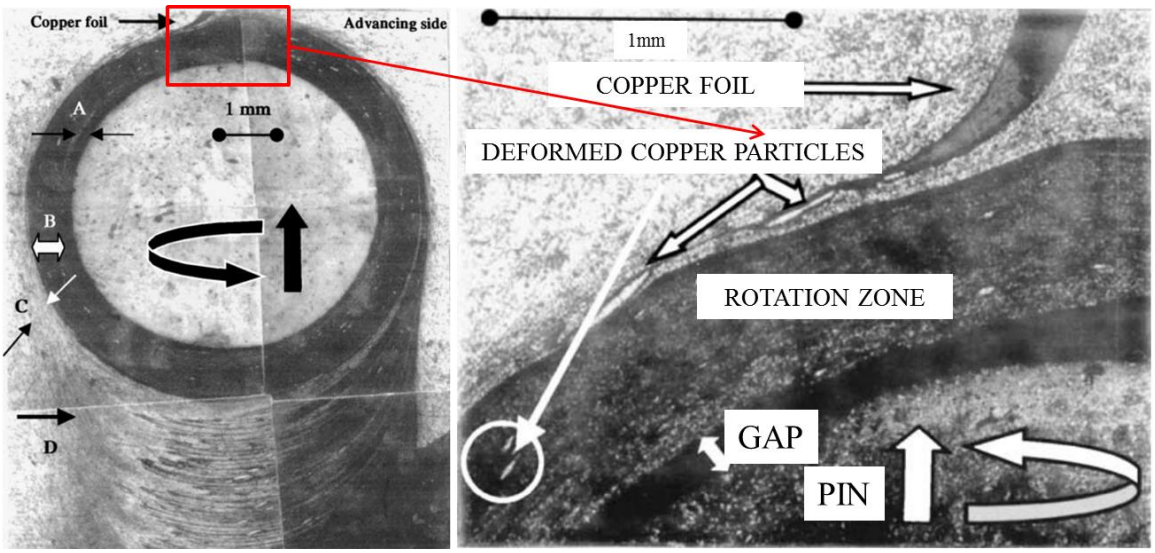

Figure 1.3: Plan view at mid thickness of weld with a frozen nib. A copper foil marker was on the faying surface of the 6061 aluminum and is seen at the top. (A) Gap without material. (B) Rotational zone or that rotates with the nib. (C) Transitional zone [12]

References

[1] Thomas, W. M., and E. D. Nicholas. "Friction stir welding for the transportation industries." Materials & Design 18.4 (1997): 269-273.

[2] C. Dawes and W. Thomas: 'Friction stir joining of aluminum alloys', TWI Bulletin (6), Cambridge, UK, November/December 1995.

[3] Thomas, W.M., Friction Stir Butt Welding. International Patent Application No PCT/GB92 Patent Application No.9125978.8, 1991

[4] Nandan, R., T. DebRoy, and H. K. D. H. Bhadeshia. "Recent advances in friction-stir welding–process, weldment structure and properties." *Progress in Materials Science* 53.6 (2008): 980-1023.

[5] Mishra, Rajiv S., and Z. Y. Ma. "Friction stir welding and processing." Materials Science and Engineering: R: Reports 50.1 (2005): 1-78.

[6] Rhodes, C. G., et al. "Effects of friction stir welding on microstructure of 7075 aluminum." *Scripta materialia* 36.1 (1997): 69-75.

[7] Liu, G., et al. "Microstructural aspects of the friction-stir welding of 6061-T6 aluminum." *Scripta materialia* 37.3 (1997): 355-361.

[8] Lakshminarayanan, A. K., and V. Balasubramanian. "Process parameters optimization for friction stir welding of RDE-40 aluminium alloy using Taguchi technique." Transactions of Nonferrous Metals Society of China 18.3 (2008): 548-554.

[9] Qian, Jinwen, et al. "An analytical model to optimize rotation speed and travel speed of friction stir welding for defect-free joints." Scripta Materialia 68.3 (2013): 175-178.

[10] Colligan, K. "Material flow behavior during friction welding of aluminum." *Welding journal* 75.7 (1999): 229s-237s.

[11] Arbegast, William J. "Modeling friction stir joining as a metalworking process." Proceedings of Hot Deformation of Aluminum Alloys III (2003): 313-327.

[12] Guerra, M., et al. "Flow patterns during friction stir welding." *Materials characterization* 49.2 (2002): 95-101.

[13] Schmidt, Henrik Nikolaj Blicher, T. L. Dickerson, and Jesper Henri Hattel. "Material flow in butt friction stir welds in AA2024-T3." *Acta Materialia* 54.4 (2006): 1199-1209.

[14] Fonda, R. W., J. F. Bingert, and K. J. Colligan. "Development of grain structure during friction stir welding." Scripta Materialia 51.3 (2004): 243-248.

[15] J. A. Schneider and A. C. Nunes Jr: 'Characterization of plastic flow and resulting microtextures in a friction stir weld', Metall. Mater. Trans. B, 2004, 35B, (4), 777–783

[16] B. Yang, J. Yan, M. A. Sutton and A. P. Reynolds: 'Banded microstructure in AA2024-T351 and A2524-T351 aluminum friction stir welds, Part I. metallurgical studies', Mater. Sci. Eng. A-Struct., 2004, A364, 55–65

[17] K. E. Knipling and R. W. Fonda: 'Texture development in the stir zone of near-a titanium friction stir welds', Scr. Mater., 2009, 60,1097–1100

[18] A. L. Pilchak, W. Tang, H. Sahiner, A. P. Reynolds and J. C. Williams:

‘Microstructure evolution during friction stir welding of mill-annealed Ti-6Al-4V’, Metall. Mater. Trans. A, 2011, 42A, (3), 745–762.
[19] Chen, Z. W., and S. Cui. "On the forming mechanism of banded structures in aluminium alloy friction stir welds." Scripta Materialia 58.5 (2008): 417-420.
[20] Krishnan, K. N. "On the formation of onion rings in friction stir welds." Materials science and engineering: A 327.2 (2002): 246-251.
[21] A. C. Nunes: ‘Prolegomena to the study of friction stir welding’, Proc. Materials Science & Technology 2010 – Joining of Advanced and Specialty Materials XII, Houston, TX, USA, October 2010, Paper 14, pp. 2651–2664.
[22] Xu, Shaowen, and Xiaomin Deng. "A study of texture patterns in friction stir welds." Acta Materialia 56.6 (2008): 1326-1341.
[23] Schneider, J. A., and A. C. Nunes Jr. "Characterization of plastic flow and resulting microtextures in a friction stir weld." *Metallurgical and materials transactions B* 35.4 (2004): 777-783.
[24] Sutton, Michael A., et al. "Banded microstructure in 2024-T351 and 2524-T351 aluminum friction stir welds: Part II. Mechanical characterization." Materials Science and Engineering: A 364.1 (2004): 66-74.
[25] Kim, Y. G., et al. "Three defect types in friction stir welding of aluminum die casting alloy." Materials Science and Engineering: A 415.1 (2006): 250-254.
[26] Lakshminarayanan, A. K., S. Malarvizhi, and V. Balasubramanian. "Developing friction stir welding window for AA2219 aluminium alloy." *Transactions of Nonferrous Metals Society of China* 21.11 (2011): 2339-2347.
[27] Zhang, Z. H., et al. "Effective predictions of ultimate tensile strength, peak temperature and grain size of friction stir welded AA2024 alloy joints." The International Journal of Advanced Manufacturing Technology 73.9-12 (2014): 1213-1218.
[28] Gadakh, Vijay S., and Adepu Kumar. "Friction stir welding window for AA6061-T6 aluminium alloy." Proceedings of the Institution of Mechanical Engineers, Part B: Journal of Engineering Manufacture 228.9 (2014): 1172-1181.
[29] Commin, Loreleï, et al. "Friction stir welding of AZ31 magnesium alloy rolled sheets: Influence of processing parameters." Acta materialia 57.2 (2009): 326-334.
[30] Gould, Jerry E., and Zhili Feng. "Heat flow model for friction stir welding of aluminum alloys." *Journal of Materials Processing and Manufacturing Science* 7 (1998): 185-194.
[31] Vilaça, Pedro, Luísa Quintino, and Jorge F. dos Santos. "iSTIR—analytical thermal model for friction stir welding." *Journal of Materials Processing Technology* 169.3 (2005): 452-465.
[32] Schmidt, Henrik Nikolaj Blich, and Jesper Hattel. "An analytical model for prescribing the flow around the tool probe in friction stir welding." (2005).
[33] Nandan, R., et al. "Three-dimensional heat and material flow during friction stir welding of mild steel." *Acta Materialia* 55.3 (2007): 883-895.
[34] Schmidt, H., Jesper Hattel, and John Wert. "An analytical model for the heat generation in friction stir welding." *Modelling and Simulation in Materials Science and Engineering* 12.1 (2003): 143.
[35] Schmidt, H., and J. Hattel. "Modelling heat flow around tool probe in friction stir

welding." *Science and Technology of Welding and Joining* 10.2 (2005): 176-186.
[36] Schmidt, Henrik B., and Jesper H. Hattel. "Thermal modelling of friction stir welding." *Scripta Materialia* 58.5 (2008): 332-337.
[37] Chao, Yuh J., X. Qi, and W. Tang. "Heat transfer in friction stir welding-experimental and numerical studies." TRANSACTIONS-AMERICAN SOCIETY OF MECHANICAL ENGINEERS JOURNAL OF MANUFACTURING SCIENCE AND ENGINEERING 125.1 (2003): 138-145.
[38] Zhu, X. K., and Y. J. Chao. "Numerical simulation of transient temperature and residual stresses in friction stir welding of 304L stainless steel." *Journal of materials processing technology* 146.2 (2004): 263-272.
[39] Song, M., and R. Kovacevic. "Thermal modeling of friction stir welding in a moving coordinate system and its validation." International Journal of Machine Tools and Manufacture 43.6 (2003): 605-615.
[40] Khandkar, M. Z. H., Jamil A. Khan, and Anthony P. Reynolds. "Prediction of temperature distribution and thermal history during friction stir welding: input torque based model." *Science and Technology of Welding and Joining* 8.3 (2003): 165-174.
[41] Schmidt, Henrik Nikolaj Blich, and Jesper Hattel. "An analytical model for prescribing the flow around the tool probe in friction stir welding." (2005).
[42] Arbegast, William J. "A flow-partitioned deformation zone model for defect formation during friction stir welding." *Scripta materialia* 58.5 (2008): 372-376.
[43] Nunes Jr, Arthur C. "Metal flow in friction stir welding." (2006).
[44] Reynolds, Anthony P. "Flow visualization and simulation in FSW." Scripta materialia 58.5 (2008): 338-342.
[45] Seidel, T. U., and Anthony P. Reynolds. "Two-dimensional friction stir welding process model based on fluid mechanics." *Science and technology of welding and joining* 8.3 (2003): 175-183.
[46] Colegrove, P. A., and H. R. Shercliff. "Two-dimensional CFD modelling of flow round profiled FSW tooling." *Science and technology of welding and joining* 9.6 (2004): 483-492.
[47] Colegrove, Paul A., and H. R. Shercliff. "Development of Trivex friction stir welding tool Part 2–three-dimensional flow modelling." *Science and technology of welding and joining* 9.4 (2004): 352-361.
[48] Colegrove, Paul A., and Hugh R. Shercliff. "3-Dimensional CFD modelling of flow round a threaded friction stir welding tool profile." *Journal of Materials Processing Technology* 169.2 (2005): 320-327.
[49] Nandan, R., G. G. Roy, and T. Debroy. "Numerical simulation of three-dimensional heat transfer and plastic flow during friction stir welding." *Metallurgical and materials transactions A* 37.4 (2006): 1247-1259.
[50] Nandan, R., et al. "Three-dimensional heat and material flow during friction stir welding of mild steel." *Acta Materialia* 55.3 (2007): 883-895.
[51] Nandan, R., et al. "Numerical modelling of 3D plastic flow and heat transfer during friction stir welding of stainless steel." *Science and Technology of Welding and Joining* 11.5 (2006): 526-537.
[52] Cho, Hoon-Hwe, et al. "Three-dimensional numerical and experimental investigation on friction stir welding processes of ferritic stainless steel." Acta

Materialia 61.7 (2013): 2649-2661.
[53] Deng, Xiaomin, and Shaowen Xu. "Two-dimensional finite element simulation of material flow in the friction stir welding process." *Journal of Manufacturing Processes* 6.2 (2004): 125-133.
[54] Xu, S., et al. "Finite element simulation of material flow in friction stir welding." *Science and Technology of Welding and Joining* 6.3 (2001): 191-193.
[55] Ulysse, Patrick. "Three-dimensional modeling of the friction stir-welding process." *International Journal of Machine Tools and Manufacture* 42.14 (2002): 1549-1557.
[56] Zhang, H. W., Zhao Zhang, and J. T. Chen. "3D modeling of material flow in friction stir welding under different process parameters." *Journal of Materials Processing Technology* 183.1 (2007): 62-70.
[57] Zhang, Zhao, and H. W. Zhang. "A fully coupled thermo-mechanical model of friction stir welding." *The International Journal of Advanced Manufacturing Technology* 37.3-4 (2008): 279-293.
[58] Chen, C. M., and R. Kovacevic. "Finite element modeling of friction stir welding—thermal and thermomechanical analysis." *International Journal of Machine Tools and Manufacture* 43.13 (2003): 1319-1326.
[59] Buffa, G., et al. "A continuum based fem model for friction stir welding—model development." *Materials Science and Engineering: A* 419.1 (2006): 389-396.
[60] Schmidt, Hattel, and Jesper Hattel. "A local model for the thermomechanical conditions in friction stir welding." *Modelling and simulation in materials science and engineering* 13.1 (2004): 77.
[61] Kuykendall, Katherine, Tracy Nelson, and Carl Sorensen. "On the selection of constitutive laws used in modeling friction stir welding." *International Journal of Machine Tools and Manufacture* 74 (2013): 74-85.
[62] Tello, Karem E., Adrian P. Gerlich, and Patricio F. Mendez. "Constants for hot deformation constitutive models for recent experimental data." *Science and Technology of Welding and Joining* 15.3 (2010): 260-266.
[63] Pan, Wenxiao, et al. "A new smoothed particle hydrodynamics non-Newtonian model for friction stir welding: Process modeling and simulation of microstructure evolution in a magnesium alloy." International Journal of Plasticity 48 (2013): 189-204.
[64] Mitsufuji, Kenta, Masahito Nambu, and Fumikazu Miyasaka. "Numerical Analysis of FSW Employing Discrete Element Method." Friction Stir Welding and Processing IX. Springer International Publishing, 2017. 311-319.
[65] Krzyzanowski, Michal, et al. "Combined discrete/finite element multiscale approach for modelling of the tool/workpiece interface during high shear processing: hot rolling and friction stir welding applications." *Materials Science Forum*. Vol. 638. Trans Tech Publications, 2010.
[66] Krzyzanowski, Michal, and Mark W. Rainforth. "Advances on modelling of the tool/workpiece interface during high shear processing." Materials Science Forum. Vol. 654. Trans Tech Publications, 2010.
[67] Cho, Jae-Hyung, Donald E. Boyce, and Paul R. Dawson. "Modeling strain hardening and texture evolution in friction stir welding of stainless steel." *Materials Science and*

Engineering: A 398.1 (2005): 146-163.
[68] Fratini, Livan, and Gianluca Buffa. "CDRX modelling in friction stir welding of aluminium alloys." International Journal of Machine Tools and Manufacture 45.10 (2005): 1188-1194.
[69] Simar, A., et al. "Sequential modeling of local precipitation, strength and strain hardening in friction stir welds of an aluminum alloy 6005A-T6." *Acta Materialia* 55.18 (2007): 6133-6143.
[70] Myhr, O. R., and Øystein Grong. "Modelling of non-isothermal transformations in alloys containing a particle distribution." Acta Materialia 48.7 (2000): 1605-1615.
[71] Myhr, O. R., Ø. Grong, and S. J. Andersen. "Modelling of the age hardening behaviour of Al–Mg–Si alloys." *Acta Materialia* 49.1 (2001): 65-75.
[72] Wagner, Richard, Reinhard Kampmann, and Peter W. Voorhees. "Homogeneous Second-Phase Precipitation." *Materials science and technology* (1991).
[73] Dong, P., et al. "Coupled thermomechanical analysis of friction stir welding process using simplified models." *Science and Technology of Welding and Joining* 6.5 (2001): 281-287.
[74] Roy, G. G., R. Nandan, and T. DebRoy. "Dimensionless correlation to estimate peak temperature during friction stir welding." Science and Technology of welding and Joining 11.5 (2006): 606-608.
[75] Tello, K., U. Duman, and P. Mendez. "Scaling laws for the welding arc, weld penetration and friction stir welding." *Proceedings of Eighth Trends in Welding Research* (2009): 172-181.
[76] Mendez, Patricio F., and Thomas W. Eagar. "The matrix of coefficients in order of magnitude scaling." *Fourth International Workshop on Similarity Methods, Nov*. 2001.
[77] Mendez, Patricio F., and Thomas W. Eagar. "Order of magnitude scaling: a systematic approach to approximation and asymptotic scaling of equations in engineering." *Journal of Applied Mechanics* 80.1 (2013): 011009.
[78] Mendez, Patricio F. "Characteristic values in the scaling of differential equations in engineering." *Journal of Applied Mechanics* 77.6 (2010): 061017.
[79] Tello, K. E., A. P. Gerlich, and P. F. Mendez. *Use of scaling laws to estimate grain size and coarsening in the stir zone of friction stir welding*. na, 2009.
[80] Mendez, Patricio F., Karem E. Tello, and Thomas J. Lienert. "Scaling of coupled heat transfer and plastic deformation around the pin in friction stir welding." Acta Materialia 58.18 (2010): 6012-6026.
[81] Arora, A., T. DebRoy, and H. K. D. H. Bhadeshia. "Back-of-the-envelope calculations in friction stir welding–velocities, peak temperature, torque, and hardness." Acta materialia 59.5 (2011): 2020-2028..

Chapter 2

Shear Localization Modeling of Friction Stir Weld Formation Process

Abstract

This paper presents a shear localization model for studying friction stir welding (FSW) formation process. With this model, shear band (SB) width, shear band formation time, and shear band propagation speed can be theoretically estimated. The shear band propagation speed in this context serves as theoretical estimate of the maximum welding speed possible for a given material and prescribed welding conditions, such as stir pin rotation speed and torque level. The model is shown to provide reasonable estimates of shear localization parameters against a set of recent experimental data on friction stir welding of titanium alloy Ti-6Al-4V. With this model, titanium alloy Ti-6Al-4V, high strength low-alloy steel 4340, and aluminum alloy 2024 are compared in terms of shear localization parameters, such as maximum shear band propagation speeds (or welding speeds).

Introduction

Friction stir welding (FSW) is a relatively new solid-state joining process, as first reported by Dawes and Thomas [1], and has many advantages over traditional welding and joining processes as recently reviewed by Nandan et al. [2] . It can be used either to

join advanced high strength materials deemed not weldable or modify material surface conditions for improved fracture and fatigue resistance of a structure that may be subjected to a hostile service environment, such as space vehicle launch and operation, as discussed by Nandan et al [2] and Nunes [3]. Recognizing the needs for an improved understanding of weld formation process associated with friction stir welding, it has been established experimentally that plastic flow phenomena in form of shear banding seem governing weld development as shown experimentally by Schneider and Nunes and [4], Yang et al. [5] for high strength aluminum alloys, by Knipling and Fonda [6] and Pilchak et al [7] for titanium alloys.

To form a quality friction stir weld, two key parameters are rotational speed of stir pin and its translational speed (or welding speed) [1], which are typically used in describing a process operating window for today's applications based on exhaustive and costly Design of Experiment (DoE) approach or trial-and-error. Numerous computational procedures have been attempted over the years to simulate one or a few aspects of the complex multi-physics and multi-scale mechanics phenomena associated with various stages of weld formation process in friction stir welding. Along this line, Dong et al. [8] employed a finite element method and established that in addition to friction heating, plastic dissipation induced heating also plays an important role in facilitating the development of a favorable plastic flow field around stir pin at least during stir pin plunging stage. As a result, a friction stir welding model solely relying on analytical-based thermal solutions considering only friction heating such as those by Schmidt et al. [9] may not be adequate in revealing some of the important mechanisms in stir zone forming process. As a case in point, an orderly banded structure (see Figure 2.1)

typically seen in good friction stir welds by various researchers [3-6] coincides with an incremental distance traveled by stir pin per revolution suggests that an essentially displacement-controlled weld formation process is at play, or more precisely, through a local shear deformation process.

A 2D fully-coupled thermal-fluid model by Seidel and Reynolds [10] considered lamina-viscous and non-Newtonian flow around an ideal cylinder. Their results suggested that material transport occurs mainly around the pin on the retreating side. Similarly, Colergrove and Shercliff [11] used commercial fluid dynamics software and simulated coupled heat conduction and fluid flow effect friction stir welding of 7075 Al alloy. A review summary on various modeling approaches is given by Nandan, Roy and DebRoy [12].

Although a plenty of numerical models for friction stir welding have been proposed or attempted over the last two decades, a modeling capability for process parameter window estimation [1] in terms of friction stir pin rotational and translational speed for a given material of interest remains elusive today. Recognizing the dominance of local plastic deformation characteristics discussed in aforementioned work [3-6], this report presents a rather different approach to friction stir weld formation modeling by focusing on shear localization process dynamics which should be directly applicable to the shear band formation process shown in Figure 2.1 as reported in [13]. We start with a coupled thermal and visco-plastic formulation by idealizing the shear formation process as a one-dimensional (1D) problem following the framework by Batra and Wei [14], but with a different definitions of boundary and initial conditions that are directly relevant to friction stir welding process.

Within this context, definitions of both time scale that governs the formation of a shear band and length scale measuring shear band width will be introduced. Together, these two parameters provide a theoretical estimate of the maximum shear band propagation speed or maximum welding speed possible for a given material and a set of welding parameters. Friction stir welding experiments reported by Pilchak et al. [7] and conducted in this study on friction stir welding of Ti-6Al-4V alloy are then used to validate the theoretical estimates of maximum welding speeds observed in experiments. Finally, three drastically different metals are examined to gain insight on their friction stir weldability in terms of shear localization parameters.

Note that material constitutive behavior in this study is assumed to follow Johnson-Cook law in terms of dependency on temperature, strain and strain-rate. One reason is that Johnson Cook parameters for the materials of interest in this investigation have been well-documented in a number of authoritative publications [15-16]. The other reason is that prior investigations such as Batra and Wei [14] discussed the feasibility of modeling FSW process in the context of Johnson Cook material model. However, a follow-on study, documented in the separate report [17] by the same authors, has shown that Sellars-Tegart model seems more effective in capturing some of the observed material behaviors under friction stir welding conditions than Johnson-Cook law.

Shear Localization Model

2.1.1 Model definition

As shown in Figure 2.1b, a localized shear band just formed neighboring stir spin (only is stir pin cavity shown here after pin was pulled out) can be clearly identified with

its width representing the tool advance for each tool revolution. The nearby material remains essentially stationary beyond a small distance from the shear band boundary. At a peak strain rate of order of $10^2 \sim 10^4$/sec at shear band surface in contact with pin surface, the associated heat transport process resulted from friction and plastic dissipation from the shear band to its surrounding material can be reasonably assumed negligible, i.e., adiabatic.

As a result, relevant shear localization problems can be further simplified as a thermal boundary layer problem (see Fig. 2) within which plastic deformation boundary layer is fully contained. Then, the governing characteristic length dimension (*H*) for such a problem definition is fully determined by 1D transient heat conduction problem in the same way as given in [14].

In Figure 2.2, stir pin rotates at a constant speed V_{pin} while exerting a shear stress $\tau = f$ in contact with the workpiece (or base metal). The resulting frictional heat flux $q = f\left(V_{pin} - V_W\right)$ is assumed to be fully consumed by the workpiece for simplicity. As the frictional heat builds up at base metal near stir pin surface, material softening occurs, resulting in rapid development of plastic straining and flow along the base metal and stir pin interface. As soon as the relative velocity, i.e., $V_{pin} - V_W$ approaches zero, a fully developed shear band is considered to be realized, corresponding to a full revolution of stir pin in 3D space. At this point in time, it is assumed a shear band width is represented as W_{SB} and time required in realizing W_{SB} represented as T_{SB}. Then, the corresponding shear band propagation speed becomes

$$V_P = \frac{W_{SB}}{T_{SB}} \tag{2.1}$$

which can be interpreted as the theoretically maximum possible (or the optimum) welding speed we set out to investigate as one of the important FSW process parameters.

2.1.2 Governing equations

Consider a domain that occupies $0 \le y \le H$, which is subjected to applied frictional stress f and a friction induced heat flux $q = f(V_{pin} - V_W)$ at the material/pin interface $y = 1$. Let the spatial coordinate (y) be normalized by H , the shear stress by τ_0 , time by H / V_{Pin} and temperature by θ_0. In terms of non-dimensional variables, the domain now occupies the region bounded by planes with $y = 0$ and $y = 1$. Initially, the material behaves elastically with a rising temperature caused by frictional heating and associated conduction transfer. However, as yield strength of material decreases with increasing temperature, plastic deformation begins to develop. The governing equations for the thermal visco elastic plastic problem can be written as follows:

$$\rho \dot{v} = \tau_{,y} \tag{2.2}$$

$$\dot{\theta} = \lambda \theta_{,yy} + \tau \dot{\gamma}_p \tag{2.3}$$

$$\dot{\gamma} = v_{,y} = \dot{\gamma}_e + \dot{\gamma}_p \tag{2.4}$$

$$\dot{\tau} = \mu \dot{\gamma}_e \tag{2.5}$$

$$\dot{\gamma}_p = \begin{cases} 0 & \left(\theta < \theta_p\right) \\ \dot{\gamma}_0 \exp\left[\left(\dfrac{\tau}{(A+B\gamma^n)(1-\theta_*^m)} - 1\right) \Big/ C\right] & \left(\theta \geq \theta_p\right) \end{cases} \qquad (2.6)$$

$$\theta_* = \frac{\theta - \theta_r}{\theta_m - \theta_r}$$

Here a superimposed dot signifies the time derivative; a comma followed by y indicates the partial differentiation with respect to y. In above equations, ρ is the mass density, v the velocity, τ the shear stress, θ the temperature, γ the shear strain which is partitioned into elastic part γ_e and plastic part γ_p. Furthermore, μ is the shear modulus and λ the thermal diffusivity of material. Eq. (2.2) expresses the balance of momentum. Eq. (2.3) is the balance of internal energy, in which all plastic energy, represented by the second term on the right hand side, is assumed to be converted into heating. Eq. (2.4) and Eq. (2.5) imply, respectively, the definition of strain rate and the Hooke's law written in rate form. Eq. (2.6) is the constitutive equation of elasto-thermo-viscoplastic relationship, where θ_p is the temperature at which material yield strength equals to applied stress. All other material parameters are assumed to be independent of temperature. At $t = 0$, the initial conditions are described as follows:

$$v(y,0) = 0, \quad \theta(y,0) = \theta_r, \quad \gamma(y,0) = f/\mu, \quad \tau(y,0) = f, \quad \gamma_p(y,0) = 0 \qquad (2.7)$$

The corresponding boundary conditions are:

$$-\lambda\theta_{,y}(1,t) = q(t) = -f(V_{Pin} - V_M), \quad \tau(1,t) = f, \quad -\lambda\theta_{,y}(0,t) = 0, \quad v(0,t) = 0 \qquad (2.8)$$

which state that at the workpiece/pin interface, heat flux is induced by friction in the form of the product of applied frictional stress and relative velocity while at the other end of

the domain (i.e., $y = 0$), $v(0,t) = 0,\ \theta_{,x}(0,t) = 0$ can be realized as long as H is sufficiently large.

The non-dimensional parameters are related to their dimensional (barred) counterparts as follows:

$$y = \bar{y} / H,\ t = \bar{t} / \dot{\gamma}_0,\ \theta = \bar{\theta} / \theta_0,\ \lambda = \bar{k} / \left(\bar{\rho}\bar{c}\dot{\gamma}_0 H^2\right),\ \rho = \bar{\rho} H^2 \dot{\gamma}_0^{\ 2} / \tau_0,$$
$$q = \bar{q} / \left(\dot{\gamma}_0 H \tau_0\right),\ \tau_0 = \bar{A},\ A = \bar{A} / \tau_0,\ B = \bar{B} / \tau_0,\ v = \bar{v} / V_{pin},\ \theta_0 = \bar{A} / (\bar{\rho}\bar{c}) \tag{2.9}$$

where c is specific heat, k thermal conductivity, and $\dot{\gamma}_0 = \dot{V}_{pin} / H$ nominal strain rate. All are written in consistent dimensionless forms.

2.1.3 Numerical implementation

The shear localization problem described by Eq. (2) through Eq. (9) can be conveniently solved numerically by writing a finite element method (FEM) code using language of technical computing such as MATLAB. [18]. In numerical implementation of Eqs.(2.2) through (2.9), a parametric programming code was developed using a weak form of the governing equations (Eqs.(2.2)-(2.6)), initial conditions and boundary conditions (Eqs. (2.7)-(2.8)) derived by a simple piecewise linear Galerking/Petrov-Galerkin method. This discretization method offers a good accuracy to the second order in space [19]. The result is a system of coupled non-linear ordinary differential equations that can be integrated using MATLAB function "*ode15s"*. An adaptive time increment method is used to compute incremental solution over time within a prescribed accuracy requirement using built-in default tolerance settings, i.e. "*Reltol"=10*$^{-3}$*, "Abstol" = 10*$^{-6}$, where *Reltol* and *Abstol* control the relative and absolute tolerances, respectively. The

resulting MATLAB program developed can be used to obtain a full solution over time from $t = 0$ to a time at which material at workpiece/pin interface reaches to a prescribed pin surface linear velocity, i.e., $v(1,t) = 1$, at which time a shear band of width W_{SB} in Eq. (2.1) is considered to be fully developed. The program execution terminates.

The coordinates of finite element model grid (i.e., nodal positions) is given by:

$$y_n = 1 - \left(\frac{301 - n}{300} \right)^4, \quad n = 1, 2, \ldots 301. \tag{2.10}$$

With Eq.(2.10), a finer resolution is attained at material/pin interface (i.e, $y = 1$) where applied shear stress and heat flux are prescribed.

Modeling of Welding Experiments

In this section, the modeling procedures described above are used to simulate a set of selected FSW experiments reported by Pilchak et al. [7] and conducted as a part of this study including introducing the definitions of shear localization parameters described in Eq.(2.1):

2.1.4 Data by Pilchak et al. [7]

A total of five mill-annealed Ti-6Al-4V friction stir welded specimens (see Table 1) were produced with good weld quality by using a range of welding parameters through prior experiences [7]. Table 1 shows welding parameters used in [7]. The Johnson Cook material constants are summarized in Table 2, taken directly from a Federal Aviation Administration (FAA) report (see [15]).

In applying the shear localization model described in Sec. 2.2.2 of this work, we

only need to investigate shear localization within a time period of one revolution of stir pin in order to estimate shear band width and time needed to generate the shear band. As such, a time domain of interest becomes $t_c = 1/\omega$, where ω is the angular velocity of pin rotation. A space domain H in Figure 2.2 can be defined as $H = 5H_c$, where $H_c = 2\sqrt{\alpha t_c}$ is a characteristic length in thermal diffusion process, in which α is thermal diffusivity of material. As to be shown in the next section, with $H = 5H_c$, an one-dimensional semi-infinite body condition is realized in Figure 2.2.

2.1.5 Modeling results

For illustration purpose, modeling results corresponding to conditions under "Weld 2-120" (see Table 2.1) are shown in Figure 2.3. Note that predicted temperature (Figure 2.3a) is normalized by material melting temperature and material flow velocity by stir pin velocity V_{pin} . In order to examine detailed transitional behavior from elastically dominated deformation to plastically deformation, the vertical axes in Figure. 3b-d, are presented in logarithmic scale. Note that the analysis terminates when the relative velocity at the interface between base material and stir pin becomes zero, i.e., $V_{pin} - V_M = 0$.

Figure 2.3a shows predicted special temperature distributions within base metal at different times in seconds. The material/pin interface temperature is relative low at the beginning ($t \approx 0.11s$) and continue to increase over time. Before time reaches to $t \approx 1.06s$, temperature throughout the domain remains relatively low and resulting plastic deformation is still barely noticeable (see Figure 2.3b-c). The same can be said about

material flow velocity, see Figure 2.3d. As the interface temperature rapidly increases due to continued friction heating, thermal softening term in Johnson-Cook model (Eq.(2.6)) begins to take effect. At time reaches to and increases beyond $t \approx 1.06s$, a localized development of plastic strain rate and plastic strain can be clearly seen near material/pin interface. Material at and near the interface starts to flow with an increasing velocity, as shown in Figure 2.3d. Even though the temperature only exhibits a slight increase during $t \approx 1.06 - 1.28s$, plastic strain, plastic strain rate, and interface material velocity increase rapidly. With the presence of high temperature gradient near the interface, e.g., $y > 0.95$, both spatial plastic strain, plastic strain rate, and velocity distributions become increasingly localized, forming two distinct zones in space after $t \geq 1.2\sec$, as shown in Figure 2.3b-c. A demarcation position separating the two zones in space occurs at $y \approx 0.985$ from material/pin interface at $t = 1.28\sec$, which can be seen in all three parameters predicted, i.e., plastic strain, strain rate, and velocity, suggesting the onset of shear band development within the small region of $y \approx 0.985 \sim 1$, often referred to as shear localization in continuous mechanics terms.

In order to verify the generality of the shear localization phenomena observed for conditions corresponding to "Weld 2-120" in Table 1, the modeling results for all five weld samples produced by Pilchak et al [7] under five different sets of welding conditions are compared in Figure 2.4. In all five cases shown in Figure 2.4, although with rather similar spatial temperature distributions (Figure 2.4a), plastic strain, strain rate, and velocity distributions indeed show a clear deflection point which moves increasingly closer to the interface from $y \approx 0.985$ to $y \approx 0.995$, as pin rotation speed increases from

120RPM to 800 RPM. Beyond the deflection point (or further increase in y), plastic strain, plastic strain rate, and velocity exhibit similar distribution characteristics among all five cases, similar to the finding discussed earlier with respect to the case for "Weld 2-120". Given the results obtained so far shown in Figure 2.3 and 2.4, it can be concluded with a reasonable degree of confidence that shear band localization phenomena associated with friction stir weld formation process are captured with the shear localization model presented in the previous section. We can then proceed to estimate theoretical welding speed for each of the five cases by extracting shear band width W_{SB} and shear band formation time T_{SB} in Eq.(2.1).

Before proceeding, it is worth noting that the temperature distributions in Figure 2.4a, show rather small spatial variation over the five sets of welding parameters, all of which reaches to the melting temperature (i.e., with normalized temperature being unity) at workpiece/pin interface. A careful examination of the modeling results associated with this phenomenon and the theoretical formulation in Eq.(2.6) suggests that this is solely due to the structure of John-Cook model. When the workpiece material at the interface rises to the pin rotational speed, the high plastic strain renders the strain-hardening term so dominant that the resulting high yield stress accelerates friction heating at the interface until the interface temperature reaches to its melting point. This also points out one limitation of Johnson-Cook model for modeling friction stir welding, which inevitably predicts melting temperature at the interface under typical welding conditions. In light of this finding, an alternative constitute model such as Sellars-Tegart type has been shown to be more appropriate for modeling friction stir welding [17], when it was incorporated

for analyzing the same set of experimental data.

2.1.5.1 Shear Band Width

Figure 2.5 is a re-plot of the plastic strain, strain rate, and velocity fields in Figure 2.3 by focusing attention in the region containing shear band development. All three predicted field parameters (plastic strain, strain rate, and velocity) indicate an essentially same demarcation position in *y*, beyond which a distinct change in rate over spatial coordinate (*y*) can be clearly seen. The region from $y \approx 0.985$ to material/pin interface, i.e., $y = 1$ can be defined the shear band width. Since *y* is normalized by $H=5H_c$, The actual SB width becomes $(1-0.985)\times 5H_c$, yielding a SB width of *0.18mm*. Figure 2.6 shows a banded structure of a friction stir welded Ti-6Al-4V sample produced in this study, which shows a width of 0.23mm. The comparison in terms of shear band widths can be considered as being acceptable, given the simplicity of the 1D assumption, temperature-independent thermal-physical properties used in Eq.(2.6), and uncertainties involved in the material constitutive model.

2.1.5.2 Shear Band Formation Time

By considering the case for "Weld 2-120" in Table 1, without losing generality, Figure 2.7 shows time-history of plots of normalized temperature, plastic strain rate, plastic strain, and velocity for material point at the material/pin interface, i.e., at $y = 1$. In logarithmic scale, plastic strain rate as a function of time shows a sudden change in its time rate at $t = 1.085s$, which can also been observed in plastic strain and velocity histories (see Figure 2.7c-d). This deflection point in time signifies the initiation of shear

band. The time duration accumulated from this point to the completion of one full revolution of stir pin rotation (i.e., $V_{pin} - V_M = 0$) defines the shear band formation time, T_{SB}. Furthermore, it is worth noting that after initiation, plastic strain and velocity histories continue to show a monotonic rise, although with a slower rate, plastic strain rate history at first increases rapidly and then show a drastic drop from its peak. Again, this phenomenon is unique to Johnson-Cook law in which plastic strain rate is governed by both thermal softening θ_*^m and strain hardening terms γ^n where m and n are thermal softening and strain hardening exponents, respectively. Before reaching its peak, plastic strain nearly remains zero until temperature increase to about $0.9T_m$ or 90% of material melting temperature. Prior to reaching to this point, the strain hardening term dominates the strain rate development as a function of time. When temperature reaches to a neighborhood of $\theta \approx 0.9T_m$, thermal softening term starts to drive a rapid increase in plastic strain rate resulting from a rapid decrease in shear strength and applied constant shear traction stress. This leads to an explosive increase in plastic strain (Figure 2.7c), which in turn increases shear strength, enabling the dominance of the strain hardening term again, resulting in a rapid decrease in plastic strain rate.

.

2.1.5.3 Welding Speed Estimation

Since both shear band width and its formation time have been already defined in the previous sections, shear band propagation speed, which is the maximum welding speed in the context of friction stir welding, can then be calculated through Eq.(2.1). The

results for the five welding conditions in Table 2.1 are compared in Figure 2.8a-c. It can be seen that both shear band width and formation time decrease with increasing rotational speed. It is important to note that shear band formation time decreases in faster rate than shear band width as a function of pin rotation speed, leading to faster shear band propagation speed or welding speed while maintaining a consistent weld quality. The theoretically estimated optimum welding speeds for all five welding conditions compare well with experimental findings from Pilchak et al. [7], in which welding parameters used to achieve acceptable weld quality were obtained experimentally (Figure 2.8c). The predicted maximum welding speed is a higher than that used in experiment, which seems reasonable since the calculation result is "maximum welding speed", while the weld speed used in experiment is decided through trials and may not be the optimum value. .

Discussions

As shown in Sec. 2.3.2.3, the shear localization modeling procedure developed here provide reasonable estimates of shear band width, shear band formation time, and theoretical maximum translational speed. In this section, the application of the present modeling are used to study different base material effect, i.e. Ti-6Al-4V, Steel 4340, Al2024. Then the issue caused by Johnson Cook constitutive law is discussed.

2.1.6 Material effects

Thus far, the analysis has been focused upon titanium alloy Ti-6Al-4V. It should be informative to examine some of the fundamental differences in shear localization process among the three rather different materials, such as titanium versus steel versus

aluminum. In doing so, two more materials are considered here: high strength low-alloy steel 4340 and high strength aluminum alloys Al 2024 on which Johnson-Cook model properties are also available from [15-16], as given in Table 2. In addition, yield strength as a function of temperature for each material is also given in Figure 2.9.

For easy comparison purpose, all calculations for the three materials are performed under the same frictional stress ($f = 60MPa$) and same rotational speed (500 RPM), and same flux (1.571×10^7 (W/m^2)). The results are summarized in Fig.10. Due to significant differences in material property, Steel 4340 has the highest plastic temperature, while Al2024 has the lowest. In Table 2, $\overline{A}$, $\overline{B}$ and n characterize material's strain hardening ability. It can be seen that Ti-6Al-4V shows the strongest strain hardening term among the three materials and Al2024 shows the weakest strain hardening term. The strain hardening ability symbolizes material's resistance to SB formation. A material possesses a higher strain hardening ability would require a higher temperature to be reached in order for its thermal softening term to overcome plastic deformation resistance. Under the same friction heat input conditions, a material with a lower strain hardening ability requires a lower temperature to overcome its plastic deformation resistance, resulting in a wider SB. This is consistent with the results shown in Fig. 10b. The high strain hardening term and low thermal conductivity of Ti-6Al-4V result in localized SB formation characterized by small SB width and short SB formation time. For Al2024, its low strain hardening ability and high thermal conductivity allow a wider SB but a relatively short SB formation time.

As for Steel4340, its strain hardening ability is not as strong as Ti-6Al-4V while its thermal conductivity is nearly 6 times bigger than Ti-6Al-4V. As a result, 4340 tends

form a wider SB with a longer SB formation time, leading to somewhat a slower welding speed than Ti-6Al-4V. In summary, the predicted maximum welding speed is the highest for Al2024 among all three materials. Interestingly enough, both Steel 4340 and Ti-6Al-4V are rather similar in maximum welding speed, with Steel 4340 being slightly lower. However, the narrowest SB width predicted for Ti-6Al-4V suggests that Ti-6Al-4V should possess the poorest FSW weldability, i.e., sensitive to pin translational speed. The widest SB width predicted for Al2024 is consistent with the fact that aluminum alloys often possess a good FSW weldability.

2.1.7 About Johnson Cook model

Although all calculation results using Johnson Cook material model seem reasonable as far as shear localization parameters are concerned, this work has identified one area that requires further investigation regarding its suitability for modeling friction stir welding process. This is illustrated in Figure 2.4a. In this figure, material at the interface for all five cases reaches melting temperature under different rotation and translational speeds, which is considered unlikely. This is because Johnson Cook [16] determined material parameters from torsional test data over a (relative low) range of strain, strain rate and temperature. The strain hardening term in Johnson-Cook model is expressed as $A + B\gamma^n$, and the relationship between plastic strain and strain hardening term is plotted in Figure 2.11. It can be seen that when plastic strain reaches to 100-200, which is usually the case when dealing with friction stir welding, the resulting hardening effects generate a yield stress to a value that is about 40 to 80 times higher than room temperature value. This suggests that Johnson-Cook model is a strain hardening

dominated material model. As such, thermal softening term does not play a significant role until material temperature reaches near melting temperature, i.e., not suited for high temperature material behavior characterization in a temperature regime below melting. Typical hot forming (e.g., forging, extrusion etc) takes advantage of thermal softening effects which are dominant at a desirable forming temperature. A great deal of evidence generated in hot forming research community show that material at such a temperature possesses little strain hardening ability if at all [20]. Furthermore, some indirect temperature measurements performed by Pilchak et al [7] suggests that the five welding conditions in Table 1 resulted in different interface temperatures which should be below material melting temperatures. For above reasons, an alternative constitutive material model will be examined in a subsequent paper [17] by the same authors, which clearly show more reasonable results than Johnson-Cook model.

Summary

A shear localization model is presented in this paper, which focuses on shear band (SB) formation phenomena associated with friction stir welding process. With this model, shear band width, shear band formation time, and shear band propagation speed can be theoretically estimated. The shear band propagation speed serves a direct estimate of the maximum welding speed for a given material to be welded under a set of specified stir pin rotational and translational speeds. The model is shown to provide reasonable estimations of shear localization parameters against recent experimental data on titanium alloy Ti-6Al-4V.

By considering three drastically different base materials, predicted shear

localization parameters clearly indicate that titanium alloy such as Ti-6Al-4V is most difficult to weld due to its narrowest shear band width among all three materials considered. Even though Steel 4340 exhibits a slightly lower welding speed Ti-6Al-4V, its significantly wider shear band width suggests a much better friction stir weldability than Ti-6Al-4V. Aluminum alloys such as Al 2024 possesses the best friction stir weldability among the three materials examined, because of its widest shear band width and a modest amount of time needed for shear band formation.

Table 2-1: Welding parameters for Ti-6-4 [7]

Conditions	ω (RPM)	Travel speed (mm/min)	R^1 (mm)	h (mm)	Torque (Nm)
Weld 2-120	120	50.8	7.85	9.91	201
Weld 2-150	150	50.8	7.85	9.91	154
Weld 2-200	200	50.8	7.85	9.91	127
Weld 4-400	400	101.6	7.85	9.91	100
Weld 8-800	800	203.2	7.85	9.91	79

Table 2-2: Material properties Ti-6Al-4V, Steel 4340 and Al2024

Material Name	$\overline{\rho}$ (kg/m^3)	$\overline{c}$ (J/kgK)	$\overline{\mu}$ (GPa)	$\overline{k}$ (W/mK)	θ_m (K)	$\overline{A}$ (MPa)	$\overline{B}$ (MPa)	C	n	m
Ti-6Al-4V	4428	580	40	6.7	1883	634	379	0.014	0.93	1.1
Steel 4340	7840	477	76	38	1520	455	237	0.006	0.37	1
Al 2024	2770	875	28	119	502	213	264	0.0083	0.73	1.7

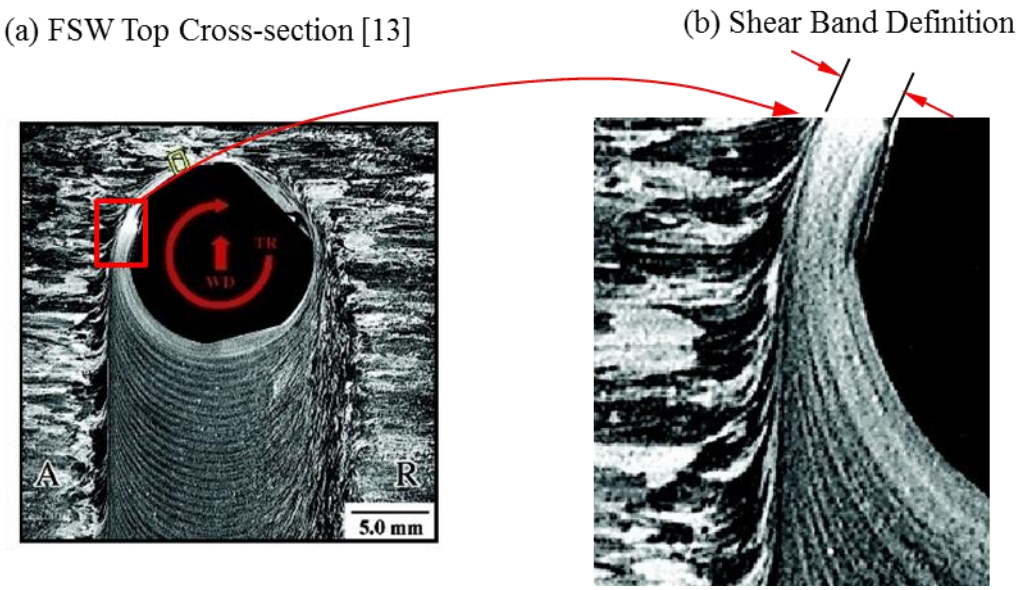

Figure 2.1: Typical banded structure in a friction stir weld and shear band definition for computational treatment

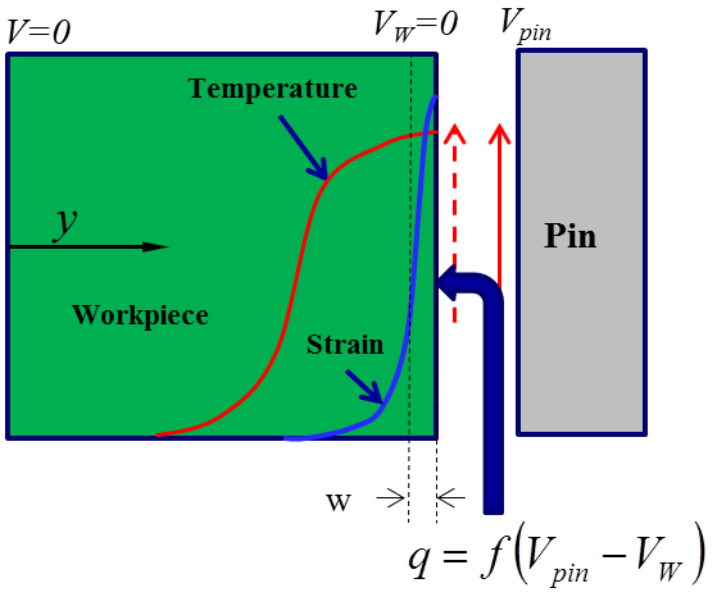

Figure 2.2: Definition of thermal boundary layer and plastic deformation boundary layer model presentation

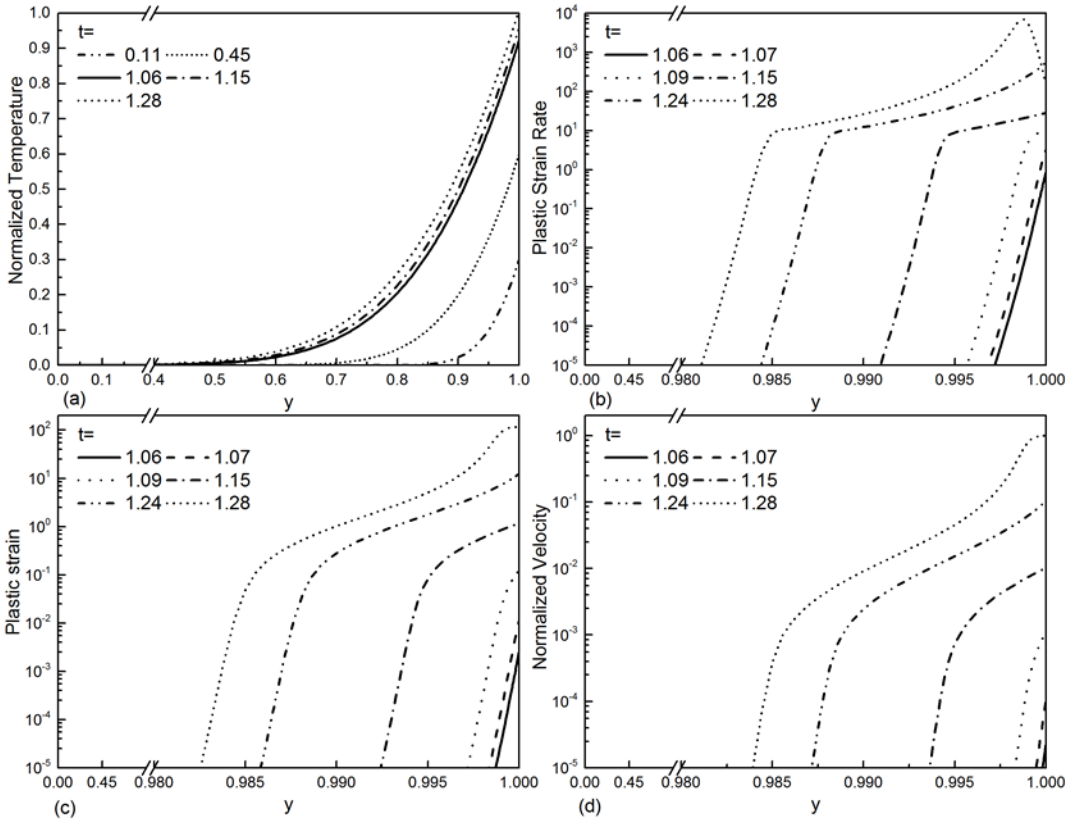

Figure 2.3: Predicted spatial distributions for Weld 2-120: (a) Temperature, (b) Plastic strain rate, (c) Plastic strain, (d) Velocity.

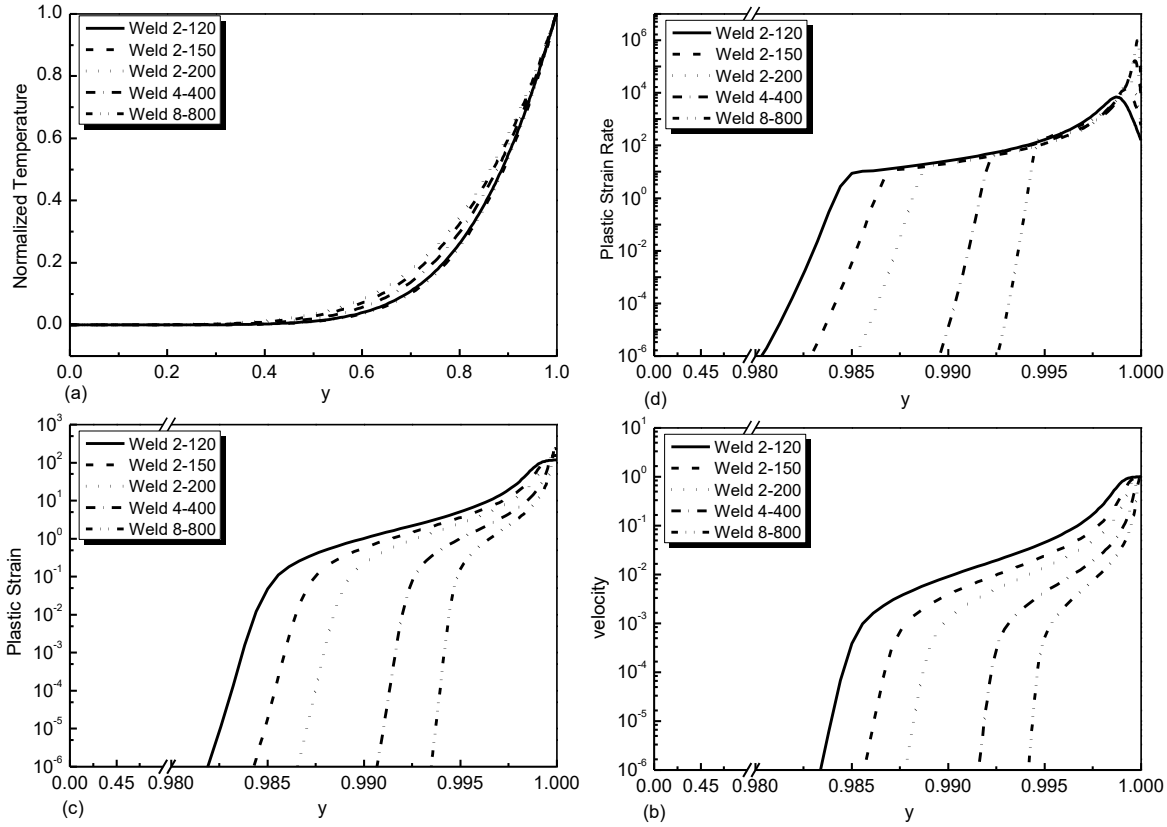

Figure 2.4: Comparison of final spatial distribution results for all five welding conditions given in Table 1: (a) temperature, (b) plastic strain rate, (c) plastic strain, (d) velocity.

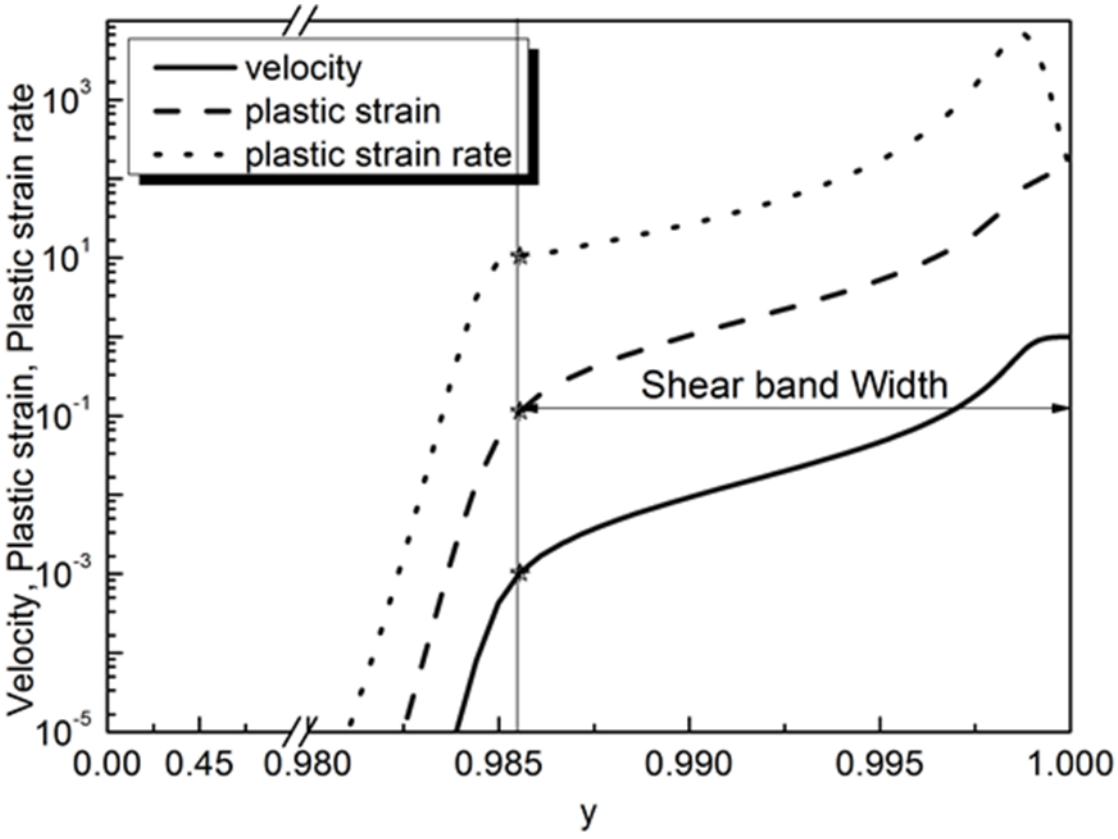

Figure 2.5: Log plot of spatial distributions of velocity, plastic strain, and plastic strain rate distribution for Weld ID 2-120.

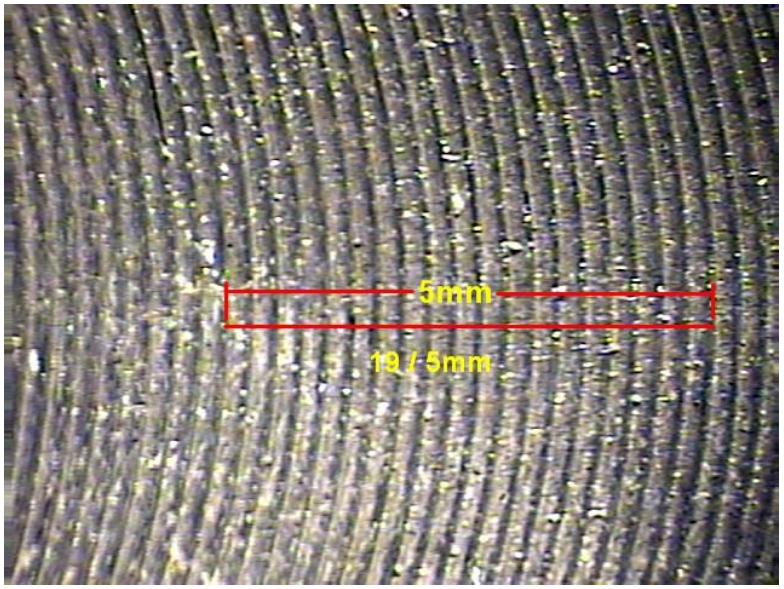

Figure 2.6: Banded structure of a friction stir welded Ti-6Al-4V sample, showing a band width about 0.23mm

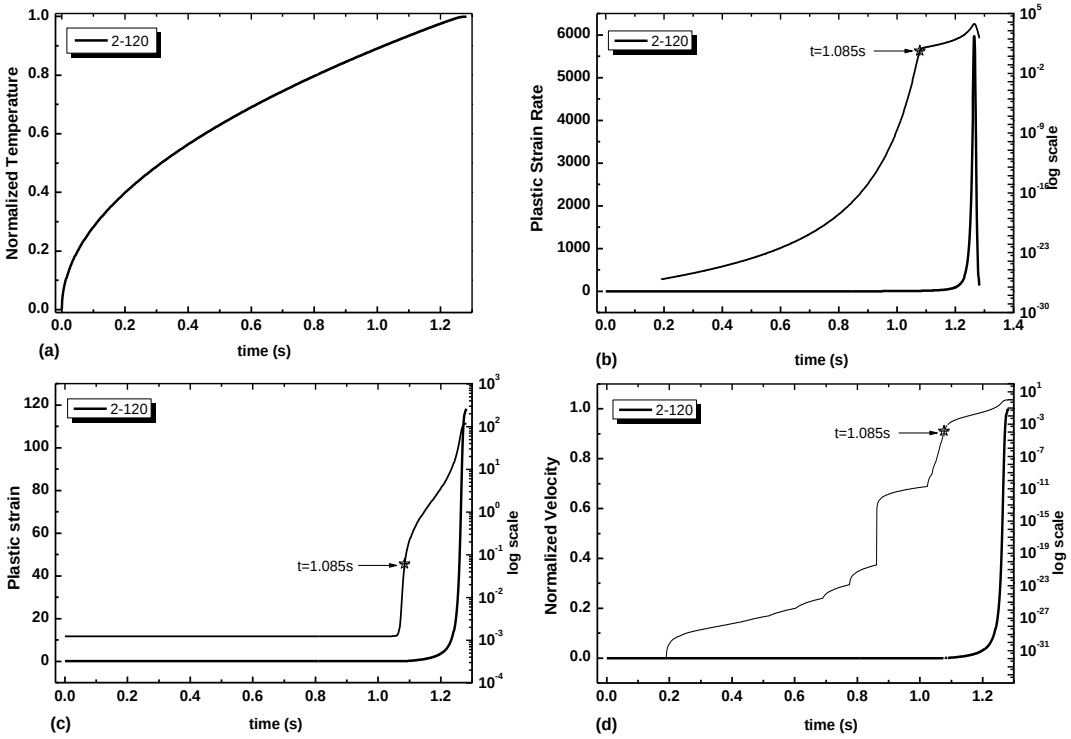

Figure 2.7: Time-history plots at interface ($y = 1$) for Weld 2-120 using both linear (thin lines) and log scale (thick lines): (a) Normalized temperature rise, (b) Plastic strain rate, (c) Shear strain, and (d) Velocity.

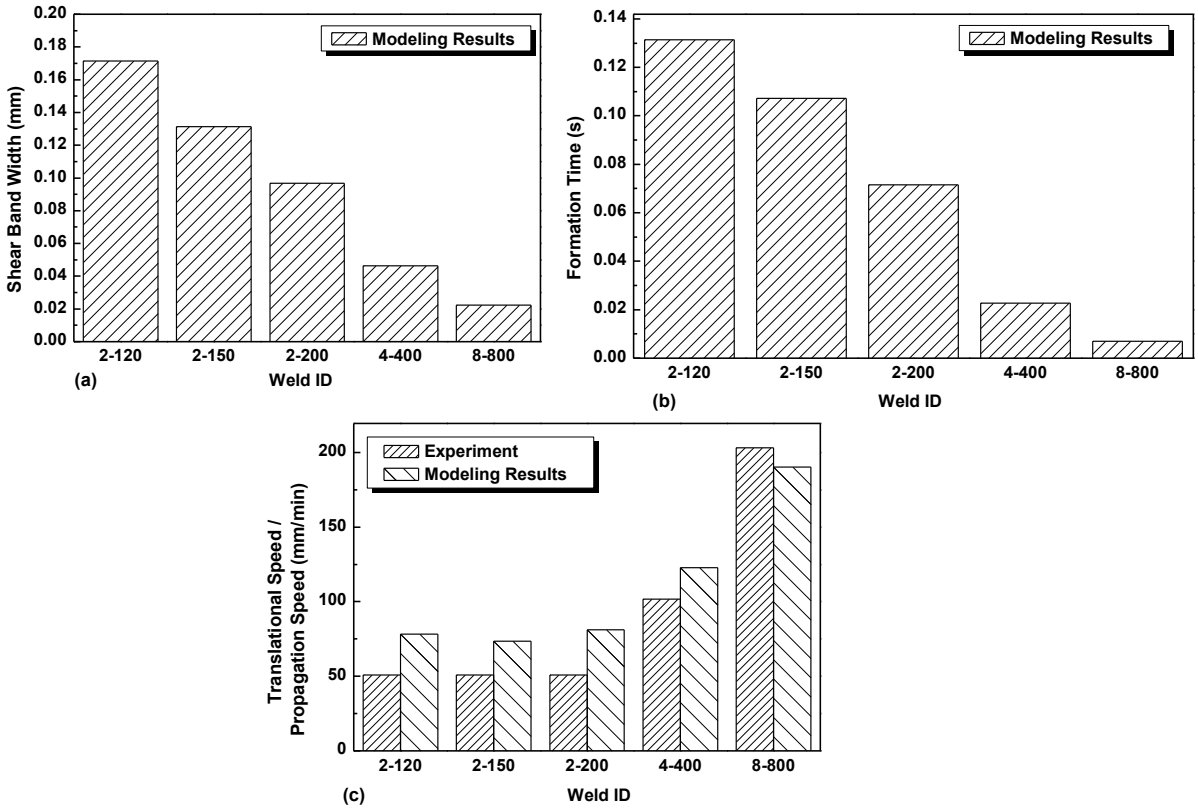

Figure 2.8: Comparison of predicted shear band width and formation time for five welding conditions in Table 1 and shear band propagation speed and applied welding speed. (a) Shear band width, (b) shear band initiation time, (c) shear band propagation speed and comparison with pin translational speed given from experiment.

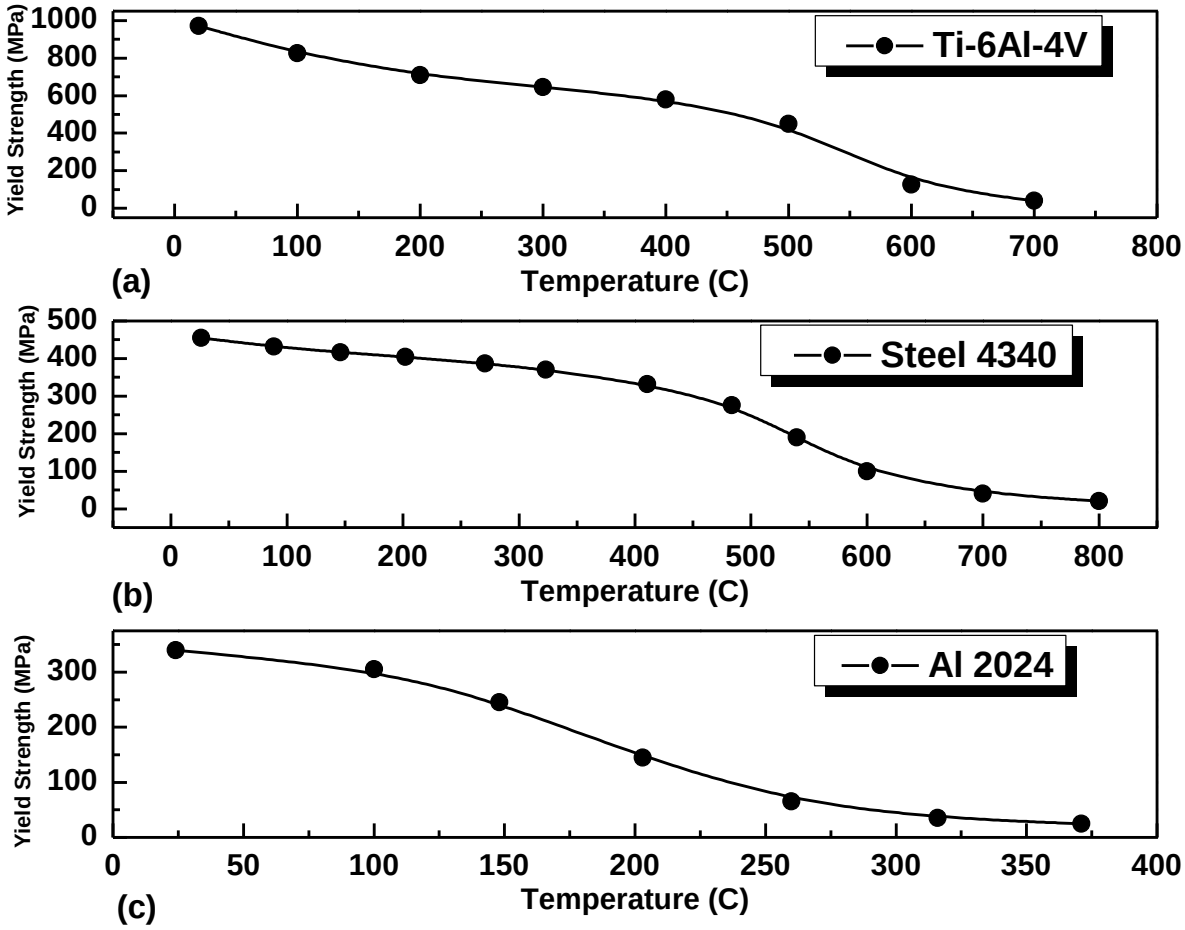

Figure 2.9: Yield strength as a function of temperature of (a) Ti-6Al-4V, (b) Steel 4340, and (c) Al2024.

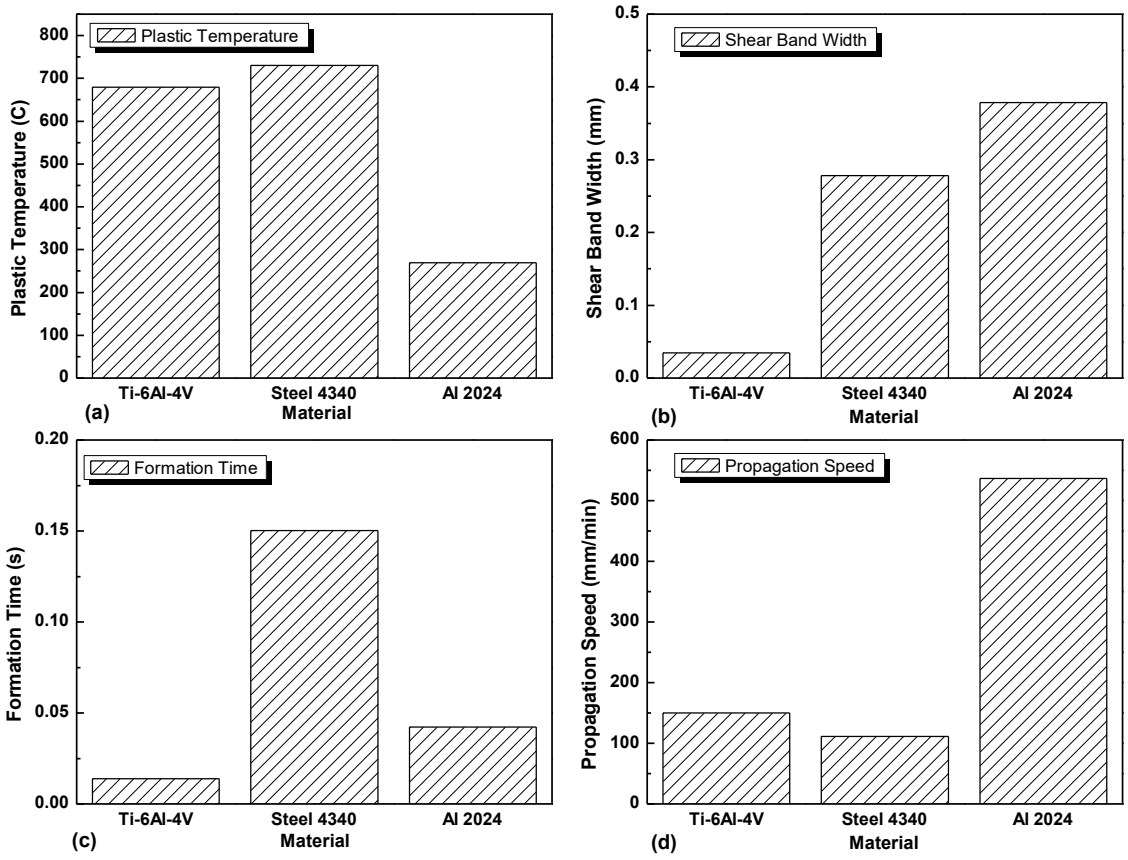

Figure 2.10: Weld penetration effect on ETS: (a) weld throat ETS at θ_c; (b) weld toe ETS

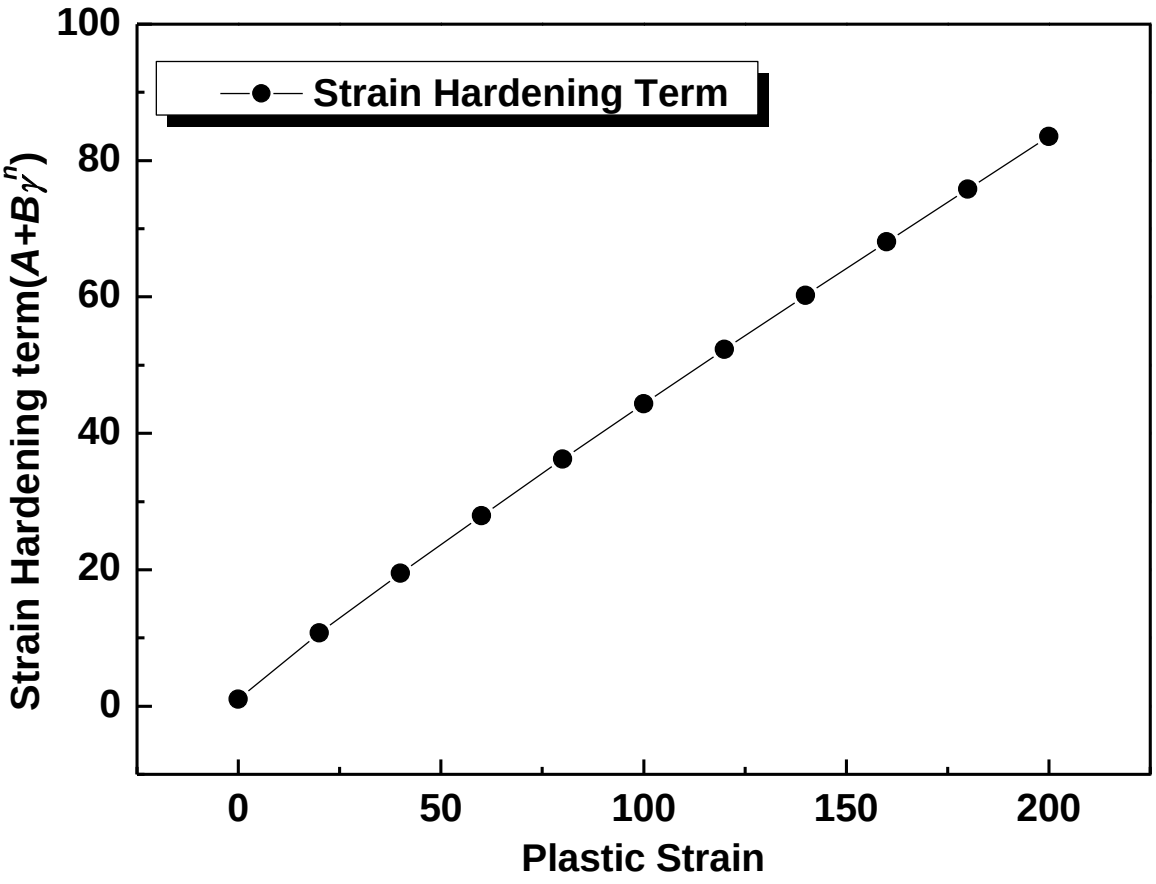

Figure 2.11: Dependency of strain hardening term

Acknowledgment

The authors acknowledge the support of this work in part by ONR Grant No. N00014-10-1-0479 at UNO and the National Research Foundation of Korea (NRF) Gant funded by the Korea government (MEST) through GCRC-SOP at University of Michigan under Project 2-1: Reliability and Strength Assessment of Core Parts and Material System.

References

[1] C. Dawes and W. Thomas, 'Friction stir joining of aluminum alloys', TWI Bulletin (6), Cambridge, United Kingdom, November/December 1995

[2] R. Nandan, T. DebRoy and H. K. D. H. Bhadeshia: 'Recent Advances in Friction Stir Welding – Process, Weldment Structure and Properties', Prog. Mater. Sci., 2008, **53,** 980-1023

[3] A.C. Nunes, 'Prolegomena to the Study of Friction Stir Welding' Proceedings of Materials Science & Technology 2010 – Joining of Advanced and Specialty Materials XII, Houston, TX, Novermber 2010.

[4] J.A. Schneider and A.C. Nunes Jr., 'Characterization of plastic flow and resulting microtextures in a friction stir weld,' Metall. Mater. Trans. B., 2004, 35, **4**, 777-783

[5] B. Yang, J. Yan, M.A. Sutton, and A.P. Reynolds, 'Banded microstructure in AA2024-T351 and AA2524-T351 aluminum friction stir welds, Part I. Metallurgical studies,' Mat. Sci. Eng. A-Struct, 2004, **364**, 55–65

[6] K.E. Knipling* and R.W. Fonda, 'Texture development in the stir zone of near-a titanium friction stir welds,' Scripta Mater., 2009, **60**, 1097–1100

[7] A.L. Pilchak, W. Tang, H. Sahiner, A.P. Reynolds, and J.C. Williams, 'Microstructure Evolution during Friction Stir Welding of Mill-Annealed Ti-6Al-4V', Metall. Mater. Trans. A., Mar. 2011, **42**,(3), 745-762.

[8] P. Dong, F. Lu, J.K. Hong, and Z. Cao, 'Coupled thermomechanical analysis of friction-stir welding process using simplified models,' . Sci. Technol. Weld. Joi., 2001, **6**, (5), 281-287.
[9] H. Schmidt, J. Hattel, and Wert. John. 'An analytical model for the heat generation in friction stir welding.' Model. Simul. Mater. Sc., 2004,**12**, (1), 143-157.
[10] T. U. Seidel and A. P. Reynolds. 'Two-dimensional friction stir welding process model based on fluid mechanics.' Sci. Technol. Weld. Joi., 2003, **8**, (3), 175-183.
[11] P. A. Colegrove and H. R. Shercliff. '3-Dimensional CFD modelling of flow round a threaded friction stir welding tool profile.' J. Mater. Process. Tech., 2005, **169**, (2), 320-327.
[12] R. Nandan, G. G. Roy and T. DebRoy, 'Numerical Simulation of Three-Dimensional Heat Transfer and Plastic Flow During Friction Stir Welding', Metal. Mater. Trans. A, 2006, **37**, (4), 1247-1259
[13] R. W. Fonda, J. F. Bingert, and K. J. Colligan. 'Development of grain structure during friction stir welding.' Scripta Mater. 2004, **51**, (3), 243-248.
[14] R. C. Batra, and Z. G. Wei. 'Shear bands due to heat flux prescribed at boundaries.' Int. J. Plasticity, 2006, **22**, (1), 1-15.
[15] Federal Aviation Administration (FAA) Office of Aviation Research Report, 'Experimental Investigations of Material Models for Ti-6Al-4V Titanium and 2024-T3 Aluminum', Washington, D.C. 20591
[16] G. R. Johnson, and W. H. Cook. 'A constitutive model and data for metals subjected to large strains, high strain rates and high temperatures.' Proceedings of the 7th International Symposium on Ballistics. Vol. 21. The Hague, Netherlands: International Ballistics Committee, 1983.
[17] X. Pei and P. Dong, 'A shear localization modeling of banded structure formation in friction stir welding' in preparation
[18] Guide, MATLAB User'S. 'The mathworks.' Inc., Natick, MA 5 (1998).
[19] R. D. Skeel, and M. Berzins, 'A method for the spatial discretization of parabolic equations in one space variable.', SIAM J. Sci. Stat. Comp., 1990,**11**,(1), 1-32.
[20] H. J. McQueen, and N. D. Ryan. 'Constitutive analysis in hot working.' Mater. Sci. Eng. A , 2002, 322, (1), 43-63.Turlier, Didier, Patrice Klein, and Florent Bérard. "FEA shell element model for enhanced structural stress analysis of seam welds." Welding in the World 58.4 (2014): 511-528.

Chapter 3

Modeling of Banded Structure in Friction Stir Weld in Strain Rate Hardening Materials of Sellars-Tegart Type

Abstract

This paper presents a shear localization model for simulating the shear band formation process uniquely associated with friction stir welding. By introducing a thermal and plastic deformation boundary layer definition, the shear band formation process can be modeled as shear localization phenomena using one dimensional coupled elastic viscoplastic model. Material constitutive behavior is assumed to follow Sellars-Tegart constitutive equation. With this model, shear band width, formation time, and propagation speed can be theoretically estimated as a measure of friction stir weldability. As such, the shear band propagation speed serves as a theoretical estimate of the maximum possible welding speed under given base material and welding conditions, such as stir pin rotational speed and torque level. The model is shown to provide reasonable estimates of shear localization parameters when compared with recent experimental data on titanium alloy Ti-6Al-4V. With this model, some fundamental questions such as why titanium alloys are more difficult to weld than aluminum alloys or steels, can be more quantitatively addressed. And consequently, potential means for mitigating some of the difficulties in friction stir welding of some of the alloys can be

theoretically examined to provide guidance for cost-effective development of welding process parameters for new applications.

Introduction

Friction stir welding (FSW) is a relatively new solid-state joining process, as first reported by Dawes and Thomas[1] and has many advantages over traditional welding processes as recently reviewed by Nandan et al.[2]. It can be used either to join advanced high strength materials deemed not weldable with traditional fusion welding processes or modify material surface conditions for improving fracture and fatigue resistance of a structure, as discussed by Nandan et al. [2] and Nunes [3]. Recognizing the needs for an improved understanding of weld formation process associated with friction stir welding, there have been numerous investigations into various aspects of friction stir welding process over the last decade or so, which resulted in numerous important findings as recently reviewed by Nandan et al. [2], spanning from heat generation mechanisms and material flow characteristics, to weld quality definitions and resulting fatigue/fracture properties. Among some of the important findings, one that is particularly of interest to this study is that plastic deformation phenomenon in the form of shear banding seems to govern weld development process, as shown experimentally by Schneider and Nunes [4], and Yang et al. [5] for high strength aluminum alloys, by Knipling and Fonda [6] and Pilchak et al. [7] for titanium alloys. Krishnan [8] investigated the formation of the banded structure in FSW of aluminum alloy AA6061, and suggested that FSW should be treated as an extrusion process. Aukrust and Lazghab [9] further found that during

extrusion of aluminum alloy AA6082 in a channel at a deformation rate of 0.175 m/s, most of the deformation occurred in a very localized material layer of 250 μm in width adjacent to the die wall, which is about in the same order of magnitude as the spacing of banded deformation typically observed in friction stir welds.

Recognizing this important finding, Nunes's first principle based model [3] by treating plastic deformation process associated with friction stir welding as a rigid plug surrounded by material that behaves as a rigid perfectly plastic solid, seems to yield rather insightful results, given his model's remarkable simplicity. However, Nunes' model [3] took shear band parameters such as band width a known priori as a part of rigid plug definition and cannot be used to establish how such a shear band is formed under given material and welding conditions.

In an attempt to directly relate the localized plastic deformation characteristics discussed in [3-6] to weld formation process, the authors recently presented a rather different approach to friction stir weld modeling by specifically focusing upon the mechanics of the shear band (SB) formation process, as illustrated in Figure 3.1. The shear localization model was based on a coupled thermo-elastic and visco-plastic formulation by idealizing the shear band formation process into a one dimensional (1D) shear localization problem similar to that examined by Batra and Wei [11], but with different definitions of boundary and initial conditions relevant to friction stir welding phenomena. With this approach, the authors were able to demonstrate rather promising results in terms of theoretically estimated shear band width and shear band propagation speed in comparison with experimental data (see Pei and Dong [12]). However, their study also revealed that the use of Johnson Cook constitutive law as a descriptor of

material strain rate hardening behavior shows one major limitation in that the predicted temperature at workpiece and pin interface reaches to material melting temperature upon shear localization regardless of welding conditions, which contradicts available experiment data and engineering intuition. As concluded by the same authors earlier, the work hardening part of material behavior tends to be grossly over-estimated in Johnson-Cook material model, resulting in the attainment of melting temperature, only at which point the thermal softening term becomes dominant. Liang and Khan [13] also discussed such a deficiency in Johnson Cook model, stating that it is not appropriate for the work hardening term to remain dominant with an increasing plastic strain in hot forming regime.

In this paper, we examine the shear band formation process associated with friction stir welding by incorporating a Sellars-Tegart type constitutive material model[14]. In view of the order of magnitude of strain, strain rate and temperature involved in friction stir welding as discussed in Pilchak [7], a constitutive model of Sellars-Tegart type should provide a more realistic description of material behavior than Johnson Cook type. The former is broadly adopted for hot forming applications as described by Puchi-Cabrera et al. [15] while the latter tends to be used for high strain rate applications such as ballistic penetration problems as demonstrated by Wei and Batra [11]. Kuykendall et al. also concluded that Johnson-Cook constitutive equation becomes invalid at high strain and strain rate since material flow stress tends to increase without a bound before reaching to melting temperature [16].

Within this context, FSW experiments by Pilchak et al. [7] are first analyzed using the fully-coupled elastic visco-plastic shear localization model. In addition to

validating the model developed in this study, the experimental data provide a realistic context for demonstrating how shear localization modeling results can be related to actual welding experiments in terms of a time scale that governs the formation of a shear band and length scale that characterizes shear band width. Together, these two parameters provide a theoretical estimate of the shear band propagation speed i.e. the maximum possible welding speed while maintaining a consistent friction stir weld quality. Finally, shear band formation characteristics in three fundamentally different base metals (e.g., aluminum, steel, and titanium) are examined to gain theoretical insights on their friction stir weldability. In addition, effective means, such as pre-heating or auxiliary spot heating, are explored for achieving a significant increase in welding travel speed in friction stir welding of titanium alloys for shipbuilding applications, as recently discussed by Dong et al. [17].

Shear Localization Model

3.1.1 Model definition

As shown in Figure 3.1, a localized deformation process in band forms can be seen around the stir spin. The formation of such a band structure has been attributed to three dimensional material flow around stir pin and investigated by numerous researchers [2-6]. Although the deformation characteristics are noticeably different between the advancing and retreating sides, the band spacing along the welding direction can be, in an averaged sense, related to the tool advance during each pin revolution, as observed by researchers such as Dong et al. [18], Nunes [3], and Fonda et al. [10]. The material outside of the band (both in the front and on the side of pin) remains essentially

stationary. As discussed in Pei and Dong [12], such a localized deformation process, to the first approximation, can be idealized as a shear localization phenomenon for establishing the conditions under which a shear band forms. At a peak strain rate of an order of $10^3 \sim 10^4$/sec at workpiece and pin surface, the associated heat transport process resulted from friction heating and plastic dissipation from the shear band to its surrounding material can be approximated as a 1D coupled heat transfer and elastic visco-plastic deformation problem in y (see Figure 3.2), with a domain length of H. Then, the analysis domain length parameter H for such a thermal boundary layer problem can be determined by 1D transient heat conduction characteristic length with respect to a reference time scale as discussed in the next section. Beyond H, an adiabatic condition can be assumed.

In Figure 3.2, stir pin rotates at a constant speed V_{pin} while exerting a shear stress (frictional stress) $\bar{\tau} = \bar{f}$ in contact with the workpiece (or base metal). The resulting frictional heat flux $\bar{q} = \bar{f}\left(V_{pin} - V_W\right)$ is assumed to be fully consumed by the workpiece for simplicity here. As frictional heat builds up at the workpiece and pin interface, material softening occurs, resulting in rapid development of plastic strain in a narrow region at the interface. As soon as the relative velocity, i.e., $V_{pin} - V_W$ approaches zero (i.e., sticking conditions), a fully developed shear band is considered to be realized within the context of plastic instability in continuum mechanics. The corresponding shear band width is denoted as W_{SB} and time required in realizing W_{SB} as T_{SB}. Then, the resulting shear band propagation speed can be estimated as:

$$V_P = \frac{W_{SB}}{T_{SB}} \tag{3.1}$$

which can be interpreted as the theoretically maximum possible welding speed that we set out to investigate as one of the important FSW process parameters in practice.

3.1.2 Governing equations

Consider the domain that occupies $0 \le \bar{y} \le H$ in Figure 3.2, which is subjected to applied frictional stress $\bar{f}$ and friction induced heat flux $\bar{q} = \bar{f}(V_{pin} - V_W)$ at the workpiece and pin interface $\bar{y} = H$. Let the spatial coordinate ($\bar{y}$) be normalized by domain size H, the shear stress by material shear strength τ_0, time by H / V_{Pin} and temperature by material reference temperature θ_0. In terms of non-dimensional variables, the domain now occupies the region is bounded by planes at $y = 0$ and $y = 1$. Henceforth, unless otherwise specified, non-dimensional variables will be used for formulating governing equations. Initially, material behaves elastically with a rising temperature caused by frictional heating and associated conduction transfer. However, as material yield strength starts to decrease upon further increasing in temperature, plastic deformation begins to develop. The governing equations for the thermo-elastic visco-plastic problem can be written as follows:

$$\rho \dot{\upsilon} = \tau_{,y} \tag{3.2}$$

$$\dot{\theta} = \lambda \theta_{,yy} + \tau \dot{\gamma}_p \tag{3.3}$$

$$\dot{\gamma} = v_{,y} = \dot{\gamma}_e + \dot{\gamma}_p \tag{3.4}$$

$$\dot{\tau} = \mu \dot{\gamma}_e \tag{3.5}$$

$$\dot{\gamma}_p = \begin{cases} 0 & \left(\theta < \theta_p\right) \\ A\left[\sinh\left(\dfrac{\tau}{\tau_R}\right)\right]^n \exp\left(-\dfrac{Q}{R\theta}\right) & \left(\theta \geq \theta_p\right) \end{cases} \tag{3.6}$$

Here, a superimposed dot on a variable signifies its derivative with respect to time; a comma followed by y indicates the partial differentiation with respect to spatial coordinate y. In above equations, ρ is the mass density, v the velocity, τ the shear stress, θ the temperature, γ the shear strain which is partitioned into elastic part γ_e and plastic part γ_p. Furthermore, μ is the shear modulus and λ the thermal diffusivity of material. Eq.(3.2) expresses the balance of momentum. Eq.(3.3) represents internal energy balance, in which plastic dissipation energy, represented by the second term on the right hand side, is assumed to be fully converted into heating. Eq.(3.4) and Eq. (3.5) state, respectively, strain rate partitioning into elastic and plastic parts, and the Hooke's law in rate form. Eq.(3.6) is the constitutive equation according to Sellars-Tegart, where θ_p is the temperature at which material yield strength equals to applied stress. Parameters A , τ_R, and n are material constants. Additionally, Q is the activation energy and R is gas constant. All other material parameters are assumed to be independent of temperature.

Note that with the above formulation, one single shear band formation event corresponding to one revolution of pin rotation out of a time continuum in which friction stir weld forms through the development of successive shear bands (see Figure 3.1).

Therefore, the boundary layer model in Figure 3.2 should be interpreted as one shear band formation event in both time and space continuums. As a result, a constant shear stress (f) should be applied at $t = 0$ and at $y \in (0,1)$ due to equilibrium considerations. Given the adiabatic assumption for each individual shear localization event, initial temperature within the boundary layer domain can be assumed to be room temperature θ_r. Based on the above considerations, the initial conditions at $t = 0$ are described as follows:

$$v(y,0) = 0, \quad \theta(y,0) = \theta_r, \quad \gamma(y,0) = f / \mu, \quad \tau(y,0) = f, \quad \gamma_p(y,0) = 0 \tag{3.7}$$

The boundary conditions are given as:

$$-\lambda \theta_{,y}(1,t) = q(t) = f(V_{pin} - V_W), \quad \tau(1,t) = f, \quad -\lambda \theta_{,y}(0,t) = 0, \quad v(0,t) = 0 \tag{3.8}$$

Note that in Eq.(3.6), τ / τ_R and $Q/(R\theta)$ are dimensionless. Other dimensionless parameters are related to their dimensional (barred) counterparts as follows:

$$\begin{aligned} &y = \bar{y} / H, \; t = \bar{t}\,\dot{\gamma}_0, \; \theta = \bar{\theta} / \theta_0, \; \lambda = \bar{k} / \left(\bar{\rho}\bar{c}\dot{\gamma}_0 H^2\right), \; \rho = \bar{\rho} H^2 \dot{\gamma}_0^{\,2} / \tau_0, \\ &q = \bar{q} / \left(\dot{\gamma}_0 H \tau_0\right), \theta_0 = \tau_0 / \left(\bar{\rho}\bar{c}\right), \dot{\gamma}_0 = H / V_{Pin} \end{aligned} \tag{3.9}$$

where τ_0 is the yield strength of material at room temperature, $\bar{c}$ the specific heat, $\bar{k}$ the thermal conductivity and $\dot{\gamma}_0 = V_{pin} / H$ is the nominal strain rate.

3.1.3 Numerical implementation

The shear localization problem described by Eq.(3.2) through Eq.(3.6) can be conveniently solved numerically by implementing a finite element procedure using MATLAB [19]. A MATLAB based parametric programming code was developed using a weak form of the governing equations (Eq.(3.2) -(3.6)), initial conditions and boundary

conditions (Eqs. (3.7)-(3.8)), derived by a piecewise nonlinear Galerking/Petrov-Galerkin method. This discretization method offers a good accuracy to the second order in space as illustrated by Skeel and Berzins [20]. The result is a system of coupled non-linear ordinary differential equations which are integrated by using MATLAB function "*ode15s"*. Note that the selection of "*ode15s*" solver instead of other ODE solvers available in MATLAB is because it is better suited in dealing with the coupled dependency among temperature, strain, strain rate and velocity over a time increment.

An adaptive time increment method is used to iteratively compute incremental solutions until convergence criteria are satisfied. To examine the effects of convergence criterion settings on solution accuracy, a set of default solution tolerance criteria were first adopted, which are "*Reltol"=10*$^{-3}$*, "Abstol" = 10*$^{-6}$, where *Reltol* and *Abstol* control the relative and absolute tolerances, respectively. Then , "*Reltol"=10*$^{-4}$ *and "Abstol" = 10*$^{-7}$ were introduced. The results from both solutions show no noticeable differences, indicating a converged solution can be achieved with either tolerance setting. The modeling procedure developed here provides a full solution over time from $t = 0$ to a time when material at workpiece and pin interface reaches to a prescribed pin surface linear velocity, i.e., $v(1,t) = 1$. The corresponding shear band of width W_{SB} in Eq.(3.1) is considered being fully developed. The time elapsed becomes shear band formation time, i.e., T_{SB} in Eq.(3.1).

The coordinates of linear elements in *y* axis is given by:

$$y_n = 1 - \left(\frac{301 - n}{300} \right)^4, \quad n = 1, 2, \ldots 301. \tag{3.10}$$

which provides a significant element refinement at the workpiece and pin interface, i.e., $y = 1$ for providing a sufficient spatial resolution for shear localization development, as demonstrated for similar problems solved by Batra and Wei [11].

Model Validation

In this section, the above shear localization modeling procedure will be applied to simulate the friction stir welding experiments reported by Pilchak et al. [7] not only for model validation purpose, but also for demonstrating how shear localization model input parameters and final results can be related to FSW process parameters and experimental results.

3.1.4 Experiments and model set up

Five mill-annealed Ti-6Al-4V plate specimens [7] were friction stir welded with acceptable quality by using different sets of welding parameters developed based on prior experiences (see Table 3-1). Temperature measurement data were also collected at two locations of stir pin (see Figure 3.3). Based on the welding parameters given in Table 3-1, the derived parameters required by the current shear localization model are: (1) time domain $t_c = 1/\omega$, where ω is the angular velocity of the pin rotation; (2) space domain $H = 5H_c$, where $H_c = 2\sqrt{\bar{\alpha} t_c}$ is a characteristic thermal diffusion length with respect to reference time t_c, and $\bar{\alpha}$ is thermal diffusivity of material; (3) friction stress $\bar{f} = T/(2\pi r_p{}^2 h)$, where r_p and h are radius and height of stir pin, respectively. Note that a factor of 5 in defining the space domain $H = 5H_c$ is used here to ensure that the

thermal boundary layer problem in Figure 3.2 is fully realized, i.e. attaining a semi-infinite body condition.

3.1.5 Modeling results

By considering a weld specimen and its welding conditions in Table 3-1, such as "Weld ID 2-120", the predicted spatial distributions of non-dimensional temperature, plastic strain, plastic strain rate, and material flow velocity are shown in Figure 3.4 at different time increments. Note that predicted temperature rise (i.e. $\theta - \theta_r$) is normalized by melting temperature (i.e. $\theta_t - \theta_r$), and material flow velocity by stir pin rotational linear velocity V_{pin}. The simulation ends when material flow velocity attains the prescribed stir pin velocity, that is, $V_{pin} - V_W = 0$.

As shown in Figure 3.4a, before time reaches to $t \approx 0.19\,s$, temperature at workpiece and pin interface is not high enough to reduce material shear strength which is still above the applied frictional stress. As a result, plastic strain, plastic strain rate, and material flow velocity are not noticeable. As temperature at and near workpiece and pin interface rapidly increases over time as a result of frictional heating, thermal softening term in Eq. (3.6) begins to take effect. As shown in Figure 3.4b, plastic strain rate begins to develop at $t \approx 0.28\,s$ near the workpiece and pin interface, which leads to the development of both localized plastic strain and flow velocity. With a continued rising in temperature, plastic strain rate, plastic strain and material flow velocity increase rapidly at and near workpiece and pin interface. At this stage, two distinct deformation zones can be identified: a region dominated by elastic deformation and a region dominated by

plastic deformation, as clearly shown in Figure 3.5 in terms of spatial distributions of plastic strain and material flow velocity at different times in logarithmic scale. It can be seen that as time increases, the plastic deformation region increases in size as temperature increases. More importantly, the spatial distribution of material flow velocity in Figure 3.5b clearly indicates the presence of discontinuity in velocity field, which is consistent with shear localization phenomenon. The material region to the right of the discontinuity forms a shear band of interest in this study, which continues to increase in size over time. This region can also be characterized as a material zone subjected to a significant level of plastic deformation as shown in Figure 3.5a.

The modeling results corresponding to five different welding conditions in Table 1 are compared in Figure 3.6. Unlike the results obtained with Johnson Cook material model in Pei and Dong [12], the predicted final temperature distributions for the five different welding conditions are significantly different from one another, as shown in Figure 3.6a. The predicted peak temperatures at workpiece and pin interface (indicated by solid square symbols) for the five weld conditions are compared in Figure 3.7 with those measured using thermocouples as documented by Pilchak, et al. [7] as a function of stir pin rotational speed. It should be noted that the measured temperatures were collected from thermocouples at about 6mm ("T1") and 10mm ("T2") away from the nearest workpiece and pin interface and therefore are expected to be consistently lower than those predicted using the current shear localization model. Nonetheless, the agreement in trend between the measured and predicted temperatures, particularly as function of pin rotation speed, is considered reasonable. In addition to a higher temperature seen at workpiece and pin interface, an increase in pin rotational speed (e.g.,

from 400 RPM for Weld ID 4-400 to 800 RPM for Weld ID 8-800 in Figure 3.6b results in a more severe plastic deformation as a result of a significantly higher strain rate.

3.1.5.1 Shear band width

In order to verify the generality of the observations discussed above with respect to Figure 3.5 corresponding to one set of welding parameters given in Table 3-1, the predicted final spatial distributions of plastic strain and material flow velocity for all five welding conditions are compared in Figure 3.8. Consistent with Figure 3.5, there exists a distinct demarcation position in space associated with each set of the five welding conditions given in Table 3-1, which signifies the presence of discontinuity in both velocity and plastic strain fields. A shear band width (W_{SB}) can be clearly identified as a region between the discontinuity position to the workpiece and pin interface. It should be noted such a shear band definition is consistent with plasticity instability theory, in which a shear band is defined as a narrow region of intense plastic deformation with distinct material flow characteristics.

3.1.5.2 Shear Band formation time

To elucidate how a shear band (SB) develops with time, we plot time history results of temperature rise, plastic strain rate, plastic strain, flow velocity at workpiece and pin interface corresponding to Weld ID 2-120, as shown in Figure 3.9. The temperature increases as a function of time in a parabolic manner because the relative speed at the interface between base material and pin decreases, resulting in decrease in frictional heat generation. At the beginning, the entire domain behaves elastically and

material flow velocity is negligible, which can be clearly seen in a logarithmic scale in Figure 3.10. As time reaches to $t \approx 0.19\,s$, a rapid increase in both material flow velocity and plastic strain can be clearly seen. Therefore, the time lapse from this point on, i.e., $t \approx 0.19\,s$ until the shear band width is fully formed (i.e. when $V_W = V_{pin}$) defines the shear band formation time (T_{SB}).

3.1.5.3 Welding Speed Estimation

With the shear band width (W_{SB}) and its formation time (T_{SB}) being estimated as discussed above, shear band propagation speed, or maximum possible welding speed can now be calculated through Eq.(3.1). The results are summarized in Figures 3.11a and 3.11b. Generally speaking, a wider shear band needs more time to complete. The estimated maximum possible FSW welding speeds using Sellars-Tegart constitutive law and that using Johnson-Cook law as well as experimental welding speeds (see Table 3-1) are compared in Figure 3.11c. It can be seen that Sellars-Tegart type of constitutive material model tends to predict a higher maximum travel speed than Johnson-Cook model. The predicted maximum possible welding speeds are higher than those used in experiments, which seems reasonable since Eq. (3.1) gives the maximum welding speed that is theoretically possible for a given material and associated welding conditions, while welding speeds used in these experiments were based on typical trial-and-error processes and are not necessarily at the maximum welding speed possible under a given combination of welding parameters used.

As a specific example, the predicted shear band width for Weld ID 8-800 [7] can

be compared with a shear band width inferred from a backscattered electron image of the same weld sample given in Pilchak [7]. The theoretically calculated shear band width is at 0.52mm which is somewhat larger than 0.4mm inferred from the image in Figure 3.12. The comparison is considered rather reasonable, given some of the uncertainties involved in the material model used (e.g., temperature-independent properties) and the idealized nature of the 1D shear localization model shown in Figure 3.2

Discussions

As shown in the previous section, the shear localization model developed here provides a reasonable estimate of theoretical maximum welding speed. Furthermore, the computed temperature and shear band width agree reasonably well with measured data. In this section, the application of this model in understanding friction stir weld formation process will be demonstrated by considering additional material type, such as aluminum alloy 2024, high strength low alloy steel (HLAS) 4340. A few auxiliary heating concepts will also be examined for exploring means for achieving maximizing welding speeds in order to be viable for shipbuilding industry [17].

3.1.6 Base material effects

Thus far, all modeling results reported in the previous section have been titanium alloy Ti-6Al-4V. In this section, two more base materials are considered: high strength low-alloy steel 4340 and high strength aluminum alloys Al 2024 on which Sellars-Tegarts based material properties are available from Tello et al. [20], as given in Table 3-2. In addition, yield strength as a function of temperature for each material is also given

in Figure 3.13, taken from Gale et al. [22]. From Eq.(3.6), it can be inferred that material activation energy Q reflects the thermal-softening ability of the material, i.e., a higher Q value suggests that a material is more difficult to become thermal-softened. This usually leads to a longer shear band formation time. While material constant A is a measure of strain rate hardening resistance. A lower value in A implies that a material possess a weaker hardenability as a function of strain rate induced by pin rotation and leads to a more localized shear deformation, exhibiting a narrow shear band.

In Table 3-2, it can be seen that Ti-6Al-4V has both the lowest conductivity $\bar{c}$ and the rate related material constant A, which implies that its shear deformation should be most localized. Steel 4340 has the highest activation energy Q and would need the longest time for temperature to become high enough in order to soften the material. The rate related constant A for Steel 4340 is much higher than that for Ti-6Al-4V and is less sensitive to localized strain rate than Ti-6Al-4V. The resulting shear band width in Steel 4340 should be wider than that in Ti-6-4V. As for Al 2024, its low activation energy Q, high strain rate resistance A, and high thermal conductivity suggests that Al2024 should have the widest shear band and shortest shear band formation time among the three materials.

To facilitate the comparison of modeling results, all calculations for the three materials are performed under the same frictional stress (f = 60MPa) and rotational speeds (500 RPM), resulting in the same heat flux (1.571×10^7 (W/m^2)). The results are summarized in Figure 3.14 in which the modeling results obtained using Johnson-Cook constitutive model [12] are also included for comparison purpose. It is interesting to note

that as far as shear band propagation speeds are concerned, the results show a close agreement between the two rather different material constitutive models than one would have expected. It can be seen that Al 2024 develops the widest shear band while Ti-6Al-4V the narrowest. As for the shear band formation time, the shear localization model predicts that Steel 4340 takes the longest time for shear band to form and complete (i.e. longest "formation time" in Figure 3.16) and that Al 2024 takes the shortest time. In summary, the predicted maximum welding speed is the highest for Al 2024 among all three materials investigated. The predicated welding speeds of both Steel 4340 and Ti-6Al-4V are in a close range with Steel 4340 being slightly lower. It is worth noting that the narrowest shear band width is predicted for Ti-6Al-4V, which suggests that Ti-6Al-4V should have the poorest FSW weldability, i.e., sensitive to pin translational speed and its variation. The widest shear band width is predicted for Al 2024, which is consistent with the fact that aluminum alloys are highly weldable with FSW.

3.1.7 Auxiliary heating effect

It is known that Ti-6Al-4V is difficult to weld with friction stir welding process, as further demonstrated quantitatively in the previous section. By intuition, any auxiliary heating in addition to friction heating at workpiece and pin interface could improve FSW weldability, as discussed in some recent publications [23-25]. The present shear localization model can be used to quantitatively assess how such an auxiliary heating method would improve a material's FSW weldablity in terms of shear localization parameters such as shear band width, shear band formation time, and the resulting welding speed. The following section considers two auxiliary heating methods: one is by

means of an auxiliary heat flux input at workpiece and pin interface; the other is through a pre-heating process so that a target temperature level can be achieved in weld area before friction stir welding takes place.

3.1.7.1 Auxiliary heat flux

By considering an auxiliary heat source being placed at workpiece and pin interface in the form of heat flux of a varying degree of intensity, Figure 3.15 plots the predicted shear band width, shear band formation time and shear band propagation speed as a function of auxiliary heating intensity (i.e., heat flux). It can be clearly seen that the presence of an auxiliary heat source, while reducing shear band width, shortens the shear band formation time, leading to essentially a linear increase in shear band propagation speed that is approximately proportional to auxiliary heat flux (see Figure 3.15c).

3.1.7.2 Pre-Heating

If a base material is initially heated in a more uniform manner within weld area to a prescribed temperature level prior to welding, the corresponding shear localization process is expected to be different from that shown in Figure 3.15 in which auxiliary heating is placed right at workpiece and pin interface. As shown in Figure 3.15a, local heating through auxiliary heat flux applied at workpiece and pin interface reduces shear band width. A more uniform pre-heating should potentially result in an increased shear band width, leading to an improved weldability. Indeed, this is the case, as shown in Figure 3.16 in which shear band width increases with pre-heating temperature level (see Figure 3.16a). A more rapid increase in shear band width above a pre-heating

temperature of about 300C (see Figure 3.16a) seems to suggest that there exists a threshold temperature level for a given material, beyond which a more drastic gain in shear band width can be obtained. Shear band formation time linearly decreases with increasing pre-heating temperature (see Figure 3.16b). The resulting welding speed is approximately proportional to shear band width (Figure 3.16a) and increases more drastically than using auxiliary heat flux at workpiece and pin interface.

Conclusions

A shear localization model incorporating Sellars Tegart constitutive equation is presented for simulating shear band formation process uniquely associated with friction stir welding processes. Comparing with experimental data on Ti-6Al-4V alloy, the model provides a reasonable estimation of shear localization parameters in terms of shear band width, shear band formation time, and shear band propagation speed. The shear band propagation speed serves as a theoretical estimate of the maximum possible welding speed for a given material to be welded under a set of specified stir pin rotational and translational speed.

With this shear localization model, parametric analyses on three different alloys, i.e., aluminum alloy Al 2024, HSLA steel 4340, titanium alloy Ti-6Al-4V have been performed to examine how shear localization parameters introduced here in this paper can be used to quantitatively rank their friction stir weldability. Furthermore, local auxiliary heating and uniform pre-heating as potential means of improving their weldablity, such as significantly improving welding speed, are also examined. Some of key findings are:

1) The predicted shear localization parameters clearly indicate that titanium alloy such as Ti-6Al-4V is most difficult to weld due to its narrowest shear band width among all three materials considered.
2) Although with its slightly lower shear band propagation speed than Ti-6Al-4V, HSLA 4340 exhibits a significantly wider shear band width, and therefore, implying a much better friction stir weldability than Ti-6Al-4V.
3) Aluminum alloys such as Al 2024 possesses the best friction stir weldability because of its widest shear band width and shortest shear band formation time among the three alloys studied

Although both local auxiliary heating and uniform pre-heating methods increase the shear band propagation speed (i.e., maximum possible welding speed), a method that provides a more uniform pre-heating in weld area is shown to be potentially much more effective than a localized heating for improving friction stir weldability for difficult-to-weld alloys such as Ti-6Al-4V.

Table 3-1: Welding parameters for Ti-6Al-4V

Weld ID	ω (RPM)	Travel speed (mm/min)	r_p [a] (mm)	h [b] (mm)	Torque (Nm)
2-120	120	50.8	7.85	9.91	201
2-150	150	50.8	7.85	9.91	154
2-200	200	50.8	7.85	9.91	127
4-400	400	101.6	7.85	9.91	100
8-800	800	203.2	7.85	9.91	79

[a]: Pin diameter
[b]: Pin height

Table 3-2: Material properties Ti-6Al-4V, Steel 4340 and Al2024 in terms of Sellas-Tegarts parameters

Material Name	$\bar{\rho}$ (kg/m^3)	$\bar{c}$ (J/kgK)	$\bar{\mu}$ (GPa)	$\bar{k}$ (W/mK)	θ_m (K)	A (s^{-1})	n	Q kJ mol^{-1}	τ_R (MPa)
Ti-6Al-4V	4428	580	40	6.7	1883	3.92E6	3.6	176	46.9
Steel 4340	7840	477	76	38	1520	1.62E16	4.69	441	119
Al 2024	2770	875	28	119	502	2.29E11	5.46	178	47.7

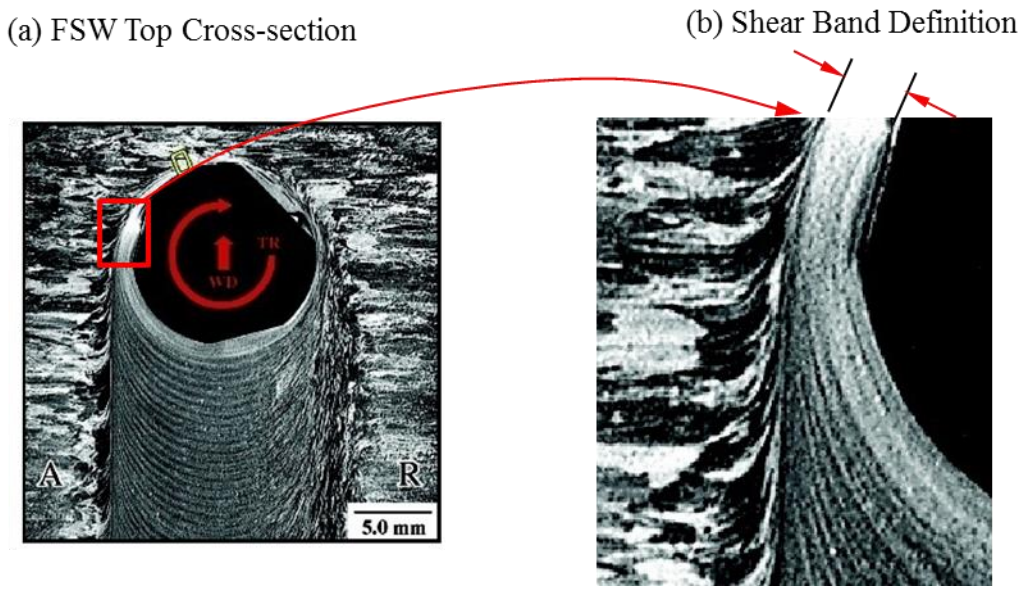

Figure 3.1: Typical banded structure in a friction stir weld and shear band definition for computational treatment

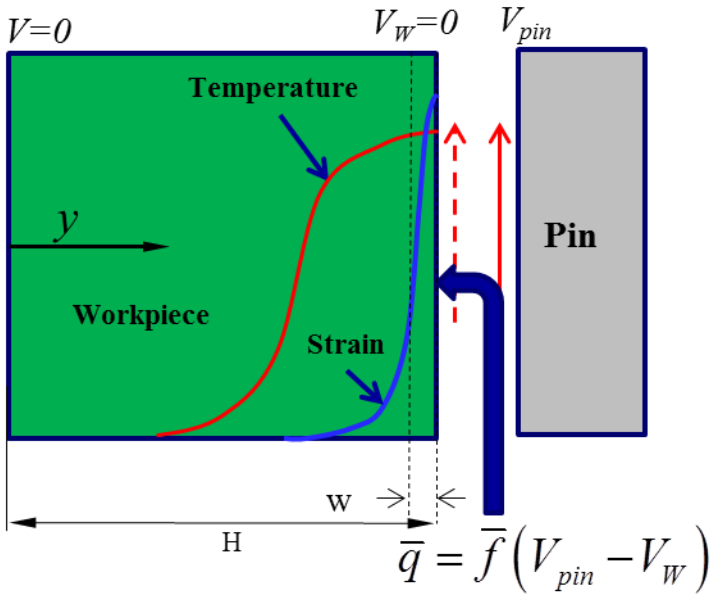

Figure 3.2: Definition of thermal and plastic deformation boundary layer problem

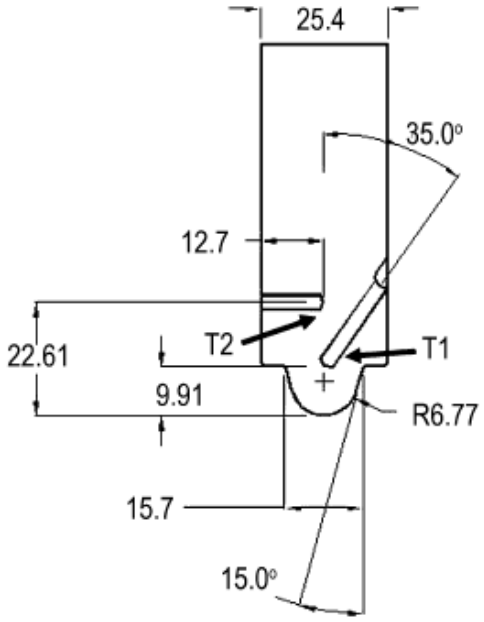

Figure 3.3: Tool geometry and thermocouple positions used in Pilchak et al. [7] (unit in mm)

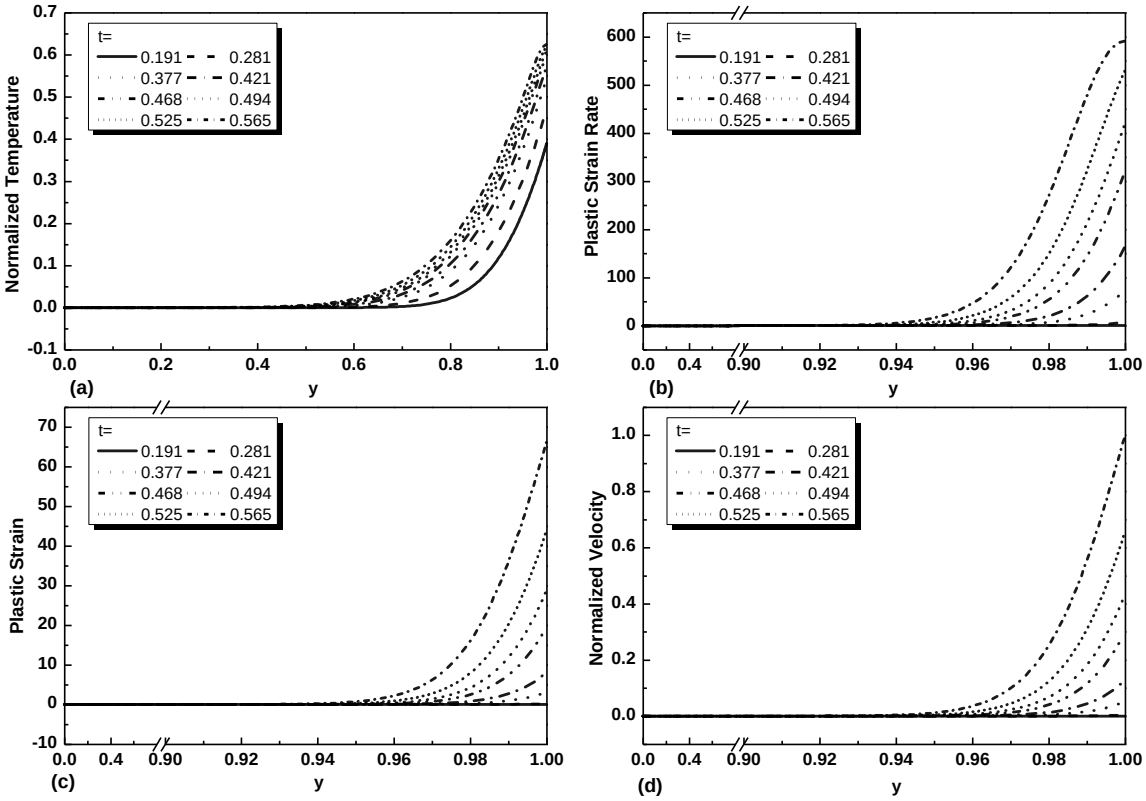

Figure 3.4: Modeling results for Weld ID 2-120: (a) Normalized temperature rise, (b) Plastic strain rate, (c) Plastic strain, (d) Normalized velocity

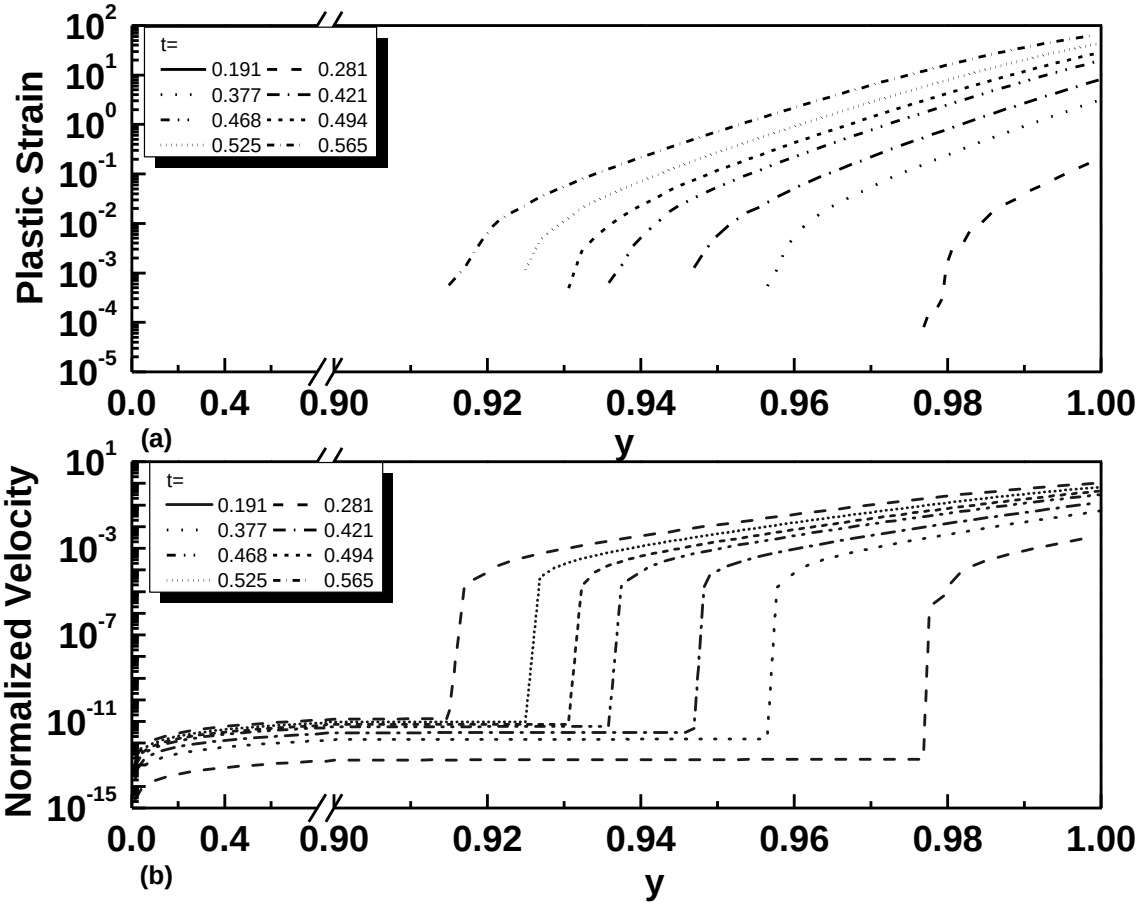

Figure 3.5: Modeling results for Weld 2-120 (in log-log scale): (a) Plastic strain; (b) Normalized velocity

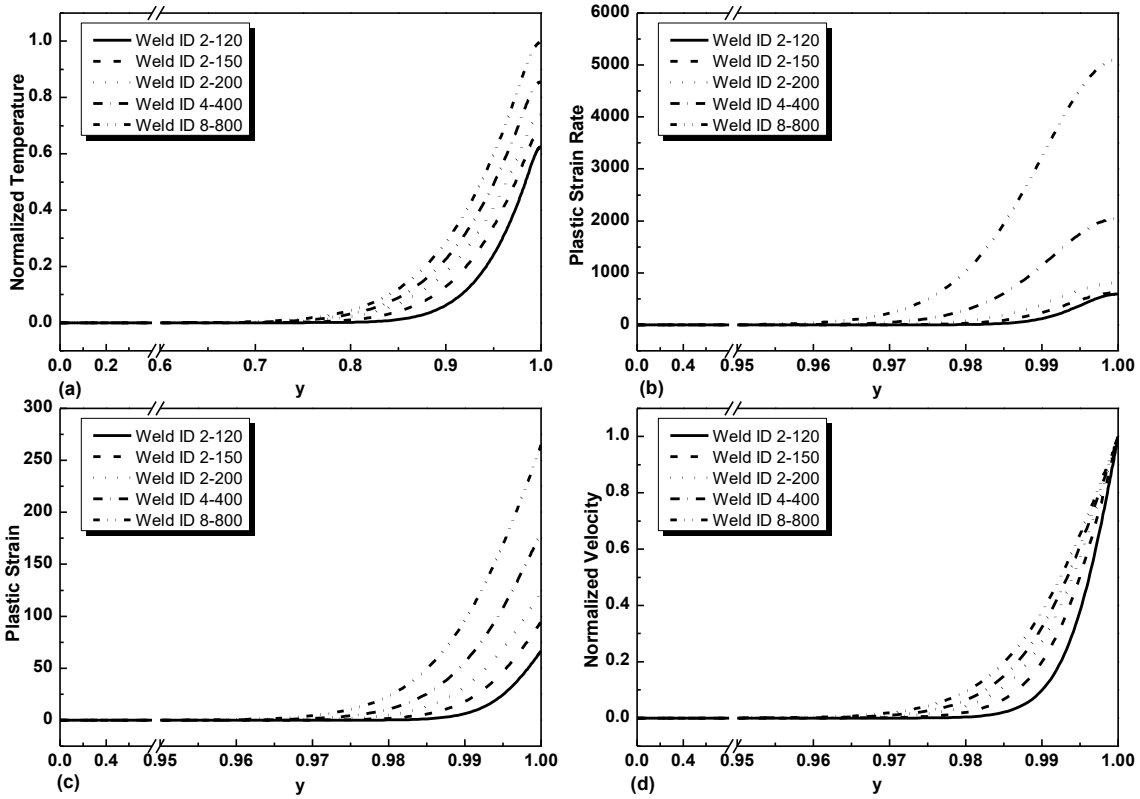

Figure 3.6: Comparison of modeling results for five different welding conditions: (a) normalized temperature rise, (b) plastic strain rate, (c) plastic strain, (d) normalized velocity.

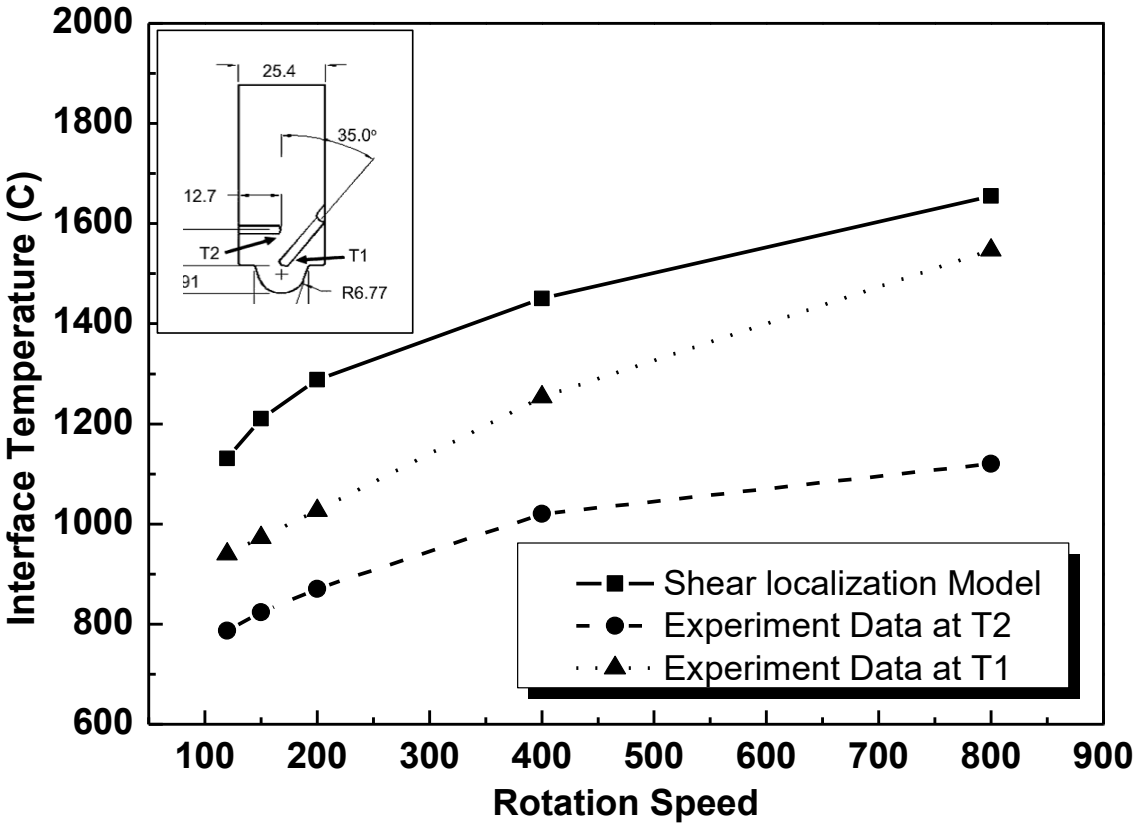

Figure 3.7: Comparison of predicted peak interface temperatures with the measurements at some distance away from workpiece/pin interface corresponding to five welding conditions documented in Pilchak et al. [7]

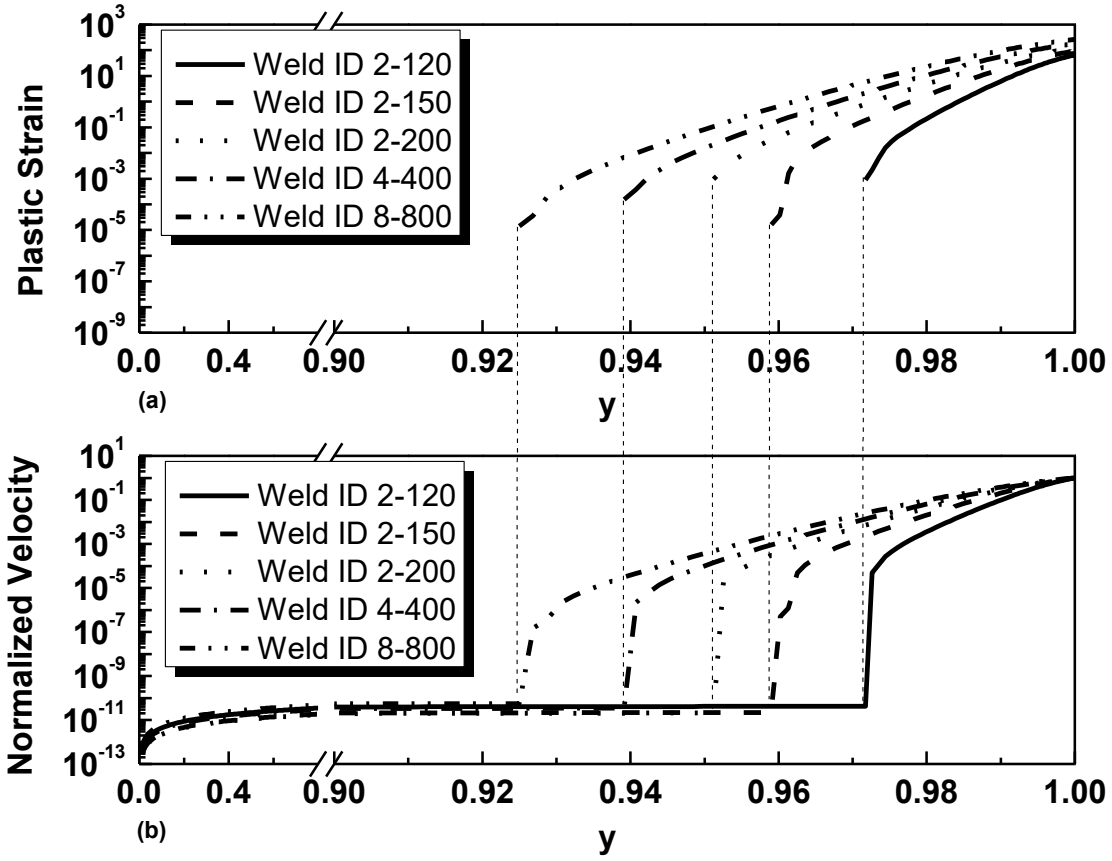

Figure 3.8: Comparison of spatial distributions for all five welding conditions in Table 3-1: (a) Plastic strain, (b) Normalized velocity.

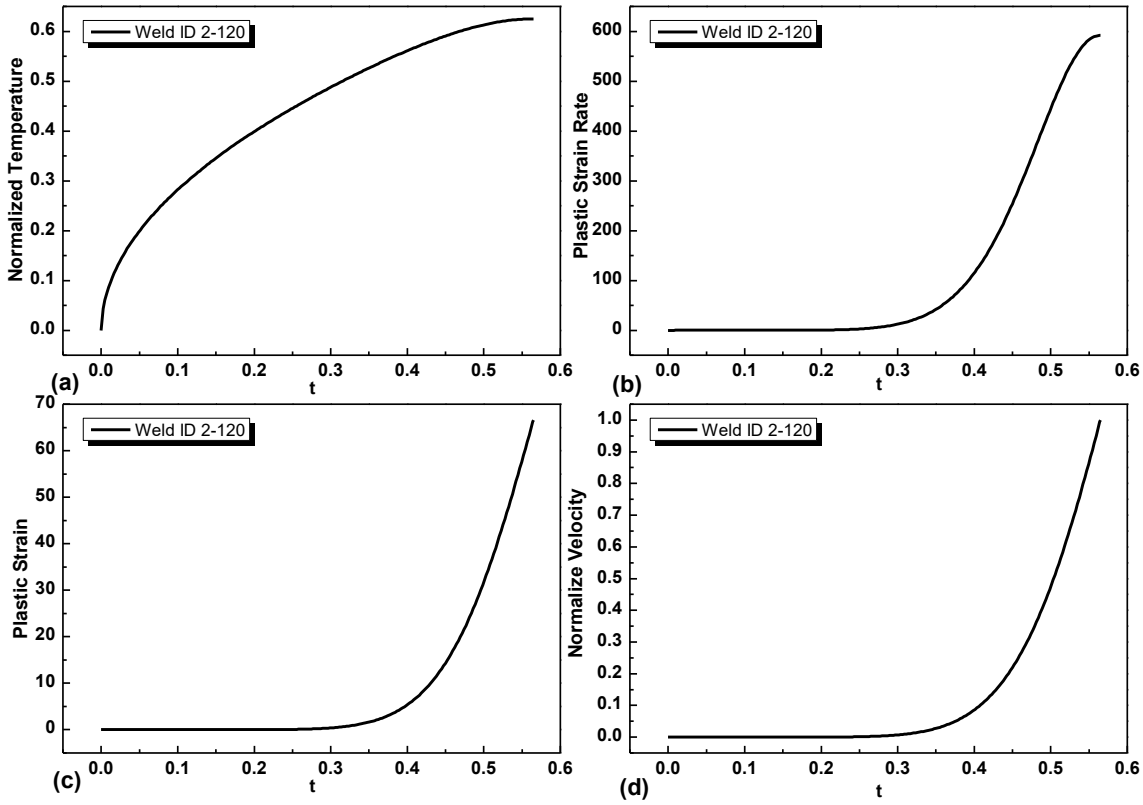

Figure 3.9: Time history plots for Weld ID 2-120 at workpiece/pin interface: (a) normalized temperature rise, (b) plastic strain rate (c) plastic strain, (d) normalized velocity

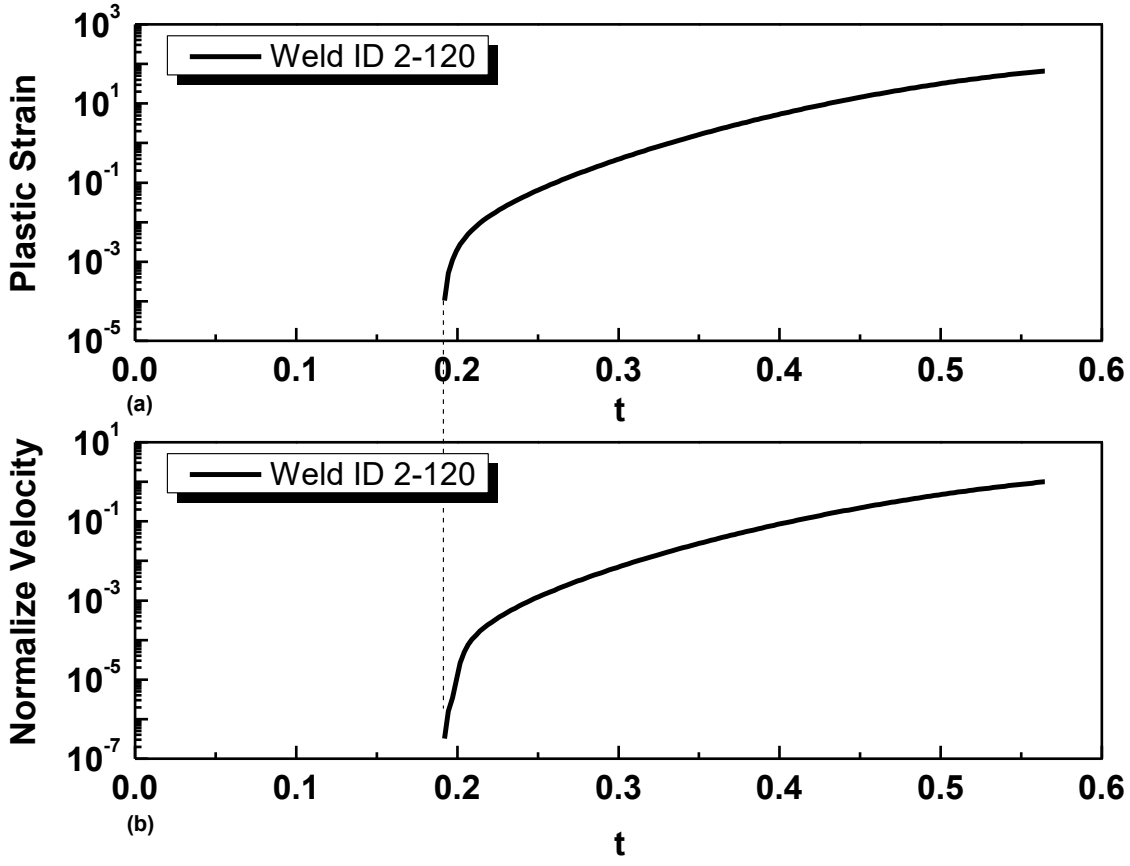

Figure 3.10: Time history plots of plastic strain and normalized velocity at workpiece/pin interface (Weld ID2-120)

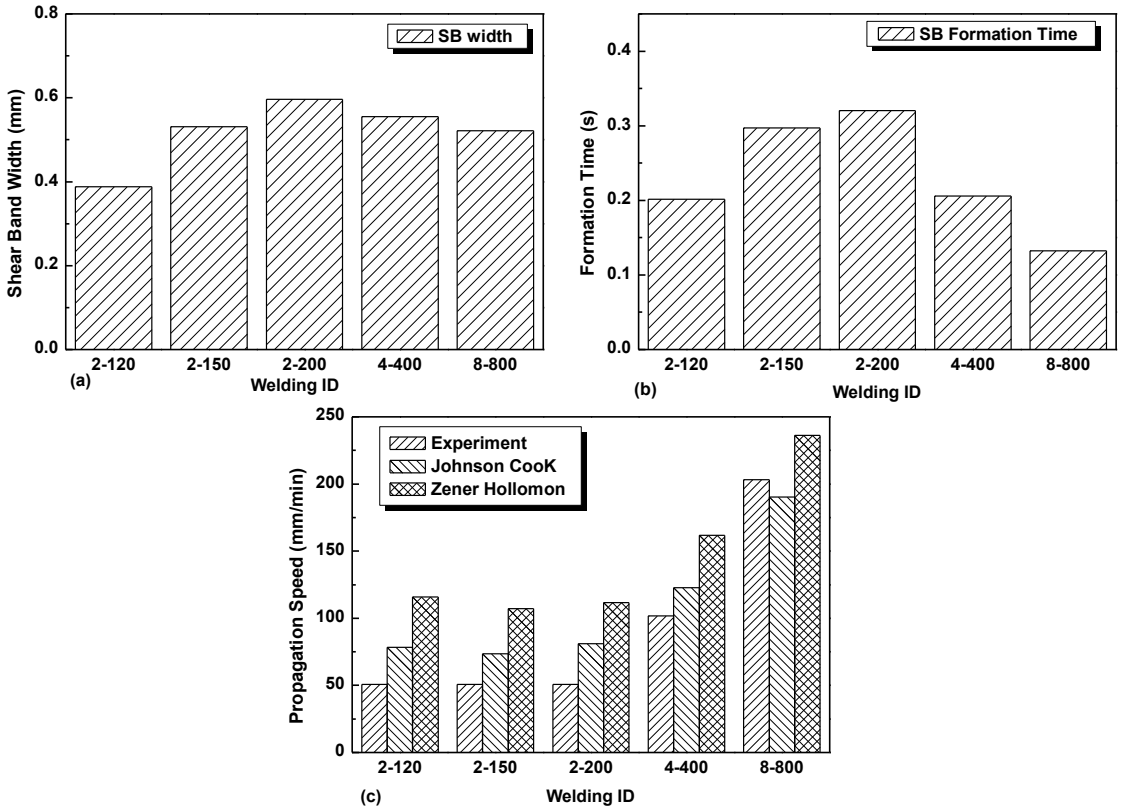

Figure 3.11: Predicted shear band width, formation time and propagation speed for all five weld conditions using both Sellars Tegart and John Cook material modes, and comparison with experiment data

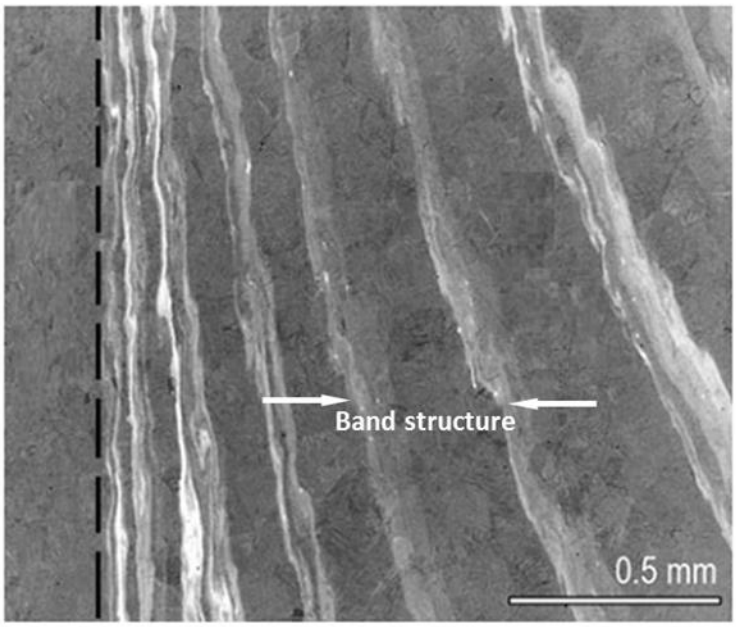

Figure 3.12: Backscattered electron image showing banded structure in the 800 rpm weld [7], in which a shear band width (W_{SB}) in the order of $0.5mm$ can be inferred.

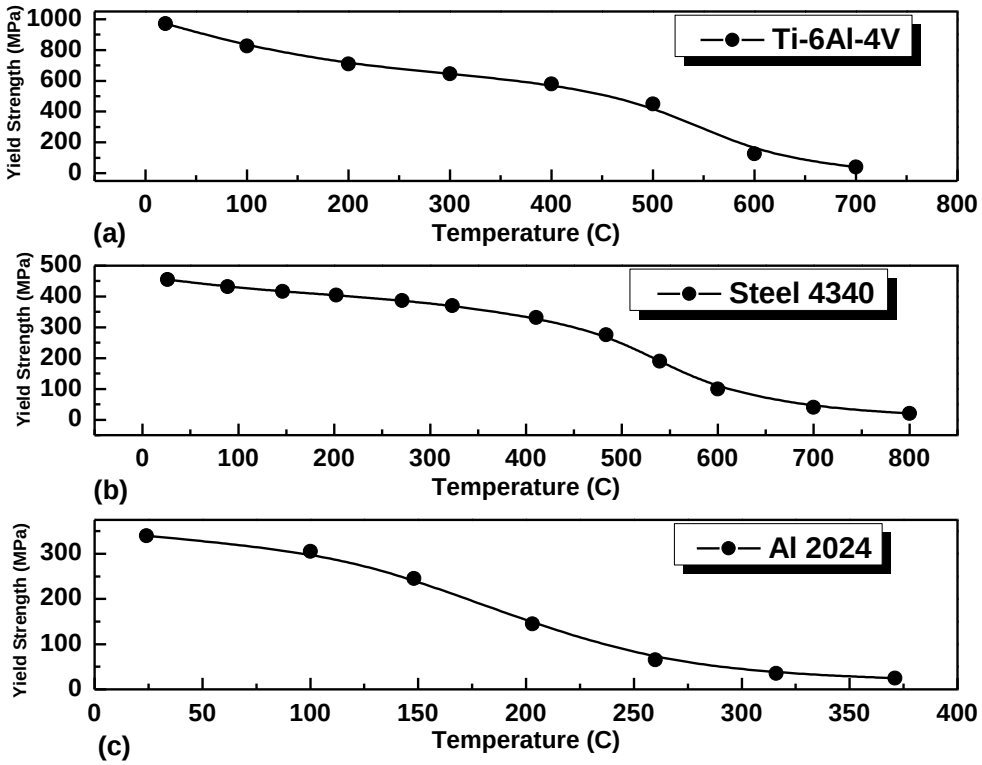

Figure 3.13: Yield strengths as a function of temperature: (a) Ti-6Al-4V, (b) Steel 4340, and (c) Al 2024 [21]

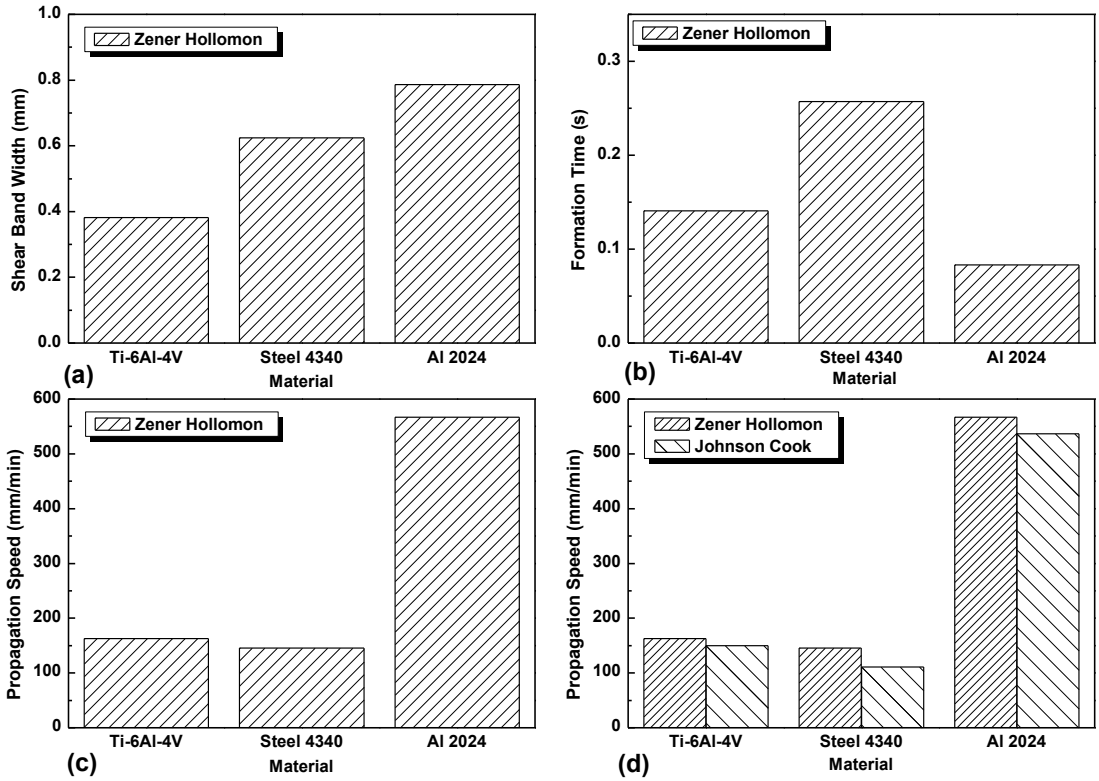

Figure 3.14: Effects of base material type on predicted shear localization parameters: (a) shear band width, (b) shear band formation time, (c) shear band propagation speed, (d) comparison of shear band propagation speed between Sellars-Tegart model and Johnson-Cook model.

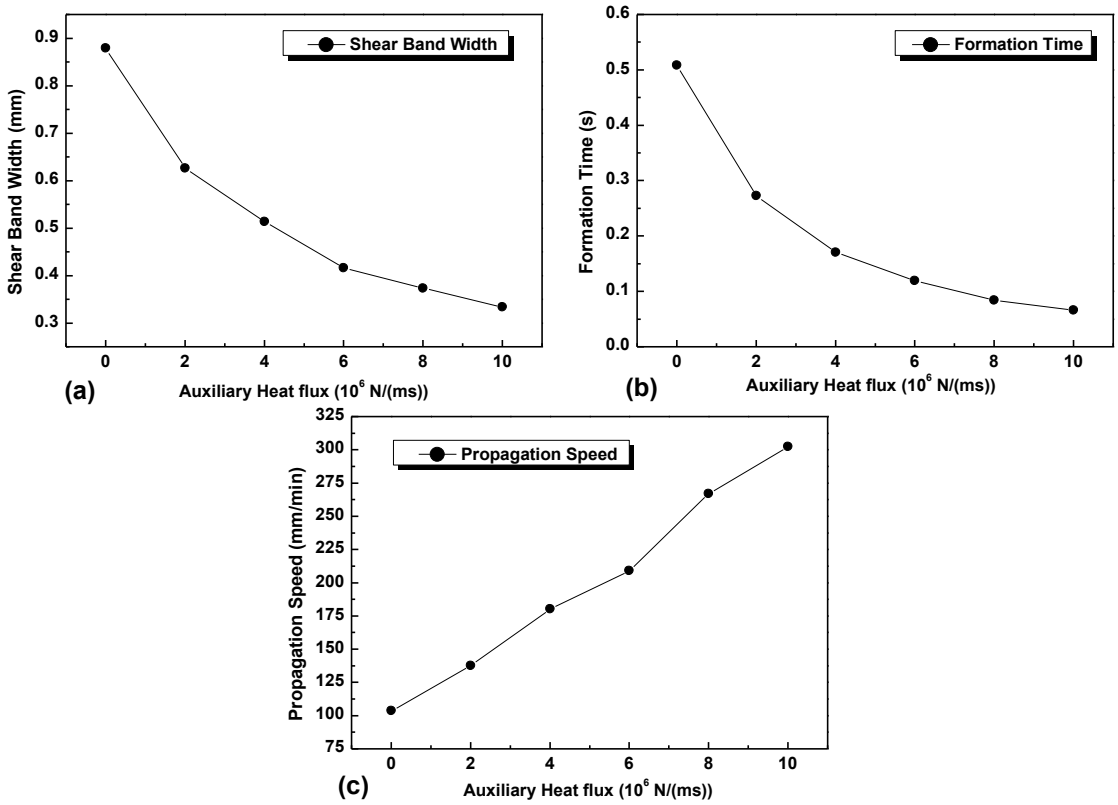

Figure 3.15: Local auxiliary heating effects on shear localization parameters (Ti-6Al-4V): (a) shear band width, (b) shear band formation time, (c) shear band propagation speed.

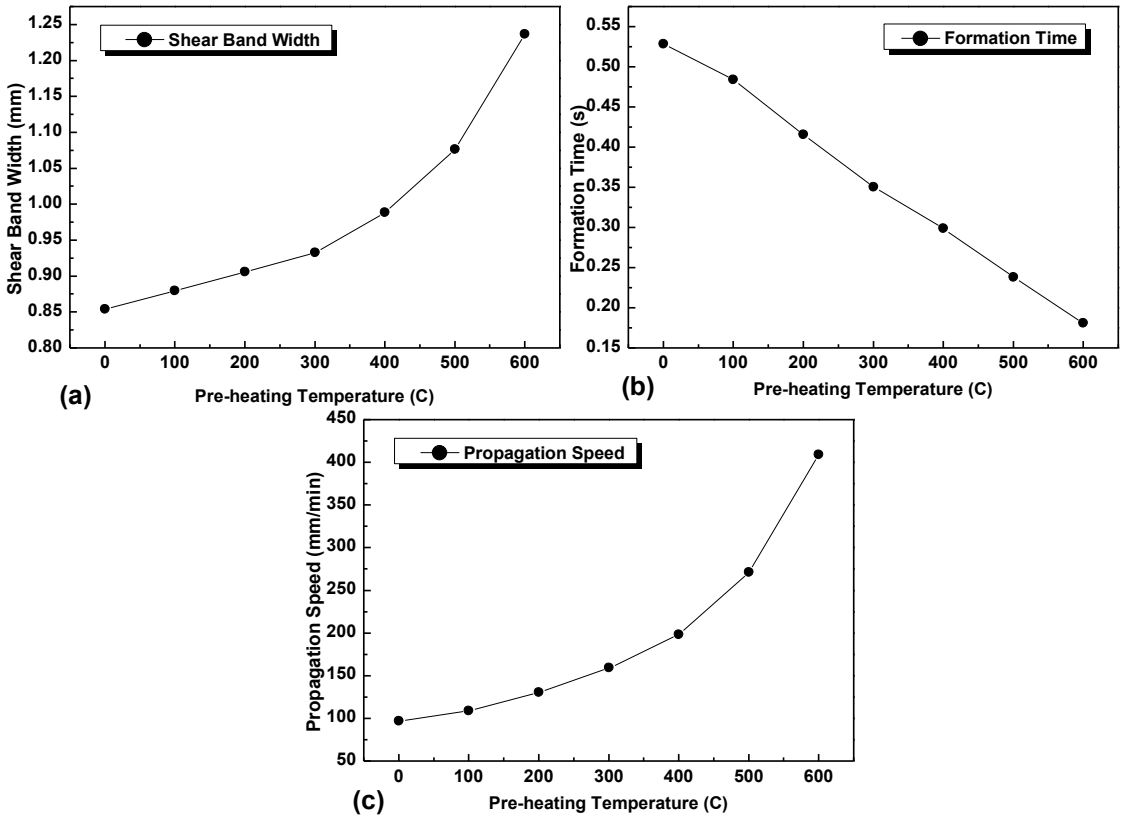

Figure 3.16: Pre-heating temperature effects on shear localization parameters (Ti-6Al-4V): (a) shear band width, (b) formation time, (c) shear band propagation speed

Acknowledgment

The authors gratefully acknowledge the support of this work in part by ONR Grant No. N00014-10-1-0479 at UNO and the National Research Foundation of Korea (NRF) Gant funded by the Korea government (MEST) through GCRC-SOP at University of Michigan under Project 2-1: Reliability and Strength Assessment of Core Parts and Material System.

References

[1] Dawes, C. J., & Thomas, W. M. (1995). Friction stir joining of aluminium alloys. TWI bulletin, 6(1), 1.

[2] Nandan, R., DebRoy, T., & Bhadeshia, H. K. D. H. (2008). Recent advances in friction-stir welding–process, weldment structure and properties. Progress in Materials Science, 53(6), 980-1023.

[3] Nunes A C. Prolegomena to the Study of Friction Stir Welding. In: Proceedings of Materials Science & Technology 2010 – Joining of Advanced and Specialty Materials XII, Houston, TX, 2010.

[4] Schneider, J. A., & Nunes Jr, A. C. (2004). Characterization of plastic flow and resulting microtextures in a friction stir weld. Metallurgical and materials transactions B, 35(4), 777-783.

[5] Yang, B., Yan, J., Sutton, M. A., & Reynolds, A. P. (2004). Banded microstructure in AA2024-T351 and AA2524-T351 aluminum friction stir welds: Part I. Metallurgical studies. Materials Science and Engineering: A, 364(1), 55-65.

[6] Knipling, K. E., & Fonda, R. W. (2009). Texture development in the stir zone of near-α titanium friction stir welds. Scripta materialia, 60(12), 1097-1100.

[7] Pilchak, A. L., Tang, W., Sahiner, H., Reynolds, A. P., & Williams, J. C. (2011). Microstructure Evolution during Friction Stir Welding of Mill-Annealed Ti-6Al-4V. Metallurgical and Materials Transactions A, 42(3), 745-762.

[8] Krishnan, K. N. (2002). On the formation of onion rings in friction stir welds. Materials science and engineering: A, 327(2), 246-251.

[9] Aukrust, T., & LaZghab, S. (2000). Thin shear boundary layers in flow of hot aluminium. International Journal of Plasticity, 16(1), 59-71.

[10] Fonda, R. W., Bingert, J. F., & Colligan, K. J. (2004). Development of grain structure during friction stir welding. Scripta Materialia, 51(3), 243-248.

[11] Batra, R. C., & Wei, Z. G. (2006). Shear bands due to heat flux prescribed at boundaries. International journal of plasticity, 22(1), 1-15.

[12] Pei, X. J., and P. S. Dong. "Shear localisation modelling of friction stir weld formation process." Science and Technology of Welding and Joining 19.5 (2014):

416-426.
[13] Liang, R., & Khan, A. S. (1999). A critical review of experimental results and constitutive models for BCC and FCC metals over a wide range of strain rates and temperatures. International Journal of Plasticity, 15(9), 963-980.
[14] Zener, C., & Hollomon, J. H. (2004). Effect of strain rate upon plastic flow of steel. Journal of Applied Physics, 15(1), 22-32.
[15] Puchi-Cabrera, E. S., Staia, M. H., Guérin, J. D., Lesage, J., Dubar, M., & Chicot, D. (2013). Analysis of the work-hardening behavior of C–Mn steels deformed under hot-working conditions. International Journal of Plasticity, 51, 145-160.
[16] Kuykendall, K., Nelson, T., & Sorensen, C. (2013). On the selection of constitutive laws used in modeling friction stir welding. International Journal of Machine Tools and Manufacture, 74, 74-85.
[17] Dong P, Nie C, Song S, Yang X, DeCan L. A math-based design-for-produceability evaluation of titanium applications in ship hull structures The 2012 SNAME Transactions, Vol. 120, PP 299-305 (ISSN 0081 1661)
[18] Dong, P., et al. Coupled thermomechanical analysis of friction stir welding process using simplified models. Science and Technology of Welding & Joining 6.5 (2001): 281-287.
[19] Guide, MATLAB User'S. The mathworks. Inc., Natick, MA 5. 1998.
[20] Skeel, R. D., & Berzins, M. (1990). A method for the spatial discretization of parabolic equations in one space variable. SIAM journal on scientific and statistical computing, 11(1), 1-32.
[21] Tello, K. E., Gerlich, A. P., & Mendez, P. F. (2010). Constants for hot deformation constitutive models for recent experimental data. Science and Technology of Welding & Joining, 15(3), 260-266.
[22] Gale, William F., and Terry C. Totemeier, eds. Smithells metals reference book. Butterworth-Heinemann, 2003.
[23] Sinclair P C, Longhurst W R, Cox C D, Lammlein D H, Strauss A M, Cook G E. Mater Manuf Process. 2010; 25(11): 1283-1291.
[24] Aydin, M. (2010). Effects of welding parameters and pre-heating on the friction stir welding of UHMW-polyethylene. Polymer-Plastics Technology and Engineering, 49(6), 595-601.
[25] Álvarez, A. I., García, M., Pena, G., Sotelo, J., & Verdera, D. (2014). Evaluation of an induction‐assisted friction stir welding technique for super duplex stainless steels. Surface and Interface Analysis.

Chapter 4

A Coupled Friction Stir Shear Localization Model Incorporating Pin Contact and 3D Transient Friction Heating

Abstract

This paper presents a sequentially coupled shear localization model incorporating both pin/workpiece contact phenomena and three-dimensional (3D) heat flow environment generated by heating between tool shoulder and workpiece. It represents a significant advancement in an early shear localization model presented by the same authors (2015,2016) which was focused on shear localization process in front of pin such that shear band development can be treated as an one-dimensional (1D) thermal viscoplastic problem, without considering shoulder/workpiece heating and contact interaction between pin and workpiece. The current model includes a novel analytical based 3D transient heat flow solution incorporating detailed spatial resolution in both heat generation at shoulder/workpiece interface, which provide a transient temperature environment within which shear localization can now be examined in detail. In addition, contact interactions at pin and workpiece interface are now explicitly considered by introducing a classical contact mechanics solution for contact between cylinder (pin) and cylindrical cavity (surrounding base metal). This refined shear localization model has been shown capable of providing more realistic and reasonable estimations for both

temperature and welding torques when comparing with available experimental data. A robust numerical procedure has also been developed for estimating optimum welding speed for a given stir tool rotational speed and welding travel speed and pin tool geometry, which shows a good agreement with experimental results for a number of applications.

Introduction

As friction stir welding (FSW) continue to gain a wider acceptance for joining lightweight materials, particular metals or dissimilar metals that are difficult to weld with conventional welding processes [e.g. 1-5], an effective computational process model that is capable of estimating process window becomes increasingly desirable for reducing the needs for time-consuming and costly Design of Experiments (DoE). There have been numerous investigation on effective computational procedures for modeling one or a few aspects of complex multi-physics and multi-scale mechanics phenomena associated with various stages of weld formation process in FSW. These models range from the simple conduction heat transfer models [e.g.6-10], to the metal flow models [e.g.11-13], to the fully coupled models [e.g. 14-17]. These investigations have illuminated several important phenomena, such as how friction heating from stir tool shoulder and stir pin contribute to stir zone formation process during FSW. However, there still exists a significant gap in modeling capabilities for enabling a direct examination of various process parameters and their effects on weld quality. Representative research efforts along this line are those by Arbegast [18] who developed a simplified model which showed a relationship between pin tool geometry (as well as its operating parameters)

and flow stress of materials being joined, by Arora et al. [19] who proposed and tested a criterion for optimum tool geometry design, but didn't address in detail how to select tool rotational speed and travel speed, and by Qian et al. [20] who proposed an analytical model for optimizing pin rotation speed and travel speed for an aluminum alloy at an assumed optimum welding temperature. One common attractiveness of these modeling procedures is that they all attempt to strike a balance between model simplicity and process details, which is essential when dealing complex thermomechanical phenomena involved in FSW, particularly of the purpose of developing robust process tools for industrial applications.

With the same objective but a different approach, Pei and Dong [21,22] presented a shear localization model to directly relate shear band formation process to weld formation in FSW, in which both shear band formation time and shear band width can be estimated for computing optimum travel speed (or welding speed). Although reasonable good agreements with experimental data have been demonstrated for FSW of aluminum alloys, steel (HSLA 4140) and titanium alloy (Ti-6-4), two major limitations in their model are that three-dimensional (3D) transient friction heating between tool shoulder and workpiece was not considered and that friction stress between pin and workpice was assumed known, available from a given applied torque. The latter limits the model's ability in estimating operating torque resulted of tool/workpiece interactions under a given set of welding process parameters such as tool rotational speed and welding travel speed, which is required for process window estimation.

To cover the two major limitations stated above, this paper is to present a refined shear localization model that incorporate both 3D transient friction heating at tool

shoulder and workpiece interface and a contact mechanics model which allows a direct estimation of welding torque resulted from tool and workpiece interactions. As such, both optimum welding speed and resulting torque can be directly estimated under given tool rotational speed and material to be welded. The effectiveness of the refined shear localization model in understanding FSW of Ti-6-4 will be demonstrated in detail along with comparisons with experimental results, for which there has been a growing interest in shipboard applications for achieving significant structural lightweighting [23].

Model Construct

Consider shear banding shown in Figure 4.1 as discussed by various authors Fonda et al. [24] and Yang et al. [25] for high strength aluminum alloys, and by Knipling and Fonda [26] and Pilchak et al.[27] for titanium alloys. A sequentially coupled shear localization model that is capable of capturing essential aspects of weld band formation process while offering a reasonable level of simplicity and computational efficiency is proposed here by idealizing the FSW as 4 stages (see Figure 4.2). During the first stage, the material under the tool shoulder is heated up by the friction between the shoulder and workpiece (Figure 4.2a). Other than friction between shoulder and workpiece, the frictional stress between the tool pin and workpiece provides additional local heat flux into the layer (the red band in Figure 4.2b) of material just in front of the pin (Figure 4.2b). Softened by the 2 heating effects aforementioned and driven by the frictional stress between the pin and workpiece, the layer of material just in front of the pin is accelerated from static to the pin tangential velocity which is known as sliding until sticking stage (Figure 4.2b). Figure 4.2c describes the stage in which the materials have already

achieved sticking stage (i.e. metal reach the same velocity as pin tangential velocity). and are swapped to the back of the pin to fill the space left by the advance of the tool. Repeat of stage 1-3 will construct a series of band structure and finally form a sound FSW joint (Figure 4.2d). In the present work, we are focusing on modeling the 1st and 2nd stage. The model firstly begins with a 3D analytical based transient heat transport model to take account the preheating effect in the 1st stage. A one dimensional shear localization model is then followed to model the material flow and heat transfer phenomena in 2nd stage which is described in Figure 4.2b-c.

4.1.1 Shoulder friction heating and 3D transient solution

In order to efficiently estimate 3D transient temperature environment generated by friction heating between stir tool shoulder and workpiece, in which localized pin/material interactions lead to shear localization and subsequent shear band formation, an analytical solution is sought, with the following assumptions and simplifications: 1) Material properties are independent of temperature, which results in a linear heat conduction problem; 2) Heat loss into the tool shoulder is considered but into ambient air is neglected. The reason is that the heat loss into ambient is negligible compare to heat conduction in the workpiece and tool shoulder within a time scale relevant to shear localization process [21,22]. 3) Heat loss through contact/gap conduction into the bottom back plate can be simplified as that the back plate is made from the same material as the plate to be weld. Thus, the above simplifications and assumptions lead to the definition of a 3D linear heat transfer problem defined in a semi-infinite body, as illustrated in Figure 4.3

Consider that a stir tool shoulder is centered at $(0,0,0)$ at time $t = 0$ with respect to the global coordinate system (x, y, z) shown in Figure 4.3a. Once the tool starts to move with a travel velocity V_T, the center of tool shoulder can be tracked as $(V_T t, 0)$. With respect to the local coordinate system moving with tool, each point on the workpiece can be expressed as $(\xi = x - V_T t, y)$, the relative velocity of each point on the workpiece under shoulder can then be given as (See Figure 4.3b):

$$\begin{aligned} v_x &= V_T - \omega r \sin\theta = V_T - \omega y \\ v_y &= \omega r \cos\theta = \omega\left(x - V_T\right) = \omega\xi \\ v(x,y) &= \sqrt{v_x^2 + v_y^2} \end{aligned} \tag{4.1}$$

Thus heat flux generated through friction between shoulder and workpiece can then be expressed as:

$$q\left(\xi, y\right) = \begin{cases} \beta\mu p_s \sqrt{\left(V_T - \omega y\right)^2 + \left(\omega\xi\right)^2} & \left(R_{pin} \le \sqrt{\xi^2 + y^2} \le R_s\right) \\ 0 & \left(otherwise\right) \end{cases} \tag{4.2}$$

In Eq.(4.1) and (4.2), ω represents angular rotational velocity of the shoulder, while μ is friction coefficient between workpiece and the shoulder, and p_s is the pressure exerted by the shoulder against the workpiece. Note that p_s can be estimated by:

$$p_s = \frac{F_z}{\pi\left(D_s^2 - D_{pin}^2\right)/4} \tag{4.3}$$

where F_z is the axial thrust force (forge load) of the shoulder against workpice, while D_{pin} and D_s represent the outer diameters of the stir pin and the shoulder, respectively. Total heat flux generated through Eq. (4.2) is partitioned between shoulder and workpiece through a constant β, expressed as [28]:

$$\beta = \frac{k_s\sqrt{\alpha_W}}{k_s\sqrt{\alpha_W} + k_W\sqrt{\alpha_s}} \tag{4.4}$$

Here k and α are thermal conductivities and thermal diffusivities of shoulder and workpiece materials, designated by subscripts s and W, respectively.

The governing equation with respect to the global coordinate system given in Figure 4.3a can be written as:

$$\frac{\partial T}{\partial t} = \frac{k}{C_p\rho}\left(\frac{\partial^2 T}{\partial x^2} + \frac{\partial^2 T}{\partial y^2} + \frac{\partial^2 T}{\partial z^2}\right) \tag{4.5}$$

where k, C_p and ρ are thermal conductivity, specific heat capacity and density of workpiece material. The solution of Eqs (4.2)-(4.5) are is based on the classical solution for an instant point source Q acting at t' that satisfies the differential equation of heat conduction in fixed coordinates Eq.(4.5). (see Eq. (23) in [29]):

$$T(r,t) - T_0 = \begin{cases} 0 & (t < t') \\ \dfrac{2Q}{\rho C_p\left[4\pi\alpha(t-t')\right]^{3/2}}\exp\left(-\dfrac{r^2}{4\alpha(t-t')}\right) & (t > t') \end{cases} \tag{4.6}$$

where $\alpha = k/(\rho C_p)$.

In the current context, the infinitesimal temperature increase $dT(r,t')$ during time period from t' to $t' + dt'$) can be expressed as:

$$dT(r,t') = \frac{2dQ}{c\rho\left[4\pi\alpha(t-t')\right]^{3/2}}\exp\left(-\frac{r^2}{4\alpha(t-t')}\right) \tag{4.7}$$

in which $dQ = qdAdt'$. Combining Eqs. (4.2) and (4.7) leads to:

$$dT = \frac{1}{\rho c\left[4\pi\alpha(t-t')\right]^{3/2}}\left\{\int_{-R+V_T t'}^{R+V_T t'}\int_{-\sqrt{R^2-(x'-V_T t')^2}}^{\sqrt{R^2-(x'-V_T t')^2}} 2\mu p\sqrt{\left(V_T-\omega y'\right)^2-\omega^2\left(x'-V_T t'\right)^2}\exp\left(-\frac{\left(x-x'\right)^2+\left(y-y'\right)^2+z^2}{4\alpha\left(t-t'\right)}\right)dy'dx'\right\}dt' \quad (4.8)$$

Integrating Eq. (4.8) with $t'' = t - t'$, noting $x = \xi + V_T t$, one can obtain temperature distribution at any given time *t* as:

$$T(\xi,y,z,t) = \int_0^t \frac{2}{\rho c\left[4\pi\alpha t''\right]^{3/2}}\left\{\int_{-R}^{R}\int_{-\sqrt{R^2-\xi'^2}}^{\sqrt{R^2-\xi'^2}} q\left(\xi',y'\right)\exp\left(-\frac{\left(\xi-\xi'+V_T t''\right)^2+\left(y-y'\right)^2+z^2}{4\alpha t''}\right)dy'd\xi'\right\}dt''+T_0 \quad (4.9)$$

It should be emphasized here that Eq.(4.9) and its derivation process described above are different from early Rosenthal type of heat flow solution based on point heat source such as the one given in [6] in that the present solution provides a detailed spatial resolution of temperature distribution on contact interface as a function of angular rotational speed ω, in addition to incorporate effects of translational velocity of stir tool (welding travel speed) while earlier solutions do not. The former is essential for differentiating shoulder's advancing side from its retreating side in terms of temperature distribution details. Furthermore, the present solution (Eq.(4.9)) captures temperature transients in addition to quasi-steady state temperature field.

As a validation of the new analytical solution given in Eq.(4.9), a detailed 3D finite element simulation of shoulder/material friction heating and heat conduction in a finite thickness plate is performed using commercial software ABAQUS [30]. The physical domain considered in the FE model has dimensions of 250x125x50 mm in x, y, z directions, with element size of 1x1x1 mm near and within shoulder/workpiece contact area. A user subroutine DFLUX is developed for modeling rotational friction heat flux generated at stir shoulder/workpiece interface as it moves along x axis, as described in Eq. (4.2). As can be seen in Figure 4.4, both the analytical results according to Eq.

(4.9) and 3D finite element results are in an excellent agreement at all three depths, proving the validity of the 3D analytical solution developed. It is worth noting that both solutions show that there is an up to about 200^0C difference in temperature on the surface between the front and back of stir pin (Figure 4.4a), and slightly difference between advancing and retreating side of the pin (Figure 4.4b), which would not have been captured by existing analytical solutions such as the one in [6]. The main advantage of the analytical solution given by Eq. (4.9) lies in the fact that it can be conveniently used for defining a transient temperature environment within which shear localization process takes place, which will be discussed in the next section.

4.1.2 Pin/workpiece Contact model

As discussed in Pei and Dong [21,22], the interaction between the pin and workpiece leading to shear localization and shear band formation within each revolution of stir pin can be idealized as a 1D shear localization problem, as further illustrated in detail in Figure 4.55b. During sliding stage when material under the shoulder has already been heated up by friction between shoulder and workpiece, stir pin has a constant tangential speed $V_{pin} = \omega R_{pin}$ (illustrated by solid red arrow line in Figure 4.5b), while exerting a frictional stress f on the workpiece (or base metal). The resulting frictional heat flux $q = \beta f(V_{pin} - V_W)$ is consumed by the workpiece, where β is defined in the same manner as in Eq. (4.4) and V_W represents material velocity at pin/workpiece interface (illustrated by red dash arrow line in Figure 4.5b), which is accelerated by the rotating pin. As the friction heat builds up at base metal side of the pin/workpiece surface, material softening occurs, resulting in a rapid development of local plastic deformation.

Sliding condition terminates as relative velocity, $V_{pin} - V_W$, approaches zero, leading to sticking stage.

Coulomb's friction law is assumed applicable for modeling pin/workpiece contact as shown in Figure 4.6, resulting frictional stress at a function of time as:

$$f(t) = \mu p_0(t) \tag{4.10}$$

where $p_0(t)$ is contact pressure between pin and workpiece at weld seam (red dot Figure 6), which can be estimated by the classical solution of contact between cylinder-in-a cylindrical groove as [33]:

$$p_0 = p_0(t) = \frac{E^*}{2}\sqrt{\frac{\delta}{R_{pin}}\left(1 - \frac{1}{R_{hole}/R_{pin}}\right)} = \frac{E^*}{2}\sqrt{\frac{V_T t}{R_{pin}}\left(1 - \frac{1}{R_{hole}/R_{pin}}\right)} \tag{4.11}$$

In Eq. (4.11), $E^*$is the effective modulus of elasticity which is expressed as:

$$\frac{1}{E^*} = \frac{1-\nu_{pin}^2}{E_{pin}} + \frac{1-\nu_W^2}{E_W} \tag{4.12}$$

representing linearized pin/workpiece interaction, and δ is the relative displacement of the pin (see Figure 4.6) upon contact with the cylindrical groove representing work piece. The resulting contact pressure distribution as a function of angular position η (see Figure 4.6) can be given as [33]:

$$p(\eta) = \frac{p_0}{\sqrt{\left(\frac{R_{pin}(1-\cos\eta)}{\sqrt{R_{pin}\delta}}\right)^2 + 1}} \tag{4.13}$$

As a result, welding torque can be calculated as:

$$\Omega = \iint_{A_s} f_s r dA + \iint_{A_{pin}} f_{pin} R_{pin} dA \tag{4.14}$$

where $f_s = \mu p_s$ represents frictional stress generated between tool shoulder and workpiece given in Eq.(4.3) and $f_{pin} = \mu p(\eta)$ frictional stress between pin/workpiece interface. Then, Eq. (4.14) can be re-written as:

$$\Omega = \int_0^{2\pi}\int_{R_{pin}}^{R_s} \frac{\mu F_z r dr d\theta}{\pi\left(R_s^2 - R_{pin}^2\right)} + \int_{-\sin^{-1}\left(\sqrt{R_{pin}\delta}/R_{pin}\right)}^{\sin^{-1}\left(\sqrt{R_{pin}\delta}/R_{pin}\right)} \frac{\mu p_{\max} R_{pin} h_{pin} d\eta}{\sqrt{\left(\frac{R_{pin}\left(1-\cos\eta\right)}{\sqrt{R_{pin}\delta}}\right)^2 + 1}} \tag{4.15}$$

The first term in Eq.(4.15) represents the torque generated by frictional stress distribution between shoulder and workpiece while the second represents torque by frictional stress distribution between pin and workpiece.

4.1.3 Shear localization model

Consider the thermal and mechanical boundary layer problem described in Figure 5. The governing equations can stated as follows, as described in [22,23, 28,31]:

$$\begin{aligned}
&\rho\frac{\partial v}{\partial t} = \frac{\partial \tau}{\partial x} \\
&\rho C_p \frac{\partial \theta}{\partial t} = k\frac{\partial^2\theta}{\partial x^2} + \tau\frac{\partial \gamma_p}{\partial t} \\
&\frac{\partial \tau}{\partial t} = G\frac{\partial \gamma_e}{\partial t} = G\left(\frac{\partial \gamma}{\partial t} - \frac{\partial \gamma_p}{\partial t}\right) = G\left(\frac{\partial v}{\partial x} - \frac{\partial \gamma_p}{\partial t}\right) \\
&\frac{\partial \gamma_p}{\partial t} = \begin{cases} 0 & (Elastic) \\ A\sinh\left(\frac{\tau}{\tau_R}\right)^n \exp\left(-\frac{Q}{R\theta}\right) & (plastic) \end{cases}
\end{aligned} \tag{4.16}$$

In Eq.**Error! Reference source not found.**, ρ is the mass density, v the material tangential velocity in y direction (see Figure. 5b), θ the temperature, τ the shear stress, γ_p plastic strain. G and C_p represent the shear modulus and specific heat capacity of the

material. Eq.$(4.16)_1$ and Eq.$(4.16)_2$ express, respectively, the balance of linear momentum and the balance of internal energy. All of plastic work, given by the second term on the right hand side of Eq. $(4.16)_2$ is assumed to be converted into heating. Eq. $(4.16)_3$ is Hooke's law written in rate form, which also implies the strain-rate has additive decomposition into elastic and plastic parts. Eq. $(4.16)_4$ represents the material constitutive behavior under thermo-viscoplastic relation due to Sellars and Tegart [32], in which, τ_R , n, Q, and R are material constants. The use of Sellars-Tegart constitutive equation is justified based on a number of earlier studies [15-17,22].

The corresponding initial conditions can be described as follows:

$$\begin{aligned} &v(x,0) = 0 \\ &\theta(x,0) = \theta_0(x) \\ &\tau(x,0) = 0 \\ &\gamma_p(x,0) = 0 \end{aligned} \tag{4.17}$$

Note that here $\theta_0(x)$ is the initial temperature distribution as a result of shoulder/workpiece friction heating obtained by the 3D transient heat conduction solution described in Eq.(4.9). The corresponding boundary conditions during sliding friction stage can be described as follows:

$$\begin{aligned} &-k\left.\frac{\partial\theta}{\partial x}\right|_{x=0} = \beta f(t)\left(V_{pin} - v\right) \\ &\tau|_{x=0} = f(t) \\ &v|_{x=R_s} = 0 \\ &\theta|_{x=H} = \theta_r \end{aligned} \tag{4.18}$$

Eq. $(4.18)_1$ represents heat flux into material from the interface due to friction heating between pin and workpiece. Eq.$(4.18)_2$ describe the traction boundary condition,

i.e., shear stress at pin/workpiece interface should equal to the frictional stress between them, and $f(t)$is obtained from the contact mechanics model given in Eq.(4.10).

At certain distance away from pin/workpiece interface, material in workpiece can be assumed to remain stationary (see Figure 4.1) throughout the deformation process, such as at outer edge of the shoulder, i.e., $v|_{x=R_s} = 0$, where R_s represents shoulder radius. Since shear localization process in the present modeling context is investigated within a very short timeframe corresponding one revolution of stir pin, a characteristic distance, *H*, can be identified, at which adiabatic conditions can be assumed [28,31], i.e., $\theta|_{x=H} = \theta_r$, where θ_r is room temperature.

The shear localization problem described by Eq.s (4.16)-(4.18) can be solved numerically by implementing a finite element procedure using MATLAB [34]. A weak form of the governing equations, initial conditions and boundary conditions is derived by a piecewise linear Galerking/Petrov–Galerkin method. This discretization method offers a good accuracy to the second order in space as illustrated by Skeel and Berzins [35]. The result is a system of coupled nonlinear ordinary differential equations (ODEs) that are integrated by using MATLAB function ode15s. Note that the selection of ode15s solver instead of other ODE solvers is because it is better suited in dealing with stiff differential equations. The coordinates of linear elements in x-axis are given by

$$x = \left(\frac{n-1}{300}\right)^4 \tag{4.19}$$

which provides a significant element refinement at the workpiece and pin interface, that is, $x = 0$, for providing a sufficient spatial resolution for shear localization development, as demonstrated for similar problems solved by Batra and Wei [28,31]. The

validation of the solving procedure mentioned above is documented in [21]. The modeling procedure developed here provides a full solution over time from $t = 0$ to a time when material at workpiece and pin interface reaches to a prescribed pin surface linear velocity, that is, $v(1, t) = 1$, i.e. sticking condition happens.

With the contact mechanics model described earlier, knowing applied torque is no longer necessary. Thus this model can be used to study shear band formation process for a given set of basic welding parameters, e.g., rotational speed ω, travel speed V_T, axial thrust force F_z, pin and shoulder diameter R_{pin} and R_s. The output parameters include estimations of peak temperature, torque required, as well as shear localization parameters such as shear band initiation time and shear band width, both of which can be used to estimate shear band propagation speed (i.e., optimum welding speed) [21,22].

Model Validation

4.1.4 Stress concentration analysis

Two sets of FSW experimental data are considered here for validating the refined shear localization model described in the previous section. The first set of was conducted by Pilchak et al. [27]. In their study 10.3-mm-thick Ti-6Al-4V plates in the mill-annealed condition was used. Five FSW welds were made using different process parameters (see Table 1). In-tool temperature measurements were made using K-type thermocouples that were placed at two points along the centerline of the welding tool, as indicated in Figure 4.7a, by spot welding the thermocouple into 3 mm diameter holes drilled in the tool. Thermocouple 2 (T2) was at shoulder level, while thermocouple 1 (T1) was 12.7 mm above T1. The other set of FSW experiments were conducted by Edwards [36]. In

contract to Pilchak's experiments, grooves were machined into the back of test plate so that thermocouples could be routed to the weld zone from the backside of the workpiece to measure the temperature. The position of the thermal couples and the welding parameters used in the experiments are plotted schematically in Figure 4.7b and listed in Table 4-1.

Both sets of experimentally measured peak temperatures at a function of tool rotational speed are compared with the ones predicted at pin/workpiece interface using the new shear localization model. It should be noted that the measured temperatures shown in Figure 4.8a were taken from about 6 mm (T1) and 10 mm (T2) away from pin/workpiece interface [27] and therefore should be consistently lower than those predicted at the pin/workpiece interface. The overall trends as a function of pin rotation speed between the measured and predicted temperatures seem rather reasonable. The temperature measurement data by Edwards [36] are compared with model predictions as a function of rotational speed in Figure 4.8b and welding travel speed in Figure 4.8c. In Figure 4.8b, all three welds were made at the same welding travel speed, i.e., $V_T = 100mm/min$ but with three different rotational speeds, while in Figure 4.8c, the welds were made with same rotational speed at 300 rpm but three different welding travel speeds. Note that all temperature measurements were taken at lower stir zone which is close to the backing plate, which explains why the predicted temperatures are noticeably higher than measured ones. It should be pointed out here that variation in temperature as a function of rotational speed seems more reasonably captured by the present model (see Figures 4.8a and 4.8b) than that as a function of welding travel speed (see Figure 4.8c). The reason may be due to the fact the estimated contact pressure is based on linearized

contact behavior which may deviate increasingly from actual contact pressure as welding travel speed become increasingly high.

However, the comparisons of predicted torques and experimentally measured ones in Figure 4.9 seem to show a rather satisfactory agreement, particularly for the cases given in Figures 4.9a and 4.9b, given some of the uncertainties involved in the material model used (e.g. temperature-independent properties) and the reduced dimension model used for simulating shear localization process. However the linearized contact behavior used in the present model seems to also overestimate the travel velocity effect on predicted torque as seen in Figure 4.9c.

Applications

4.1.5 Details of shear band formation process

One important application of the refined shear localization model developed in this study is its ability to elucidate some of the details associated with shear band formation process unique to FSW. For illustration purpose, the 4th joint listed in Table 1, discussed earlier, which is FSWed under rotation speed of 400 RPM and travel speed of 101.6 mm/min is considered. Figure 4.10 summarizes predicted velocity field within workpiece right in front of pin at various time in seconds during one pin revolution. Note that material velocity is normalized by the tangential velocity of the pin, i.e. ωR_{pin}. Final velocity distribution is plotted in solid black line upon sticking condition (i.e. $V_W = \omega R_{pin}$) is attained, i.e., at $t = 0.163s$. Material velocity decreases rapidly from unity to zero within a very thin layer of about 0.1mm. This thin layer is referred to as "shear band" by the authors early in Ref. [18,19,24,27]. A magnified plot of this region is

also given in the same figure for clarity. Interestingly, it can be seen that material points in workpiece essentially remains stationary before $t = 0.158s$. Figure 10a suggests that it only takes very short time interval right before $t = 0.158s$ for material in front of the pin to reach to the tangential velocity ωR_{pin} of pin and to form a narrow shear layer from $t = 0.158s$ to $t = 0.163s$. This behavior suggests that formation of banded structure in FSW is discontinuous in time. Material in front of the pin seems to "hibernate" a moment and then be swapped away suddenly, resulting in band texture. This finding confirms the experimental observations described by Krishnan [37], in which he designed an experiment to observe the band formation process during FSW, concluding that "tool seems to wait for a short time during which the rotation of the tool produces heat and the forward motion of the tool extrudes the hot metal."

4.1.6 Shear propagation speed

With this refined shear localization model, both shear band initiation time and the resulting shear band width within one pin revolution can be estimated under a given set of welding parameters. Here, shear band initiation time is defined as a time interval it takes for workpiece material in contact with pin interface to be accelerated from zero to pin tangential velocity ωR_{pin}. And shear band width is defined as the width of the thin layer formed, as marked in Figure 4.10. Such a band width definition is also confirmed by those measured experimentally (see [21]). Once shear band initiation time and shear band width formed, shear band propagation speed can be calculated as:

$$V_{prop} = \frac{W_{SB}}{T_{SB}} \tag{4.20}$$

W_{SB} and $T_{SB}$is the shear band (SB) width and shear band initiation time. Obviously, so calculated shear band propagation speed given in Eq.(4.20) is determined by welding conditions and material constitutive behavior. It also highlights the fact that the presence of a well-developed shear band is a necessary condition for a achieving a quality weld through a successive formation of banded structure. Otherwise, various forms of weld defects may result, as discussed in detail in a subsequent publication by the same authors [38].

4.1.7 Optimum welding speed estimation

The developments described in early sections allow an implementation of a numerical algorithm for estimating optimum welding speed in the form of Eq.(4.20) for a given set of welding parameters such as rotational speed ω, axial force F_z, tool geometry. Start with a trial travel speed V_T which can then be used to compute the resulting shear band propagation speed V_{prop} given in Eq.(4.20). If the calculated V_{prop} is less than the trial value which will be updated with a reduced travel speed (otherwise with an increased trial travel speed) until both the trial value becomes sufficiently close to V_{prop}. The corresponding final value of V_T is then the theoretically estimated "optimum" travel speed for the set of welding parameters. The numerical algorithm is described in Figure 11, which is implemented in MATLAB code for performing all computations discussed next.

Four sets of experimental determined FSW process windows reported by different authors (Ref. [23,34-36]), which are expressed in terms of tool rotational speed and travel speed, are compared with the model estimated optimum travel speeds in Figure 4.12.

The procedure outlined in Figure 4.11 is used for computing optimum travel speed according to Eq. (4.20)). Figure 4.12a shows the process window reported by Mashinini [39] in which the author first visually examined FSW welds and categorize them as either "defect" joints or "without visual defect" joints (marked as "w/o visual defect" in Figure 4.12). For those labeled with "without visual defect", the author also performed tensile tests and marked some of these joints as "UTS optimum" for high UTS strengths attained. For consistency purpose, the authors of this paper adopted the same designations for the rest of the process windows in Figures 4.12 b-d when applicable. It can be seen that the calculated optimum welding speed lines in Figures 4.12a-d from this study are overall consistent with the experimental results

Conclusions

This paper presented a refined shear localization model incorporating both pin/workpiece contact phenomena and three-dimensional (3D) heat flow environment generated by heating between tool shoulder and workpiece. The model represents the following major advancements for attaining capabilities in FSW window estimation:

(a) A new analytical based 3D transient heat flow solution that captures detailed spatial resolution of friction heat generation and dissipation as stir tool shoulder rotates in angular direction and translate welding direction. The resulting temperature distribution clearly indicates temperature differences between advancing and retreating sides

(b) A contact mechanics model is introduced to capture detailed interactions between pin and workpiece at interface, which enables a direct estimation of welding torque required under a given set of welding parameters

(c) As a result, the refined shear localization model is capable of estimating temperature profile in workpiece in front of pin and resulting welding torque, in addition to providing detailed information how shear localization develops and shear band size, which allows an improved understanding on weld formation mechanisms in FSW

(d) A robust numerical algorithm is also developed for using the refined shear localization model in evaluation of the optimum combination of pin rotational speed and welding speed to ensure a quality weld in FSW, as validated using available experimental data.

Table 4-1: FSW joint performed by Pilchak et al.[27] and Edwards and Ramulu [36] and tested against by proposed shear localization model

Data Source	ω (rpm)	V_T(mm/min)	F_z(kN)	$R_{shoulder}$(mm)	R_{pin}(mm)	h_{pin}(mm)
Pilchak [23]	120	50.8	33	12.7	7.85	9.91
Pilchak [23]	150	50.8	17	12.7	7.85	9.91
Pilchak [23]	200	50.8	8	12.7	7.85	9.91
Pilchak [23]	400	101.6	5	12.7	7.85	9.91
Pilchak [23]	800	203.2	7	12.7	7.85	9.91
Edwards[32]	200	100	45	12.5	7.5	6
Edwards[32]	300	100	15	12.5	7.5	6
Edwards[32]	400	100	10	12.5	7.5	6
Edwards[32]	300	50	12	12.5	7.5	6
Edwards[32]	300	150	20	12.5	7.5	6

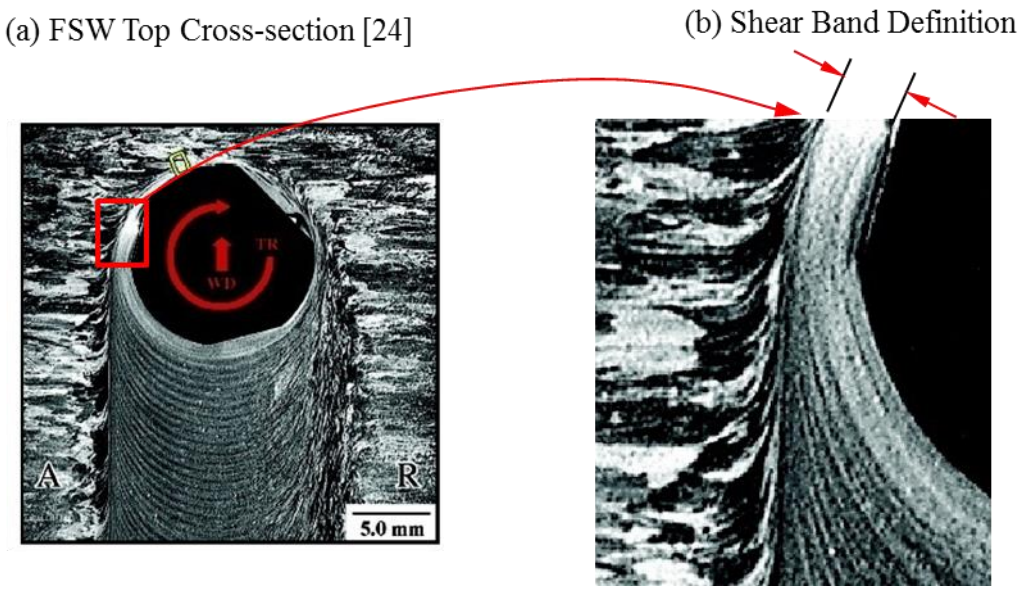

Figure 4.1: Typical band structure in a friction stir weld (picture from [24]) and shear band definition for computational treatment: (a) FSW top cross section and (b) shear band definition.

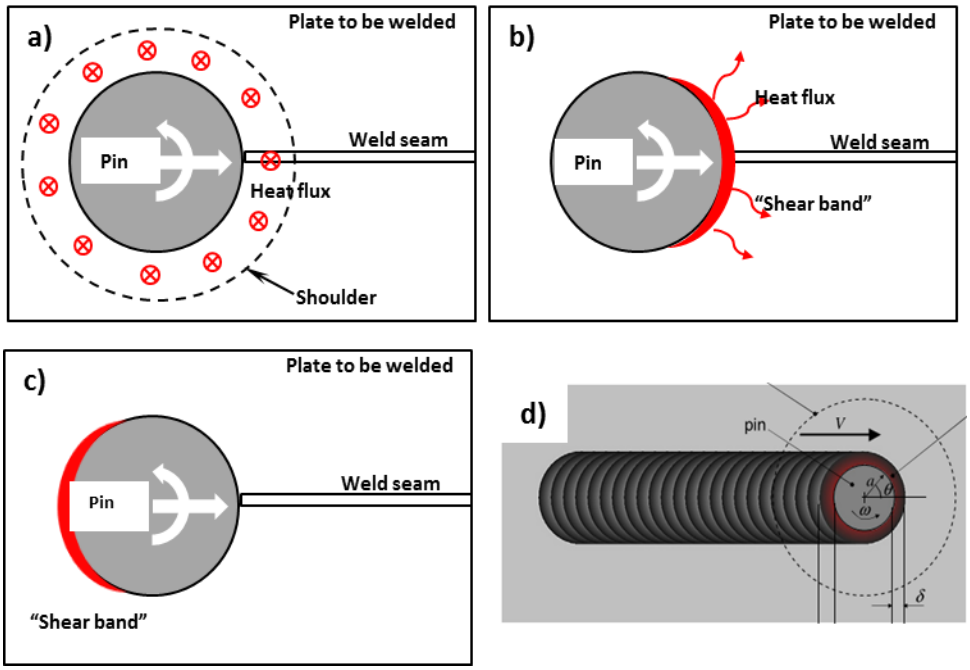

Figure 4.2: Four stages to form a FSW joint: (a) Shoulder/workpiecel interface heating and 3D heat conduction; (b) Pin/workpiece interface sliding and sticking – shear localization; (c) In-plane (2D) Shear flow and band rotation; (d) Formation of banded structure through consecutive shear bands of δ in width

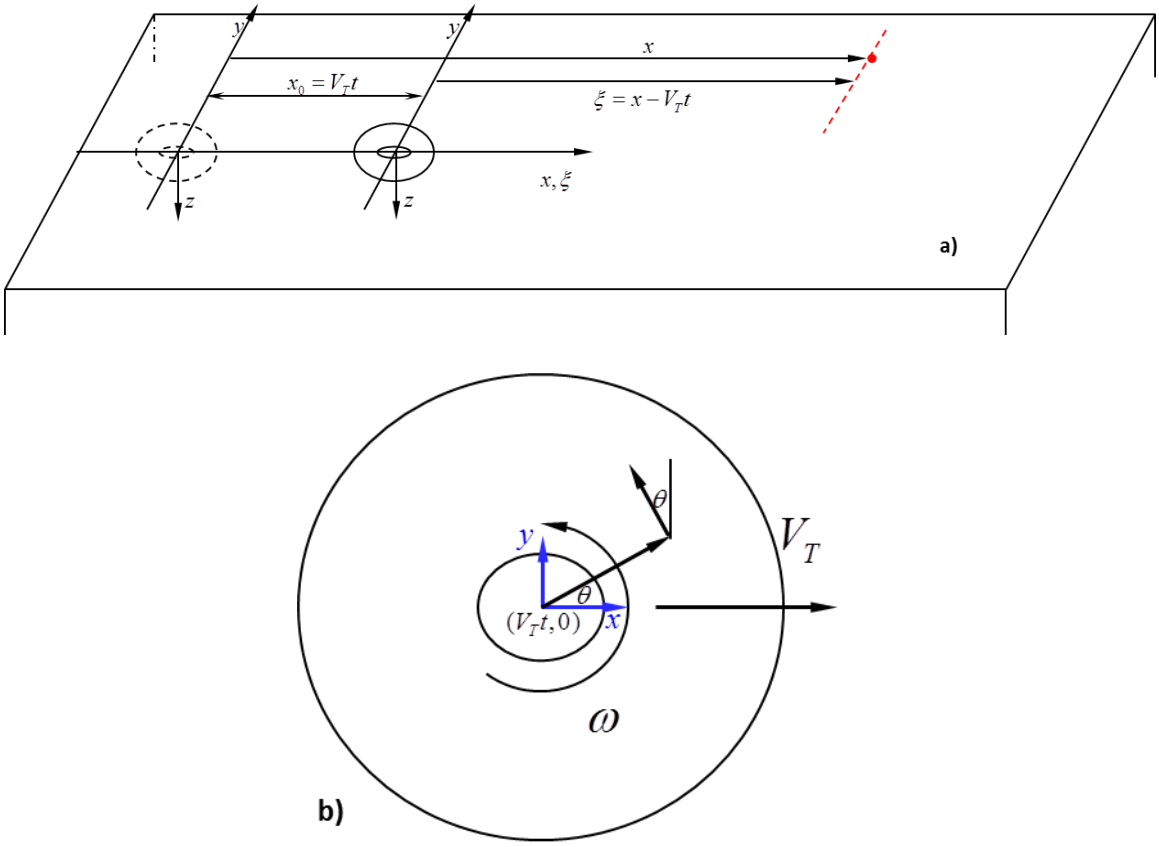

Figure 4.3: Definition of 3D transient heating conduction problem due to shoulder/material interface friction heating (a) global coordinate definition (b) local coordinate system under shoulder

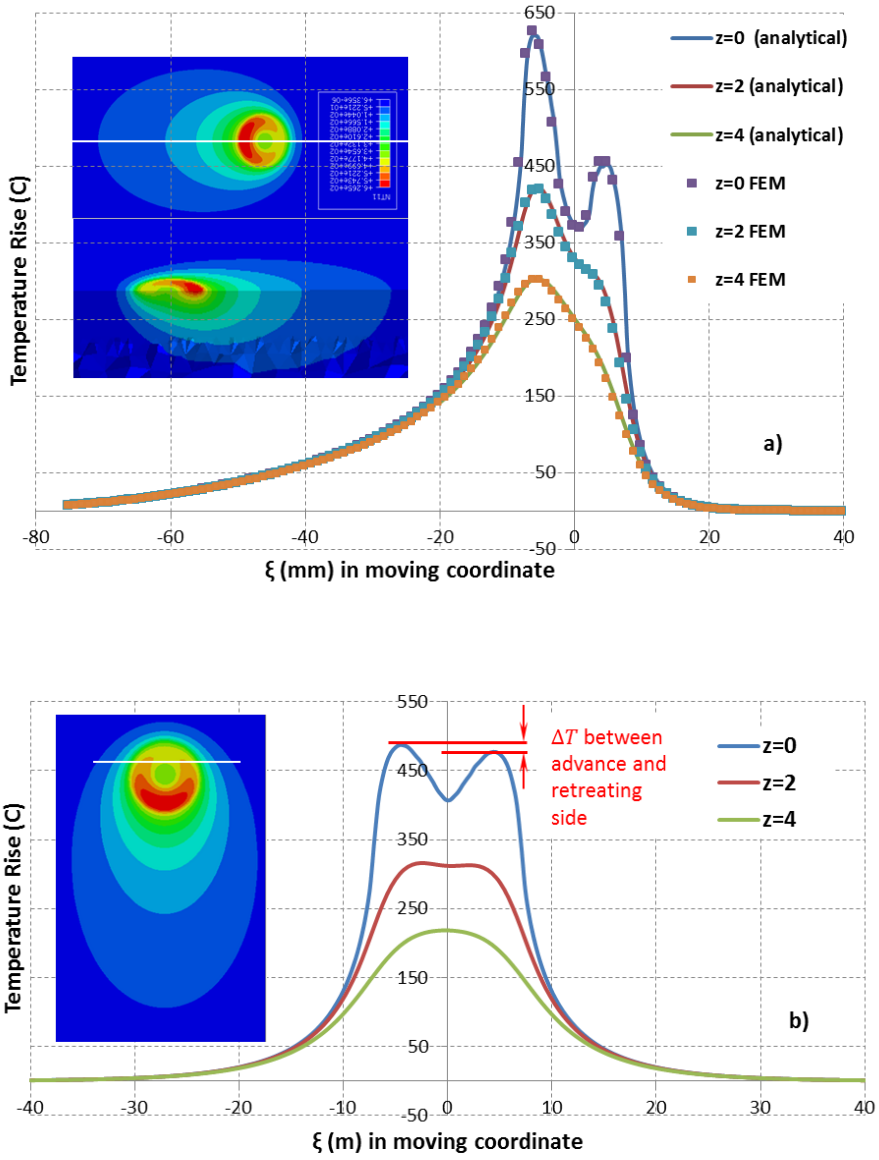

Figure 4.4: Comparison of transient temperature distributions at three depths between analytical (Eq. 9) and 3D finite element solutions for a plate of 50mm in thickness (a) longituditional cross-section (b) transverse cross-section

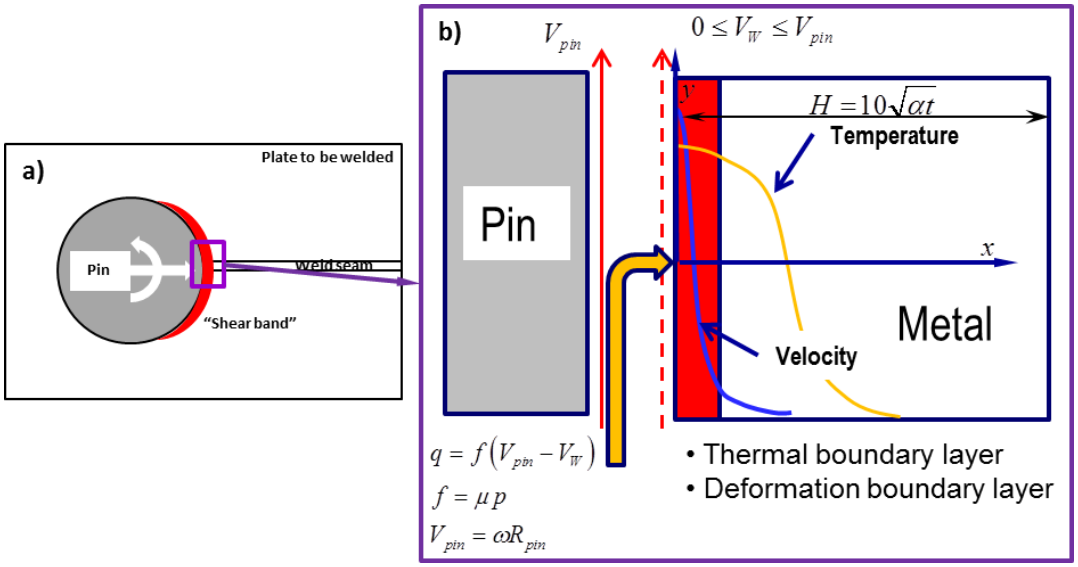

Figure 4.5: Problem definition for pin/workpiece interaction and shear localization: (a) Interaction between the pin and workpiece; (b) 1D thermal and deformation boundary layer problem definition

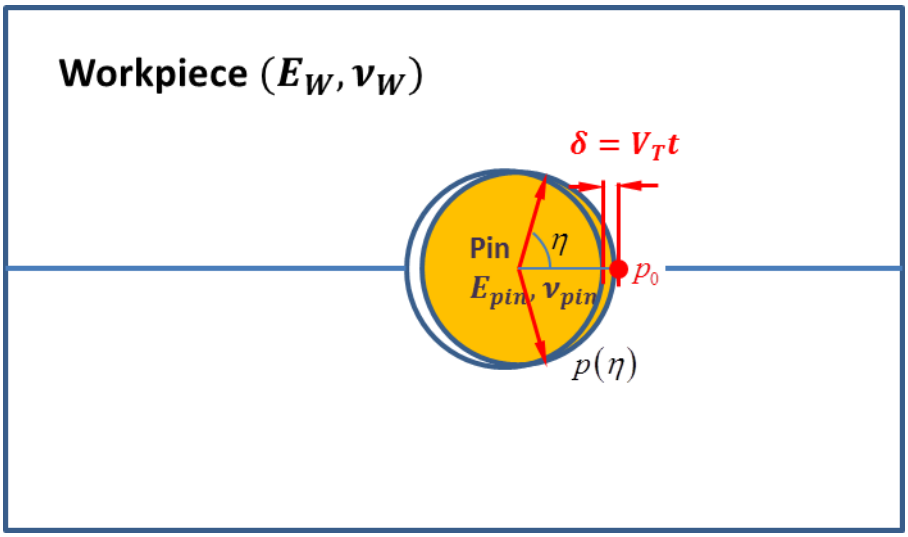

Figure 4.6: Schematically illustration of contact pressure between pin and workpiece

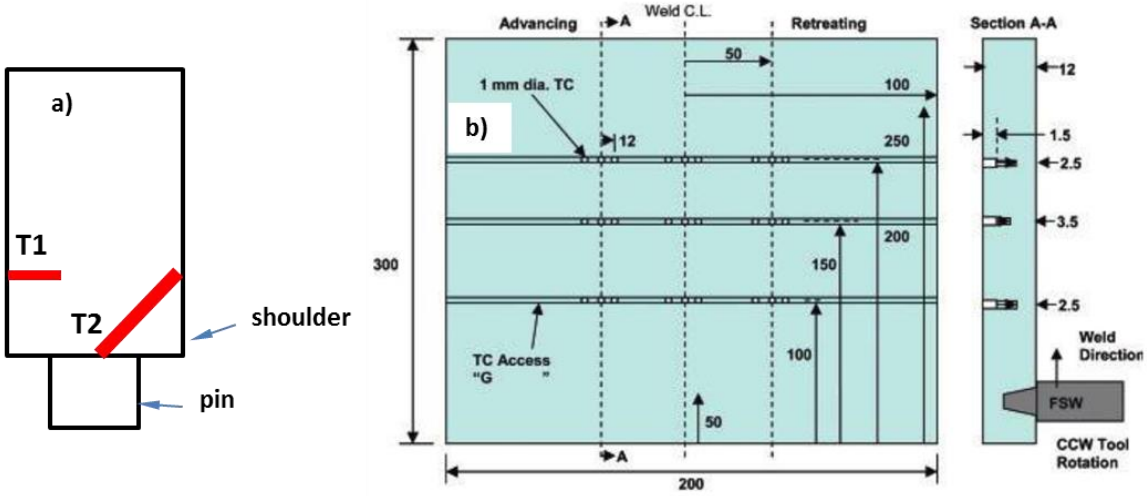

Figure 4.7: Schematic of temperature measurement in FSW experiment performed by different author: (a) Plichak et al.[27] (b) Edwards and Ramulu [40]

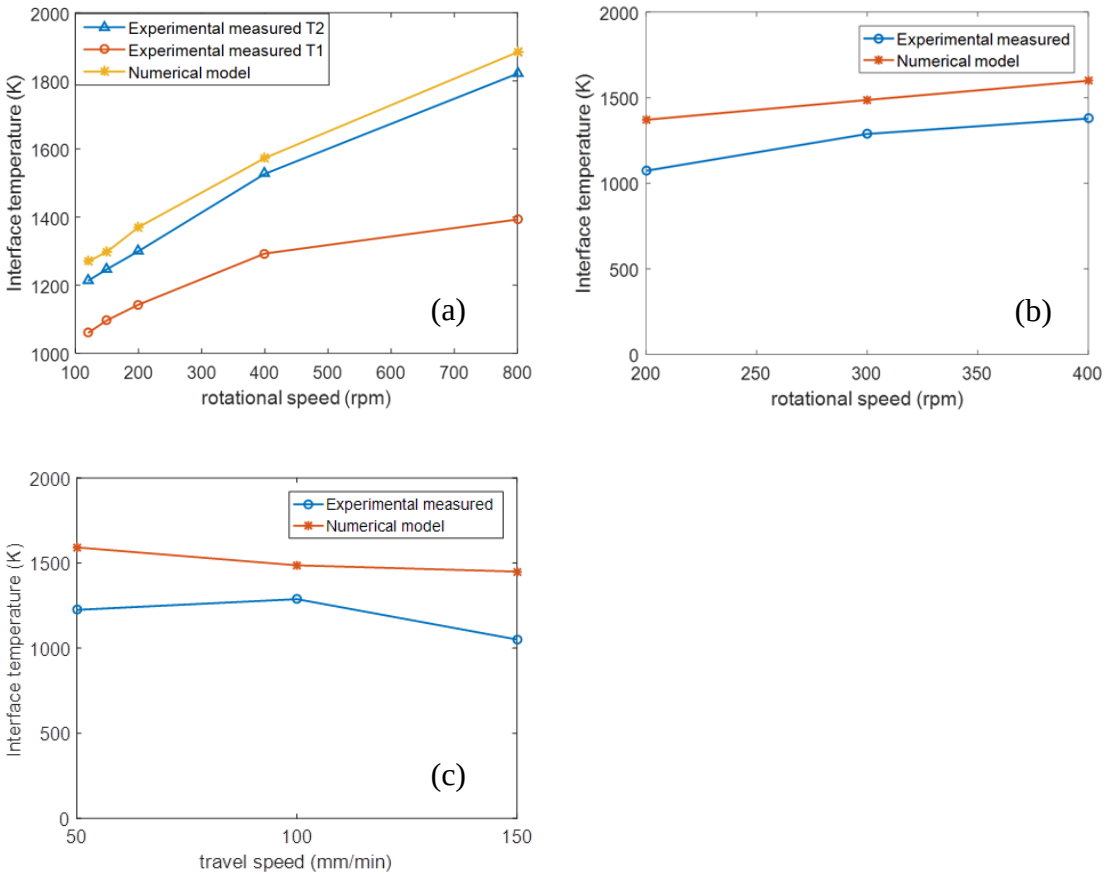

Figure 4.8: Comparison of model predicted temperature with experimental measured temperature: (a) Plichak et al.[27] (b) Edwards and Ramulu [40] different rotational speed (c) Edwards and Ramulu [35] different travel speed.

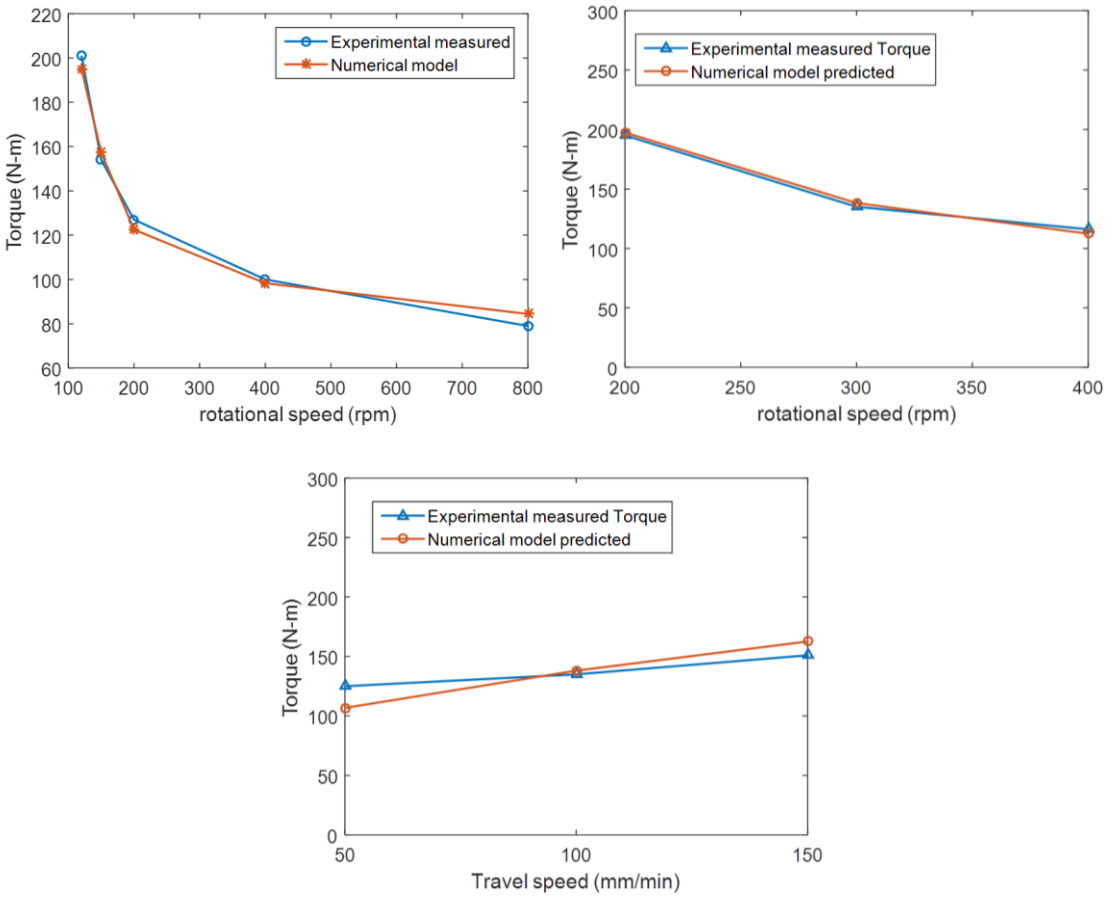

Figure 4.9: Comparison of model predicted torque with experimental measured temperature: (a) Plichak et al.[23] (b) Edwards and Ramulu [35] different rotational speed (c) Edwards and Ramulu [35] different travel speed

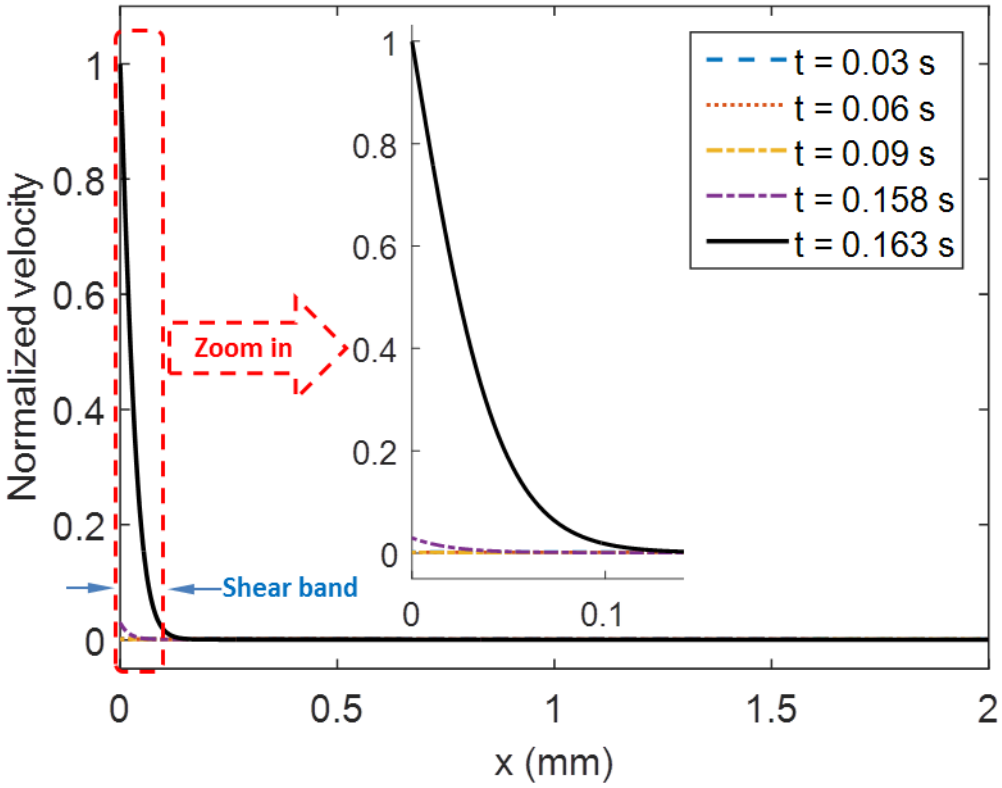

Figure 4.10: Velocity profile at different time and illustration of shear band definition

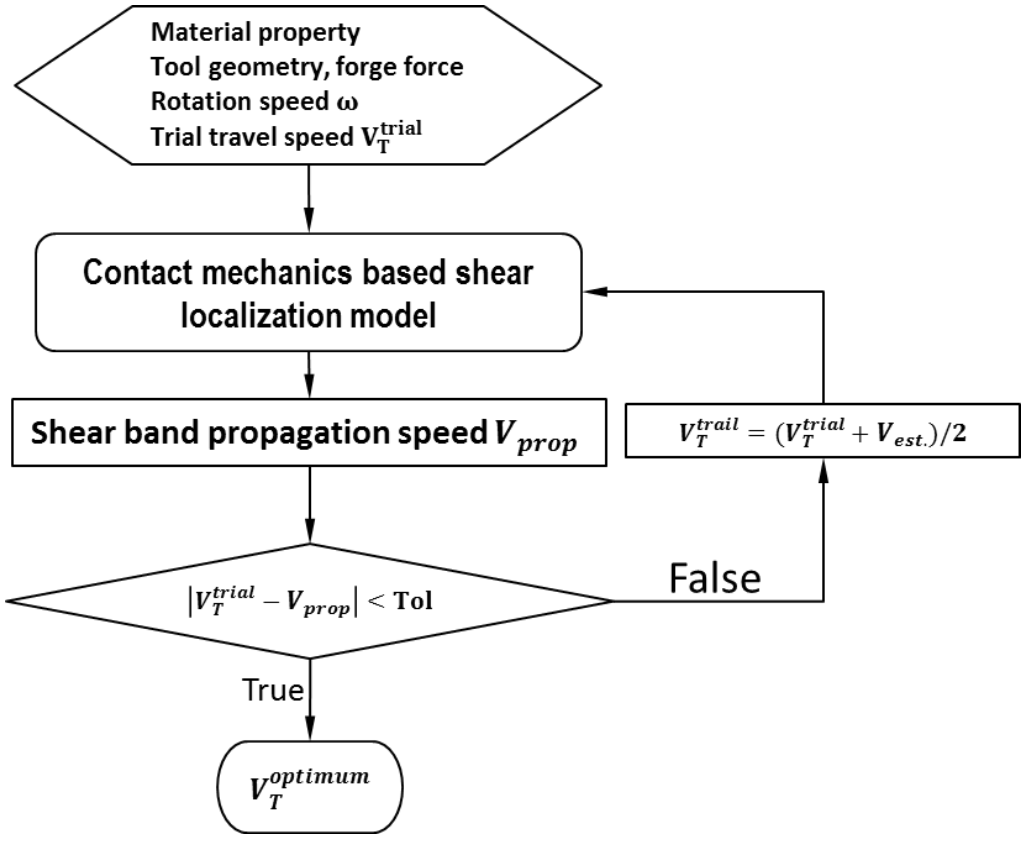

Figure 4.11: Algorithm to estimate optimum combination of travel speed and rotational speed based on shear localization model

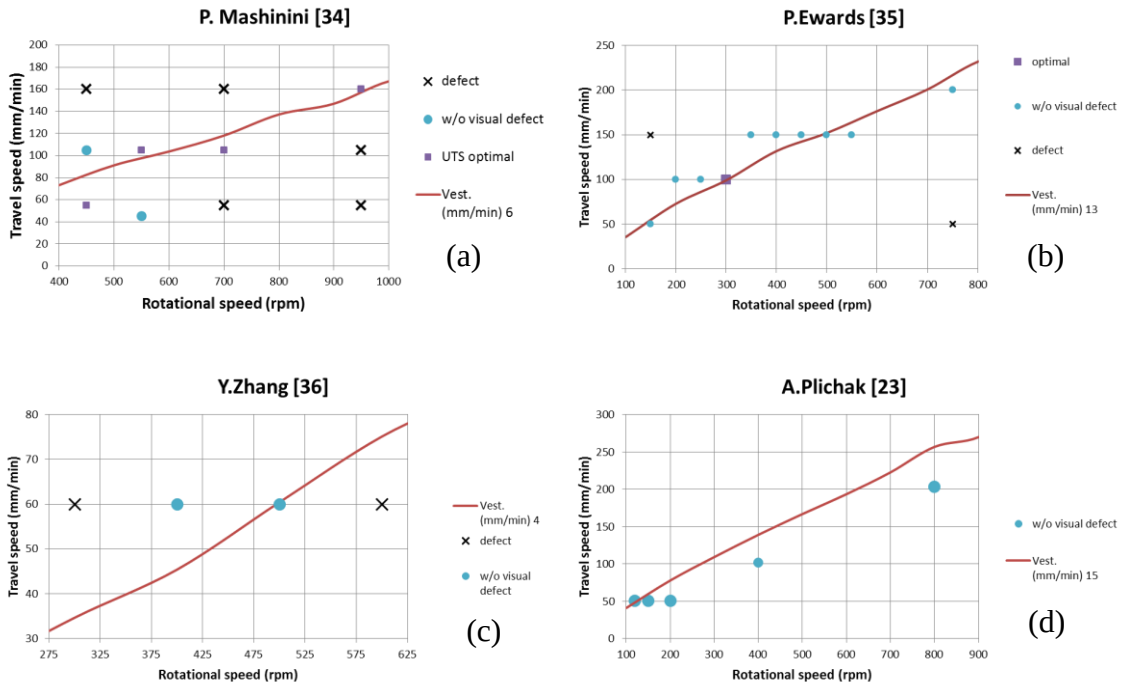

Figure 4.12: Comparison of predicted process line with experimental data: (a) Mashinini [34] (b) Ewards [35] (c) Zhang [36] d) Plichak [23]

References

[1] Thomas, W. M., and E. D. Nicholas. "Friction stir welding for the transportation industries." Materials & Design 18.4 (1997): 269-273.

[2] Nandan, R., T. DebRoy, and H. K. D. H. Bhadeshia. "Recent advances in friction-stir welding–process, weldment structure and properties." Progress in Materials Science 53.6 (2008): 980-1023.

[3] Mishra, Rajiv S., and Z. Y. Ma. "Friction stir welding and processing." Materials Science and Engineering: R: Reports 50.1 (2005): 1-78.

[4] Nandan, R., T. DebRoy, and H. K. D. H. Bhadeshia. "Recent advances in friction-stir welding–process, weldment structure and properties." Progress in Materials Science 53.6 (2008): 980-1023.

[5] He, Xiaocong, Fengshou Gu, and Andrew Ball. "A review of numerical analysis of friction stir welding." Progress in Materials Science 65 (2014): 1-66.

[6] Gould, Jerry E., and Zhili Feng. "Heat flow model for friction stir welding of aluminum alloys." Journal of Materials Processing and Manufacturing Science 7

(1998): 185-194.
[7] Vilaça, Pedro, Luísa Quintino, and Jorge F. dos Santos. "iSTIR—analytical thermal model for friction stir welding." Journal of Materials Processing Technology 169.3 (2005): 452-465.
[8] Schmidt, H., and J. Hattel. "Modelling heat flow around tool probe in friction stir welding." Science and Technology of Welding and Joining 10.2 (2005): 176-186.
[9] Schmidt, Henrik B., and Jesper H. Hattel. "Thermal modelling of friction stir welding." Scripta Materialia 58.5 (2008): 332-337.
[10] Chao, Yuh J., X. Qi, and W. Tang. "Heat transfer in friction stir welding-experimental and numerical studies." TRANSACTIONS-AMERICAN SOCIETY OF MECHANICAL ENGINEERS JOURNAL OF MANUFACTURING SCIENCE AND ENGINEERING 125.1 (2003): 138-145.
[11] Schmidt, Henrik Nikolaj Blich, and Jesper Hattel. "An analytical model for prescribing the flow around the tool probe in friction stir welding." (2005).
[12] Nunes Jr, Arthur C. "Metal flow in friction stir welding." (2006).
[13] Reynolds, Anthony P. "Flow visualization and simulation in FSW." Scripta materialia 58.5 (2008): 338-342.
[14] Colegrove, Paul A., and Hugh R. Shercliff. "3-Dimensional CFD modelling of flow round a threaded friction stir welding tool profile." Journal of Materials Processing Technology 169.2 (2005): 320-327.
[15] Nandan, R., G. G. Roy, and T. Debroy. "Numerical simulation of three-dimensional heat transfer and plastic flow during friction stir welding." Metallurgical and materials transactions A 37.4 (2006): 1247-1259.
[16] Nandan, R., et al. "Three-dimensional heat and material flow during friction stir welding of mild steel." Acta Materialia 55.3 (2007): 883-895.
[17] Nandan, R., et al. "Numerical modelling of 3D plastic flow and heat transfer during friction stir welding of stainless steel." Science and Technology of Welding and Joining 11.5 (2006): 526-537.
[18] Arbegast, William J. "Modeling friction stir joining as a metalworking process." Proceedings of Hot Deformation of Aluminum Alloys III (2003): 313-327.
[19] Arora, A., A. De, and T. DebRoy. "Toward optimum friction stir welding tool shoulder diameter." Scripta materialia 64.1 (2011): 9-12.
[20] Qian, Jinwen, et al. "An analytical model to optimize rotation speed and travel speed of friction stir welding for defect-free joints." Scripta Materialia 68.3 (2013): 175-178.
[21] Pei, X. J., and P. S. Dong. "Shear localisation modelling of friction stir weld formation process." Science and Technology of Welding and Joining 19.5 (2014): 416-426.
[22] Pei, Xianjun, and Pingsha Dong. "Modeling of banded structure in friction stir weld in strain rate–hardening materials of Zener–Hollomon type." The Journal of Strain Analysis for Engineering Design 50.3 (2015): 175-189.
[23] Dong, P., et al. "A math-based design-for-produceability evaluation of titanium applications in ship hull structures." Transactions-Society of Naval Architects and Marine Engineers 120.1 (2013): 299-305.
[24] Fonda, R. W., J. F. Bingert, and K. J. Colligan. "Development of grain structure

during friction stir welding." Scripta Materialia 51.3 (2004): 243-248.
[25] Yang, Bangcheng, et al. "Banded microstructure in AA2024-T351 and AA2524-T351 aluminum friction stir welds: Part I. Metallurgical studies." Materials Science and Engineering: A 364.1 (2004): 55-65.
[26] Knipling, K. E., and R. W. Fonda. "Texture development in the stir zone of near-α titanium friction stir welds." Scripta materialia 60.12 (2009): 1097-1100.
[27] Pilchak, A. L., et al. "Microstructure evolution during friction stir welding of mill-annealed Ti-6Al-4V." Metallurgical and Materials Transactions A 42.3 (2011): 745-762.
[28] Wei, Zhigang, and R. C. Batra. "Modeling and simulation of high speed sliding." International Journal of Impact Engineering 37.12 (2010): 1197-1206.
[29] Radaj, Dieter. Heat effects of welding: temperature field, residual stress, distortion. Springer Science & Business Media, 2012.
[30] Hibbit Karlson and Sorensen Inc 2003 ABAQUS Version 6.12
[31] Batra, R. C., and Z. G. Wei. "Shear bands due to heat flux prescribed at boundaries." International journal of plasticity 22.1 (2006): 1-15.
[32] Sellars, C. M., and WJ McG Tegart. "Hot workability." International Metallurgical Reviews (2013).
[33] Johnson, Kenneth Langstreth, and Kenneth Langstreth Johnson. Contact mechanics. Cambridge university press, 1987.
[34] Guide, MATLAB User'S. "The mathworks." Inc., Natick, MA 5 (1998): 333.
[35] Skeel, Robert D., and Martin Berzins. "A method for the spatial discretization of parabolic equations in one space variable." SIAM journal on scientific and statistical computing 11.1 (1990): 1-32.
[36] Edwards, P., and M. Ramulu. "Peak temperatures during friction stir welding of Ti–6Al–4V." Science and Technology of Welding and Joining 15.6 (2010): 468-472.
[37] Krishnan, K. N. "On the formation of onion rings in friction stir welds." Materials science and engineering: A 327.2 (2002): 246-251.
[38] Pei, X. J., and P. S. Dong. "A selectively-coupled shear localization model for friction stir welding process window estimation." preparing.
[39] Mashinini, Peter Madindwa. Process window for friction stir welding of 3 mm titanium (Ti-6Al-4V). Diss. 2011.
[40] Edwards, P., and M. Ramulu. "Effect of process conditions on superplastic forming behaviour in Ti–6Al–4V friction stir welds." Science and technology of welding and joining 14.7 (2009): 669-680.
[41] Zhang, Yu, et al. "Microstructural characteristics and mechanical properties of Ti–6Al–4V friction stir welds." Materials Science and Engineering: A 485.1 (2008): 448-455.

Chapter 5 A Selectively-Coupled Shear Localization Model for Friction Stir Welding Process Window Estimation

Abstract

This paper presents a novel computational modeling procedure for studying the joint formation mechanism in friction stir welding (FSW). The proposed model combines three-dimensional (3D) transient heating with one-dimensional shear localization process for simulating band structure formation process of FSW, in which shear band width estimation must satisfy both mass conservation and plastic flow continuity conditions formulated in a two-dimensional configuration. Any deviations from the latter conditions can be attributed to certain types of defect formatted during welding, which can be mechanistically attributed to common references to defect types such as “lack of fill”, “abnormal stirring”, “surface galling”, and “excessive flash”, etc. As a result, the selectively-coupled shear localization model can be used for estimating FSW process window in terms of welding speed and stir tool rotation speed for a given application, which can be further refined in a cost-effective manner by significantly reducing the needs for a full-blown Design of Experiments (DoE). To demonstrate this capability, the model is exercised for three types for aluminum alloys on which process windows were determined through DoE and published by various investigators. The theoretically estimated process windows are in good agreement with experimental results.

Introduction

Friction stir welding (FSW) has numerous advantages over conventional fusion processes, particularly for joining metals or dissimilar metals that are difficult to weld with traditional methods [1,2], which has been viewed as a key enabler for achieving structural lightweighting [2,3]. However, FSW process development for a given application, i.e., establishing a process window in terms of welding travel speed and pin rotation speed, relies largely on empirical process, typically requiring detailed Design of Experiments (DoE) which can be rather time-consuming and costly. Once developed, it may not be transferrable to conditions where there may be only some minor changes in joint configuration, material selection, plate or sheet thickness. Although a plenty of numerical models for FSW have been proposed or attempted over the last two decades, only few efforts were made in the development of effective computational modeling procedures which can be used to establish an approximate description of process window and associated key process parameters [4]. This kind of model with the capability to estimate process window based on unique physics associate with FSW is highly desired. Then, selected welding trials can be used to confirm and finalize the process window for final adoption of an actual application. Due to multi-physics and multi-scale mechanics nature associated with FSW process [2,5], an effective modeling procedure aimed at constructing process window, particularly for practical applications, should focus on capturing most relevant phenomena to weld formation process during FSW and simplifying other aspects of the process details. To identify what phenomena can be considered most relevant to weld formation process, results and insights gained by

numerous past investigations into various aspects of FSW process physics and mechanics will be highlighted and credited as a basis from which this study is built upon.

Based on experimental observations of various aspects of FSW process, mathematical modeling procedures reported in the literature may be characterized by the following general categories with a varying degree of complexity in two or three dimensional (2D or 3D): (a) conduction heat transfer models with equivalent frictional heat flux [e.g., 6-10]; (b) material flow models based on experimental observation [e.g., 11,12] , using knowledge of fluid mechanics[e.g. 13-15], or stemmed from an analogy with metalworking such as extrusion [16,17] or metal cutting [18,19]; (c) fully-coupled thermo-viscoplasticity flow models [e.g. 20-29]. A detailed review of some of these modeling methods and their impacts on improved understanding of weld formation process has been recently given by He et al. [5].

Another type of FSW modeling is the use of simplified models with reduced dimensions (e.g. 1D model) for certain aspects of FSW process, which can greatly simplify computational procedures particularly when multi-physics coupling effects are considered [e.g. 4, 30-32]. This simplification is extremely necessary when the numerical model is used to identify group of welding parameters for engineer application, since an appropriate 1D model can reduce computational time tremendously while capture the key features of FSW. One example along this line is the one dimensional (1D) model introduced by Qian et al [4] in which optimum combination of rotation speed and travel speed was estimated based on balance of material flow at a favorable temperature. Another example is the 1D model developed by Mendez et al [30] which couples heat transport and localized plastic flow within a thin shear layer around pin once a

characteristic temperature is reached. The resulting expressions were not only consistent with experimentally observed trends for cases investigated, but also offer a functional relationship among process and material parameters which can be used for speeding up process window development efforts.

The thin shear layer considered by Mendez et al. [30] was intended to represent a typical band width in banded structure that are uniquely associated with a quality FSW of high strength aluminum alloy, as shown Figure 5.1 [33-35] for illustration purpose, which can be shown being formed through a shear localization process discussed by Pei and Dong [31,32]. Recognizing the importance of shear banding characteristics, Nunes [19,20], by-passing heat transport model, directly introduced a rotational plug model which assumes a predetermined shear layer rotating with stir pin in the context of rigid plasticity, leading to a rather useful torque to rotational speed relationship for supporting process window development. However, the formation process of these band structures remains to be taken considered in these simplified models with reduced dimensions.

Therefore, an improved understanding of conditions under which desirable band structures are formed and their relationship to weld quality becomes critically important for process window estimation. As evidence, Schneider and Nunes [36] and Yang et al. [37] showed experimentally that localized plastic flow phenomena in form of band structures govern weld formation process in studying FSW of high strength aluminum alloys. Knipling and Fonda [38] and Pilchak et al. [39] concluded the same in studying FSW of titanium alloys. As shown in Figure 1, the band structures can be characterized as a series of overlapping near-circular ring bands approximately equally spaced corresponding to stir pin advance per revolution [34-35,40]. Guerra et al. [41] observed

that material within band region experienced a rotation of approximately the same velocity as that of stir pin (i.e. reaching to sticking condition at pin/material interface). These experimental observations seem to point to one important finding that nearly all defect-free welds tend to exhibit well-defined banded structures, such as the one shown in Figure 5.1.

Then, the question becomes how material in a banded region get accelerated from its initial stationary state during friction stage to sticking condition, and deformed into well-defined bands. Among numerous investigators, Chen [42] pointed out that band structure is formed as a result of localized forging and subsequent sweeping by the flank of stir pin into cavity created by advancing pin. Krishnan [40] further postulated that each bands is formed thorough a cylindrical extrusion process for material between advancing pin and base material within each pin revolution. Meanwhile there exists a short dwell time, presumably for friction heat to build up to a required level before next extrusion event corresponding to next pin revolution. Nunes [19,20] compared this type of band formation process seen in FSW as being similar to that in metal cutting and argued that because of the unique character of metal deformation in terms of banded structure, a velocity "discontinuity" occurs in FSW and determines much of the character of the welding mechanism. Xu and Deng [43] studied texture patterns of AA6061 FSW welds both experimentally and numerically. They found that texture patterns observed correlate well with equivalent plastic strain contours obtained from their finite element model, suggesting that texture patterns were formed though a high level plastic deformation.

Most of the existing modeling approaches discussed above, as far as band

structures are concerned, treat shear banding (e.g., band width) either as a known a priori through experimental observations [e.g.,19,20] or as a kinematic flow phenomenon [e.g. 20-29,43]. To the authors' best knowledge, little modeling work has been done in elucidating how these band structures are formed during FSW. Pei and Dong [31,32] attempted to model the formation process of these band structures using a 1D shear localization model with some rather interesting findings. They found that material constitutive model of Sellars-Tegart type is more suitable for modeling shear band formation process than Johnson-Cook type of model. They were able to estimate shear band width and its formation time, therefore, shear band propagation speed or welding speed for a given application under rather idealized 1D condition, which is not capable to provide any planar information on shear banding.

In the present work, we first present an integrated shear localization model which has the following three components: (a) 3D analytical based transient heat transport model; (b) 1D finite element based shear localization model; (c) 2D analytical shear flow kinematic model, which are coupled in a selective manner. This modeling scheme takes advantage of computational efficiency demonstrated in authors' 1D shear localization model while giving adequate considerations of coupled interactions among transient friction heating resulted from tool shoulder/pin and workpiece interface, rapid shear localization within a thermal and deformation boundary layer and shear band formation after sticking conditions are reached, and subsequent shear flow or velocity distribution in a 2D configuration. The latter allows the estimation of a defective weld as result of insufficient heat input, or abnormal stirring, or surface galling etc. Finally, the model is implemented for estimating FSW process windows for joining a series of aluminum

alloys including AA2024 [4,44], AA2219[45] and AA6061[46], on which experimentally determined process windows are available for validation purposes. A good agreement between the model estimated and experimentally determined process windows has been achieved.

Model Construct

Based on the assessment of existing experimental investigation and computational modeling results discussed in the previous section, a model construct that is capable of capturing essential aspects of weld formation process while offering a reasonable level of simplicity and computational efficiency is proposed here by considering the following (see Figure 5.2):

(a) Shoulder/workpiece friction heating and 3D transient heat conduction: As illustrated in Figure 5.2a, existing research efforts (see [30]) have shown that tool shoulder/material interface friction heating and its subsequent heat transport in work piece creates a thermal environment around stir zone, which directly influences shear localization process through pin/material interaction. As a result, 3D temperature distribution must be estimated with a sufficient detail, based on which pin/workpiece interaction is further studied.

(b) Pin/workpiece interface friction heating and shear localization from sliding to sticking: As demonstrated by a number of researchers [4,30-32], under rather high strain rate conditions typical of friction stir welding processes, both thermal and deformation boundary layer phenomena can be introduced so that a 1D shear localization model can be effectively used to capture plastic dissipation dominated

shear localization and shear band formation process from pin/workpiece interfacing sliding up to sticking, as illustrated in Figure 5.2b. That is, other than friction between shoulder and workpiece, the frictional stress between the tool pin and workpiece also provides additional heat flux into the layer of material just in front of the pin (Figure 5.2b). This layer of metal (the red band in Figure 5.2b) is softened by the 2 heating effects aforementioned. Driven by the frictional stress between the pin and workpiece, the softened material just in front of the pin is accelerated from static to the pin tangential velocity, i.e. ωR_{pin} which is known as sliding until sticking stage.

(c) Shear band rotation and in-plane (2D) material flow continuity: Once sticking condition at pin/workpiece interface is attained, material within the shear layer metal (the red band in Figure 5.2b-c) is swapped to the back of the pin to fill the space left by the advance of the tool (Figure 5.2c). During this stage, material velocity within a shear band must satisfy continuity and mass conservation conditions. To the first approximation, 2D rotational material flow within shear band is assumed here, which has been shown to provide a reasonable estimation on weld formation process [12,13,19], through a series of successively formed shear bands as shown in Figure 5.2d.

In what follows, the three parts of the model construct and their coupling in a selectively manner for estimating conditions that are required for forming a quality weld as illustrate in Figure 5.2d are presented.

5.1.1 Shoulder friction heating and 3D heat transport

In order to efficiently estimate 3D transient temperature environment generated by friction heating between stir tool shoulder and workpiece, in which pin/material interactions lead to shear localization and subsequent shear band formation, an analytical solution is sought, with the following assumptions and simplifications: 1) Material properties are independent of temperature, which results in a linear heat conduction problem; 2) Heat loss into the tool shoulder is considered while heat loss into ambient is assumed negligible within a time scale of shear localization considered here [31,32]; 3) Heat loss through contact/gap conduction into the workpiece back plate can be approximated as an equivalent conduction process as if the workpiece is extended beyond its thickness encompassing back plate and fixture support. Thus, the above simplifications and assumptions lead to a 3D linear transient heat transfer problem defined in a semi-infinite body, as illustrated in Figure 5.3.

Consider that a stir tool shoulder is centered at $(0,0,0)$ at time $t = 0$ with respect to the coordinate system (x, y, z) shown in Figure 5.3. Once the tool starts to move with a travel velocity V_T, the center of tool shoulder can be tracked as $(V_T t, 0)$, with respect to which heat flux generated through friction between shoulder and workpiece can then be expressed as:

$$q(\xi, y) = \begin{cases} \beta\mu p_s \sqrt{(V_T - \omega y)^2 + (\omega\xi)^2} & \left(R_{pin} \le \sqrt{\xi^2 + y^2} \le R_s\right) \\ 0 & (otherwise) \end{cases} \tag{4.21}$$

In Eq.(4.21), ω represents angular rotational velocity of the shoulder, while μ is friction coefficient between workpiece and the shoulder, and p_s is the pressure exerted by the

shoulder against the workpiece. Note that p_s can be estimate by:

$$p_s = \frac{F_z}{\pi\left(D_s^2 - D_{pin}^2\right)/4} \tag{4.22}$$

where F_z is the axial thrust force (forging load) of the shoulder against workpice, while D_{pin} and D_s represent the outer diameters of the stir pin and the shoulder, respectively. Total heat flux generated through Eq. (4.21) is partitioned between shoulder and workpiece through a constant β, expressed as [47]:

$$\beta = \frac{k_s\sqrt{\alpha_m}}{k_s\sqrt{\alpha_m} + k_m\sqrt{\alpha_s}} \tag{4.23}$$

Here k and α are thermal conductivities and thermal diffusivities of shoulder and workpiece materials, designated by subscripts s and m, respectively.

It should be pointed out here that the above formulation on fiction heat generation in the form of Eq. (4.21) not only captures the bulk heat generation resulted from rotational friction between shoulder and workpiece at angular rotational speed ω and linear friction along welding direction at welding speed V_T, but also provides a detailed spatial resolution on friction heating and subsequent transient conduction as the shoulder rotates with respect to its own axis, which is essential for differentiating shoulder advancing side from its retreating side . The latter has not been addressed in existing analytical models in the literature such as presented in [6] to our best knowledge.

The governing equation with respect to the coordinate system given in Figure 5.3 can be written as:

$$\frac{\partial T}{\partial t} = \frac{k}{C_p\rho}\left(\frac{\partial^2 T}{\partial x^2} + \frac{\partial^2 T}{\partial y^2} + \frac{\partial^2 T}{\partial z^2}\right) \tag{4.24}$$

where k, C_p and ρ are thermal conductivity, specific heat capacity and density of workpiece material. The above differential equation can be analytically solved using Green function and method of superposition, as presented in [48], which involves a detailed derivation process that is too lengthy to be included here due to space limitation. The resulting transient temperature solution as a function of position and time can be expressed as:

$$T(\xi,y,z,t)=\int_0^t \frac{2}{\rho c\left[4\pi\alpha t"\right]^{3/2}}\left\{\int_{-R}^{R}\int_{-\sqrt{R^2-\xi'^2}}^{\sqrt{R^2-\xi'^2}} q(\xi',y')\exp\left(-\frac{(\xi-\xi'+V_T t")^2+(y-y')^2+z^2}{4\alpha t"}\right)dy'd\xi'\right\}dt"+T_0 \quad (4.25)$$

It is worth emphasizing the analytical solution given in Eq.(4.25) captures transient temperature development distribution and provides spatial resolution of friction heating as the shoulder rotates with respect to its own axis while traveling in welding direction. Existing analytical solutions in the literature (e.g., given in [6]) only provided quasi-steady state temperature field by only taking into account of bulk frictional heat generation between tool shoulder.

As a validation of the assumptions used in deriving the transient analytical solution given in Eq.(4.25), a detailed 3D finite element simulation of shoulder/material friction heating and heat conduction in a finite thickness plate is performed using commercial software ABAQUS [49]. The physical domain considered in the FE model has dimensions of 250x125x50 mm in x, y, z directions, with element size of 1x1x1 mm near and within shoulder contact zone. A user subroutine is developed for modeling rotational friction heat flux generated at stir shoulder/workpiece interface as it moves along *x* axis. As can be seen in Figure 5.4, both the analytical solution (Eq.(4.25)) and 3D finite element results are in an excellent agreement at all three depths, proving the

validity of the 3D analytical solution developed. It should be noticed that there exists a noticeable temperature difference between the front and back of stir pin, which would not have been captured by existing analytical solutions (e.g., [6]). Obviously, the main advantage of the analytical solution given by Eq. (4.25) lies in the fact that it can be conveniently used for defining transient temperature environment within which shear localization process takes place. Furthermore, as to be demonstrated in a later section, this level of temperature distribution detail as a function of $\omega, V_T, F_z, D_s, D_{pin}$ through Eqs. (4.21) and (4.22) can be used to screen out some inappropriate welding conditions as boundary of a welding process window.

5.1.2 Pin/workpiece interaction and shear localization

As discussed in Pei and Dong [31,32], the interaction between the pin and workpiece leading to shear localization and shear band formation within each revolution of stir pin can be idealized as a 1D shear localization problem, as illustrated in Figure 5.5b. During sliding stage, stir pin has a constant tangential speed $V_{pin} = \omega R_{pin}$ (illustrated by solid red arrow line in Figure 5.5b), while exerting a fractional stress $f = \mu p$ in contact with the workpiece (or base metal). The resulting frictional heat flux $q = \beta f(V_{pin} - V_M)$ is consumed by the workpiece, where β is defined in the same manner as in Eq. (4.23) andV_M represents material velocity at pin/workpiece interface (illustrated by red dash arrow line in Figure 5b), which is accelerated by the rotating pin. As the friction heat builds up at base metal side of the pin/material surface, material softening occurs, resulting in a rapid development of local plastic deformation. Sliding condition terminates as relative velocity, $V_{pin} - V_M$, approaches zero, leading to sticking

stage. During sticking stage, since there exists no relative motion between pin and material at the interface, i.e. $V_M = V_{pin}$, friction-induced heating vanishes and plastic dissipation heating dominates, which further energizes the shear localization process.

The aforementioned process can be modeled by the following set of partial differential equations [50, 51,31,32]:

$$
\begin{aligned}
&\rho \frac{\partial v}{\partial t} = \frac{\partial \tau}{\partial x} \\
&\rho C_p \frac{\partial \theta}{\partial t} = k \frac{\partial^2 \theta}{\partial x^2} + \tau \frac{\partial \gamma_p}{\partial t} \\
&\frac{\partial \tau}{\partial t} = G \frac{\partial \gamma_e}{\partial t} = G\left(\frac{\partial \gamma}{\partial t} - \frac{\partial \gamma_p}{\partial t} \right) = G\left(\frac{\partial v}{\partial x} - \frac{\partial \gamma_p}{\partial t} \right) \\
&\frac{\partial \gamma_p}{\partial t} = \begin{cases} 0 \quad (Elastic) \\ A \sinh\left(\frac{\tau}{\tau_R} \right)^n \exp\left(-\frac{Q}{R\theta} \right) \quad (plastic) \end{cases}
\end{aligned}
\tag{4.26}
$$

In Eq.(4.26), ρ is the mass density, v the material tangential velocity in y direction (see Figure 5.5b), θ the temperature, τ the shear stress, γ_p plastic strain. G and C_p represent the shear modulus and specific heat capacity of the material. Eq.$(4.26)_1$ and Eq.$(4.26)_2$ represent, respectively, the balance of linear momentum and the balance of internal energy. All of plastic work, given by the second term on the right hand side of Eq. $(4.26)_2$ is converted into heating. Eq. $(4.26)_3$ is Hooke's law written in rate form, which also implies the strain-rate is partitioned into elastic and plastic parts. Eq. $(4.26)_4$ represents the material constitutive behavior modeled in the form of thermo-viscoplastic relation as proposed by Sellars and Tegart [52], in which, τ_R , n, Q, and R are material constants. The use of Sellars-Tegart constitutive equation is justified based on a number of earlier studies [20,27,53], including the study [32] by the same authors of this paper.

$$
\begin{aligned}
&v(x,0)=0\\
&\theta(x,0)=\theta_0(x)\\
&\tau(x,0)=0\\
&\gamma_p(x,0)=0
\end{aligned}
\tag{4.27}
$$

Note that here $\theta_0(x)$ is the initial temperature distribution as a result of shoulder/workpiece friction heating obtained by the 3D transient heat conduction solution described in Sec. 5.2.1. The corresponding boundary conditions during sliding friction stage can be described as follows:

$$
\begin{aligned}
&-k\left.\frac{\partial\theta}{\partial x}\right|_{x=0}=\beta f(t)\left(V_{pin}-v\right)\\
&\tau\big|_{x=0}=f(t)=\mu p(t)\\
&v\big|_{x=R_s}=0\\
&\theta\big|_{x=H}=\theta_r
\end{aligned}
\tag{4.28}
$$

Eq. $(4.28)_1$ represents heat flux into material from the interface due to friction heating between pin and workpiece. Eq.$(4.28)_2$ describe the traction boundary condition, i.e., shear stress at pin/workpiece interface should be the same as friction stress, for which Coulomb's friction law is assumed. In Eq.(4.28), $p(t)$ represents contact pressure between pin and workpiece, which can be described as:

$$
p(t)=\frac{E^*}{2}\sqrt{\frac{V_T t}{R_{pin}}\left(1-\frac{1}{R_{hole}/R_{pin}}\right)}
\tag{4.29}
$$

by considering a pin (with a radius of R_{pin}) being situated inside a cylindrical wall (with a radius of R_{hole}) [54]. In Eq.(4.29), E^* is an effective modulus of elasticity, representing linearized pin/workpiece interaction.

At certain distance away from pin/workpiece interface, material in workpiece can

be assumed to remain stationary (see Figure 5.1) throughout the deformation process, such as at outer edge of the shoulder, i.e., $v|_{x=R_s} = 0$, where R_s represents shoulder radius. Since shear localization process in the present modeling context is investigated within a very short timeframe corresponding one revolution of stir pin, a characteristic distance, H, can be identified, at which adiabatic conditions can be assumed, i.e., $\theta|_{x=H} = \theta_r$, where θ_r is room temperature.

As soon as sticking condition is attained, the corresponding temperature and velocity boundary conditions can be described as follows:

$$\begin{aligned} \theta\big|_{x=0} &= \theta_{pin} \\ v\big|_{x=0} &= V_{pin} \\ v\big|_{x=R_s} &= 0 \\ \theta\big|_{x=H} &= \theta_r \end{aligned} \tag{4.30}$$

Note that as a result of pin/workpiece sticking, both material temperature and velocity at interface are set being equal to the values of pin.

The shear localization problem described by Eqs (4.26)-(4.27) can be solved numerically by implementing a finite element procedure using MATLAB [55]. A weak form of the governing equations, initial conditions and boundary conditions is derived by a piecewise linear Galerking/Petrov–Galerkin method. This discretization method offers a good accuracy to the second order in space as illustrated by Skeel and Berzins [56]. The result is a system of coupled nonlinear ordinary differential equations (ODEs) that are integrated by using MATLAB function ode15s. Note that the selection of ode15s solver instead of other ODE solvers is because it is better suited in dealing with stiff differential equations. The modeling procedure developed here provides a full solution over time

from t= 0 to the end of one revolution, i.e. $t = 2\pi/\omega$. The coordinates of linear elements in x-axis are given by

$$x = \left(\frac{n-1}{300} \right)^4 \tag{4.31}$$

which provides a significant element refinement at the workpiece and pin interface, that is, $x = 0$, for providing a sufficient spatial resolution for shear localization development, as demonstrated for similar problems solved by Batra and Wei[50,51]. The validation of the solving procedure mentioned above is documented in [36].

It is important to note that the shear localization model described above provides detailed information on shear band formation time and final shear band width (δ) within one pin revolution, among other field parameters associated with shear localization process, such as transient material velocity, temperature, shear strain and strain rate distributions.

5.1.3 Shear band rotation and material flow continuity

As a shear band of width δ is developed through shear localization process as described in Sec. 5.2.2 (see also Figure 5.5), material within the shear band must flow in such a way that satisfies mass balance and continuity conditions, as discussed by Reynolds [57] and Qian et al. [4]. Note that Arbegast [16,17] studied defect formation mechanisms with mass balance principle in conjunction with the extrusion analogy. Here, we adopt the same mass conservation principle but in a 2D configuration and impose continuity conditions as described in Figure 6, leading to the following material flow conditions:

$$V_T\left[\left(R_{pin}+w_{\theta_1}\right)\sin\theta_1-\left(R+w_{\theta_2}\right)\sin\theta_2\right]=Q_{\theta_2}-Q_{\theta_1}=\omega R_{pin}\left(w_{\theta_1}-w_{\theta_2}\right) \quad (4.32)$$

Note that in Eq. (4.32) above, w_θ is material flow layer width at θ, e.g., $w_{-90^\circ}=w_a$ corresponding to material flow layer width at advancing side, while $w_{90^\circ}=w_r$ is the layer width at retreating side. From Eq.(4.32), w_θ is given by:

$$w_\theta=\frac{R_{pin}+w_{0^\circ}\left(\omega R_{pin}/V_T\right)}{\left(\omega R_{pin}/V_T-\sin\theta\right)} \quad (4.33)$$

Eq. (4.33) yields maximum flow layer width at $\theta=90°$ (note that $w_{0^\circ}=2\pi V_T/\omega$):

$$w_{\max}=\frac{2(\pi+1)R_{pin}}{\omega R_{pin}/V_T-1} \quad (4.34)$$

Eq. (4.33)-(4.34) above are derived by imposing mass balance principle and material flow continuity conditions in terms of pin tool radius (R_{pin}) and processing parameters (V_T,ω) without considering material constitutive behavior, in a similar manner to previous developments presented by Arbegast [16] and Schmidt [13]. As such, the material shear flow layer width defined by w_{max} required for ensuring mass balance and flow layer continuity must be met through shear localization process, i.e.,

$$\delta\geq w_{\max} \quad (4.35)$$

where δ represents the width of shear band formed during transient pin/material interactions before extrusion process takes place and will be further illustrated in the following section. Eq. (4.35) represents one contribution from this study, which directly relates shear flow conditions described by Eq. (4.33) and (4.34) to shear localization process described by Eq.(4.26) -(4.30) leading to the development of shear localization

band width δ which takes into account of both transient thermos-mechanical interactions between stir pin and work piece and material constitutive behavior. For instance, in the derivation of w_θ, it is assumed that material velocity within w_θ is uniformly distributed and same as pin tangential velocity, i.e., being ωR_{pin}. However, this condition may or may not be achievable under a given set of welding parameters and material behavior, which must be determined by examining shear localization process governed by Eq. (4.26) -(4.30) in which material constitutive behavior is explicitly considered.

Modeling Results

5.1.4 Conditions for quality weld

In this section, the three-part selectively-integrated shear localization modeling procedure presented in Sec. 5.2 will be first used to demonstrate how it can be used to gain insights on some of the well-documented FSW experiments while illustrating some of the important features of the model developed. Consider the experimental study reported by Guerra et al. [34]. In their work, AA6061 plates of 6.3mm in thickness were friction stir welded using a rotation speed of 1000 rpm and travel speed of 180 mm/min. They used a faying surface tracer to monitor material flow during FSW. Two distinct material flow zones were identified, i.e. a uniform "rotation zone" around pin within which metal has the same velocity as pin tangential velocity ωR_{pin}. The "rotation zone" is surrounded by a narrow "transition zone" across which material velocity exhibits a rapidly decreasing from pin tangential velocity, ωR_{pin} to near zero. This finding was then further confirmed by Schmidt et al. [12]. The modeling results obtained in this study

under the given material and welding conditions are shown in Figure 5.7. The predicted velocity distribution (normalized by pin tangential velocity ωR_{pin}) at end of shear band formation (i.e. at t=0.06s) is shown in Figure 5.7a, which shows a region of constant velocity (measured as δ from pin/workpiece interface) and a region with a rapid decrease in velocity until stationary condition is attained at about 1mm. The material flow velocity results in Figure 5.7a seem to show a consistent trend with experimental evidence [34] as shown as a macrograph given in the same figure (see Figure 5.7a). It is the presence of such a uniform velocity region (or band structure) that is fundamental to friction stir weld formation process. This region of δ in width is referred to as shear band width in Eq. (4.35) and hereafter.

To further examine the shear band development process, material velocity distributions in front of the pin at different times are plotted in Figure 5.7b. Here time is normalized by the time of one pin revolution i.e. $2\pi/\omega$. The blue dash line prescribes the velocity field when pin finishes at $t = 0.37\, rev$, at which material just starts to show some movement, indicating the beginning of shear localization process. As the pin continues to rotate to $t = 0.41\, rev$, material velocity at the interface reaches to the tangential velocity of the pin (ωR_{pin}), attaining interface sticking conditions, which indicate the beginning of shear band formation process. Beyond this point in time, a region of uniform velocity increases rapidly from $t = 0.41\, rev$ up to about $t = 0.6\, rev$, as indicated by the flat portion of velocity distribution in Figure 5.7b, then slows down or shows no noticeable growth from $t = 0.6\, rev$ up to $t = 1\, rev$. The modeling results imply that shear band formation is not a continuous process even within the time frame of one revolution, which seems to be consistent with experimental observations by Krishnan

[33].

To take a further look at the phenomena, the time-history plot of material velocity and temperature at pin/workpiece interface, i.e. at $x = 0$ are examined here (see Figure 5.8). During the first quarter of the revolution, material point at the interface is static, and velocity suddenly began to develop from zero to pin tangential velocity from 0.25 rev to 0.41 rev (see Figure 5.8a). The accompanying temperature distributions follow a rather different behavior, as shown in Figure 5.8a and b. Material temperature begins to increase at an almost constant rate at the beginning and then at a decreasing rate as relative sliding velocity between pin and material interface, i.e., $V_{pin} - V_M$ approaches zero. The temperature distribution at the end of sliding is plotted as red-dashed line in Figure 5.8b and compared with the temperature distribution (blue line) corresponding to the onset of the sliding (contributed by shoulder/workpiece friction heating (see Sec. 5.2.1). A rapidly localized temperature rising can be seen right in front of the pin as a result of friction heat between pin and metal, which is the major contribution for developing shear localization.

All The numerical results further support the postulation of Krishnan [40] based on his experiment observation: “the tool appears to wait for a short time to produce frictional heat and extrude a cylindrical shaped material around to the retreating side of the joint”. And the comparison of temperature field in Figure 7b also verified the observation by Mendez [30] “the peak temperature near the pin is affected more by the concentrated heat of the deformation around the pin than by the large, but distributed, heat of the shoulder”. The yellow dotted line describes the temperature distribution at the end of one revolution (Figure 5.8b). It is interesting to note that during sticking stage,

temperature distribution becomes non-monotonic, with peak temperature occurring inside shear band, caused mainly by self-energizing plastic dissipation. As peak temperature moves away from pin/workpiece interface, a narrow band of approximately uniform velocity forms as material at peak temperature position is accelerated to attain the speed of pin, i.e., ωR_{pin}.

With the modeling results illustrated in Figures 5.7 and 5.8, the resulting shear band width represented by δ can be estimated as shown in Figure 5.7b, i.e., $\delta = 0.31\ mm$. As discussed in Sec. 5.2.3, the flow velocity continuity conditions require that Eq. (4.35) be satisfied, in which w_{max} is calculated through Eq. (4.34) as $w_{max} = 0.24mm$. Since for this case, $\delta > w_{max}$, a continuous circumferential shear band formation is expected, leading to a well-defined banded structure. Such a condition is further illustrated in Figure 5.9. Figure 5.9b-i schematically shows material velocity within w_θ, i.e. rotating with the pin with the same angular speed, leading to a uniform velocity distribution as pin advances during one revolution. This results in a well-defined banded structure, which is illustrated in Figure 5.9b-ii. As a result, a successive formation of band structure leads to a quality FSW joint.

5.1.5 Conditions for poor quality weld

It is equally important to investigate various conditions that have experimentally determined not being able to produce a quality weld, so that underpinning mechanics in terms of both shear localization phenomena and subsequent material flow characteristics can be clearly revealed. Here, some of the reported cases found producing poor quality welds reported by Kim et al. [58] are considered.

5.1.5.1 Insufficient Shear Band Width

Under the material and welding conditions as discussed in the previous section (see Figure 5.9), except with an increased pin rotation speed to 1100 and 1600 RMP, Kim et al. [58] showed that both cases produced poor weld quality welds, referred to as "abnormal stirring" as given in Figures 10a and 10c, respectively. The corresponding shear localization velocity fields in front of stir pin, obtained from the 3-part shear localization model presented in early sections, are also given in the same figures. The modeling results indicate inadequate shear band width δ for the case with 1100 RPM and near zero δ value for the case with 1600 RPM, both of which violate the conditions described in Eq.(4.35).

Therefore, the predicted material velocity results suggest that the root cause for "abnormal stirring" in Figures 5.10a and 5.10c can be attributed to insufficient shear band width in front of pin within each pin revolution. In case of "abnormal stirring" in Figure 10a, the root cause can now be explained as follows: A high rotation speed at 1100RPM used results in a non-uniform velocity field within w_θ, with a rapidly decreasing flow velocity away from the interface, leading to increasingly thinner band as shown in Figure 5.10b-ii. One consequence of such shear flow characteristics can be as depicted by Stage *iii* in Figure 5.10b in a form of incomplete banded structure, contributing to void formation more likely at the advancing side than the retreating side, as observed experimentally in [58,45]. However according to Eq.(4.34), w_{max} decreases with V_T, as long as $\delta > 0$, suggesting that a sound weld is still possible with a slower travel speed provided that Eq. (4.35) is satisfied. This explains that even though at a higher rotational

speed, the permissible travel speed can be higher, but at a very high rotational speed is used, a lower travel speed should be used in order to maintain weld quality, as experimentally demonstrated in [58] and illustrated in Figure 5.13.

With an even higher rotation speed at 1600 rpm (see Figure 10c), there exists no uniform velocity region δ in Figure 5.10a. The highly localized velocity field (Figure 10c), as illustrated as Stage i in Figure 5.10d would result in an even thinner band width at the advancing side (Stage ii in Figure 5.10d), potentially leading to even more "abnormal stirring" weld (illustrated in macrograph in Figure 5.10c). It is important to note that with a rotation speed of 1600 rpm in this case, δ approaching zero, no matter what travel speed is used, Eq. (4.35) will not be satisfied. Thus reducing the travel speed helps little in this case. This finding suggests that rotation speed should have an upper limit, as substantiated experimentally in [58].

5.1.5.2 Insufficient Local Plastic Flow

Another type of defective welds is shown in Figure 5.11a in which X-Ray radiography and cross-section macrograph of a weld with lack of material fill can be clearly seen, which may be attributed due to insufficient material flow. Under given material and welding conditions, the predicted velocity distributions in front of pin at different times are shown in Figure 5.11b. Similar to that in Figure 5.7b, the interface material was accelerated from stationary to pin tangential velocity at $t = 0.54\,rev$ in reaching to its sticking condition. Then, a uniform shear flow velocity region can be seen being developed from $t = 0.54\,rev$ to $t = 0.559\,rev$ (indicated by yellow dot-dashed line in Figure 5.11b, but without a noticeable velocity transition region. However, at

$t = 0.56\,rev$, the uniform velocity region quickly vanishes and a linear velocity field appears with material velocity being equal to pin tangential velocity at $x = 0$ (material/pin interface) to zero at $x = R_s$, as shown in purple dotted line in Figure 5.11b. This linear distribution of material velocity exactly corresponds to the velocity field as a result of simple shear deformation for linear elastic material (also demonstrated in Figure 5.11b which suggests that plastic deformation ends at $t = 0.56\,rev$, and material begins to deform elastically. This can be further demonstrated in Figure 5.11c in which plastic strain rate at different time is plotted. To compare different level of amplitude, the plastic strain rate is plotted in log scale. As illustrated in Figure 5.11c, during sliding the plastic the plastic strain rates decrease monotonically from the pin/workpiece interface as shown in blue dash line and red solid line. After sliding condition is achieved, the plastic strain rate suddenly decreases to a negligible level near the interface but achieves a highest value at the velocity discontinuity position as shown in velocity profile in Figure 5.11b. However this plastic strain rate also reduced tremendously from $\mathrm{t} = 0.559$ rev to $\mathrm{t} = 0.560$ rev, which suggests the end of local plastic deformation. The reason that the localized plastic flow seen $t = 0.559\,rev$ cannot be maintained is that when the rotation speed is not high enough, a sufficient temperature level near the interface cannot be sustained through heat generation by plastic dissipation work due to lack of sufficiently high plastic stain rate, in addition to relatively low surrounding temperature as result of pin/workpiece sliding friction before sticking and shoulder friction heating at a rather low rotation speed. These effects can be seen in temperature distributions shown in Figure 5.11d corresponding to before and after sticking conditions are reached. This results in an unfinished band structure due to lack of plastic flow, as shown in Figure 5.11e-ii. Even

though at the beginning of sticking stage there exists a uniformly material flow around the pin (Figure 5.11e-i), the plastic material flow is not able to preserve for one band formation. And the unfinished band structures finally contribute to “cold weld” defect such as lack of fill or “ wormhole” [17] as shown in Figure 5.11e-iii.

5.1.5.3 Incomplete Shear Band Generation

As discussed in Sec. 5.1 and Sec. 5.2.3, an adequate shear band width, i.e., $\delta \geq w_{max}$ must be reached within one pin revolution in order to subsequently form a well-defined circumferential band. This further implies that sticking conditions must be achieved after initial sliding within one revolution. Consider a type of defective welds that are often characterized as “surface galling”, as shown in Figure 5.12 taken from [17]. By considering welding parameters used (rotation speed: 600 rpm; welding travel speed: 50 mm/min), the predicted velocity distributions corresponding to different times during one pin revolution are shown in Figure 5.12. It can be seen that at $t = 1\ rev$, material velocity at interface only reaches one tenth of pin tangential velocity, which suggests that sticking condition was never achieved within one revolution, and results in surface galling defect and overheating. This is mainly because the welding travel speed is too low to generate an enough contact pressure (p) (which can be inferred from Eq. (5.9)) between pin and workpiece, resulting in not high enough friction stress $(f = \mu p)$ at interface for accelerating material to attain sticking condition.

5.1.5.4 Overheating due to shoulder/workpiece friction

Excessive flash is a common defect in FSW welding, which is usually caused by

over applied axial forging load F_z [17,57,58]. Too high forging load leads to large amount of friction heat generated between tool shoulder and workpiece and cause overheating. When the maximum temperature at the shoulder pin interface approaches material solidus temperature, defect of excessive flash will develop as shown in Figure 5.13. This overheating effect can be examined by shoulder heating model given in Sec. 5.2.1.

5.1.6 Summary of shear localization results and FSW joint quality

As discussed in Sec 5.3.1 and 5.3.2, the certain relationship can be drawn between the results of proposed shear localization model and FSW joint quality. Different defects formation mechanism during FSW can be explained according to corresponding shear localization model results. These relationships are summarized in Table 5-1. Given the FSW parameters and metal to be joined, process window in terms of rotation speed and travel speed can also be estimated based on the present model.

Model-based Process Window Estimation

In practice, FSW process window is determined in terms of both pin rotation speed and welding travel speed through Design of Experiment (DoE) approach, see representative work along this line in [e.g. 17,38,43]. One such experimentally determined process window from [38] is shown in Figure 5.14, along with regimes corresponding to weld defect types observe outside the region referred to as “defect free joints”.

The selectively-coupled shear localization model presented in the previous sections can be used for achieving a model-based process window estimation in the

following manner:

(a) Minimum pin rotation speed, below which "cold" welds could be produced, is first estimated

(b) Then at a given rotation speed greater than the minimum rotation speed, a set of four limiting conditions on travel speed are determined as follows: (1) upper limit above which insufficient local plastic flow happens resulting in "too cold weld defects" discussed in Sec. 5.3.2.2; (2) upper limit above which insufficient shear band width happens leading to abnormal stirring as described in Sec. 5.3.2.1 begins to develop; (3) lower limit below which incomplete shear band generation causing surface galling is predicted (Sec. 5.3.3.3); and (4) lower limit below which excessive flash is predicted (Sec. 5.3.3.4).

The numerical algorithms implementing the above procedure are summarized in Figure 5.16. The predicted process windows are compared with four sets of experimental determined process windows corresponding to Al2024 [4,44], Al6061[46], and Al2219[45]. The results are shown in Figure 5.14. In this the figure, the upper limit of travel speed is determined by criteria (1) and (2). The first lower bound in blue dashed line is determined according to criterion (3), while criterion (4) leads to the construction of second lower limit of travel speed (the orange dashed line). It can be seen that several defective weld cases experienced in experiments are included in the estimated windows; on the other hand, some defect free welds are excluded from the predicted windows. The authors attribute these discrepancies to some simplifications associated with the selectively-integrated shear localization model and its use of temperature-independent material properties in 3D heat flow model and uncertainties involved in material

constitutive model. However, the overall estimation of these process windows seem rather reasonable, which can be used to a general guidance for supporting a cost-effectively planning Design of Experiments in refining the estimated process window for practical applications.

Conclusions

A selectively-coupled shear localization model has been presented which combines three-dimensional (3D) transient heating with one-dimensional shear localization process for simulating FSW formation process, in which shear band width estimated must satisfy both mass conservation and plastic flow continuity conditions formulated in a two-dimensional configuration. The effectiveness of the model in providing a theoretical means for FSW process window estimation has been demonstrated on three aluminum alloys on which experimentally determined process windows were published by a number of researchers recently. A good agreement has been achieved between the model-based estimations and experimentally determined process windows for all three types of aluminum alloys. Furthermore, some of the major weld defect formation mechanisms have been elucidated in details as a result of insights gained from the selectively-coupled shear localization model. These are:

(1) In order to form continuous banded structure per pin revolution in a consecutive manner, shear band width (δ) formed within one revolution must be equal or larger than the maximum plastic flow band width (w_{max}) or (Eq. (5.15))

(2) If shear band width (δ) is less than plastic flow band width (w_{max}) , the defect type of "abnormal stirring" tends to develop

(3) If not enough plastic flow is generated during one revolution, the defect type of "cold welds" tends to develop

(4) If sticking condition is not attained within one revolution, the defect of "surface galling" may occur

(5) If maximum temperature generated from friction heating between shoulder and workpiece approaches solidus temperature of workpiece, the defect type of "excessive flash" tends to develop.

Table 5-1: FSW joint performed by Pilchak et al.[27] and Edwards and Ramulu [36] and tested against by proposed shear localization model

Welding condition	(900rpm|300mm min^{-1})	(1000rpm|397mm min^{-1})	(1100rpm|400mm min^{-1})
Shear localization result	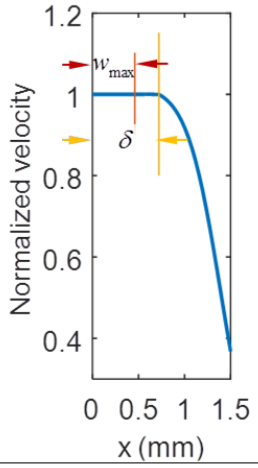	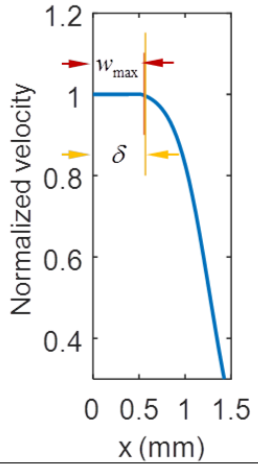	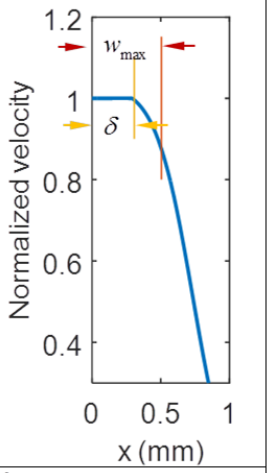
Comments	$w_\theta < \delta$, good weld, but can be welded faster	$w_\theta = \delta$, good weld, and welded with optimum travel speed	$\delta < w_\theta$, slight abnormal stirring, should be welded with smaller travel speed
Welding condition	(1600rpm|400mm min^{-1})	(500rpm|300mm min-1)	(600rpm|50mm min^{-1})
Shear localization result	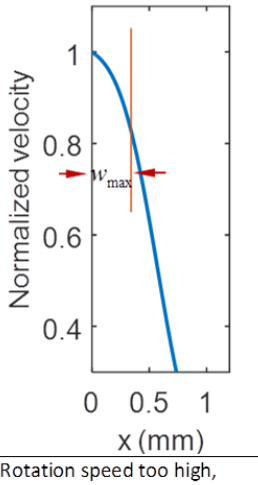	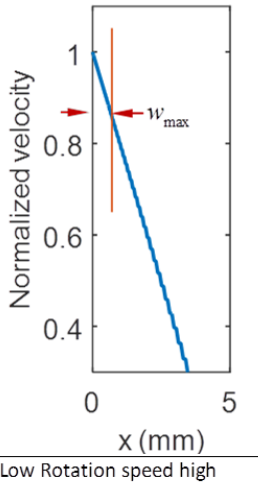	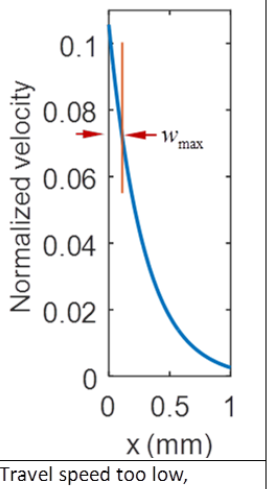
Comments	Rotation speed too high, very localized velocity distribution, severe abnormal stirring defect	Low Rotation speed high travel speed, insufficient plastic flow, too cold weld defect such as lack of fill	Travel speed too low, sticking condition not achieved within one revolution, surface galling

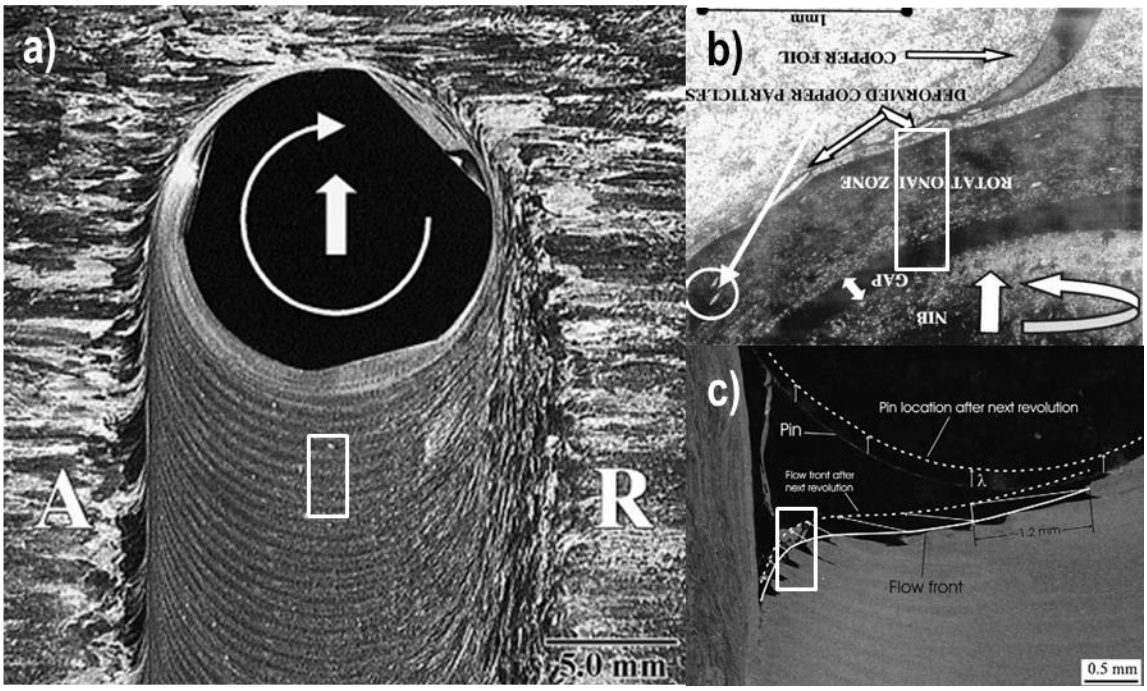

Figure 5.1: Typical banded structure in typical FSW welding a)whole picture [29] b) banded structure in front of pin [32] c) banded structure behind of pin [31]

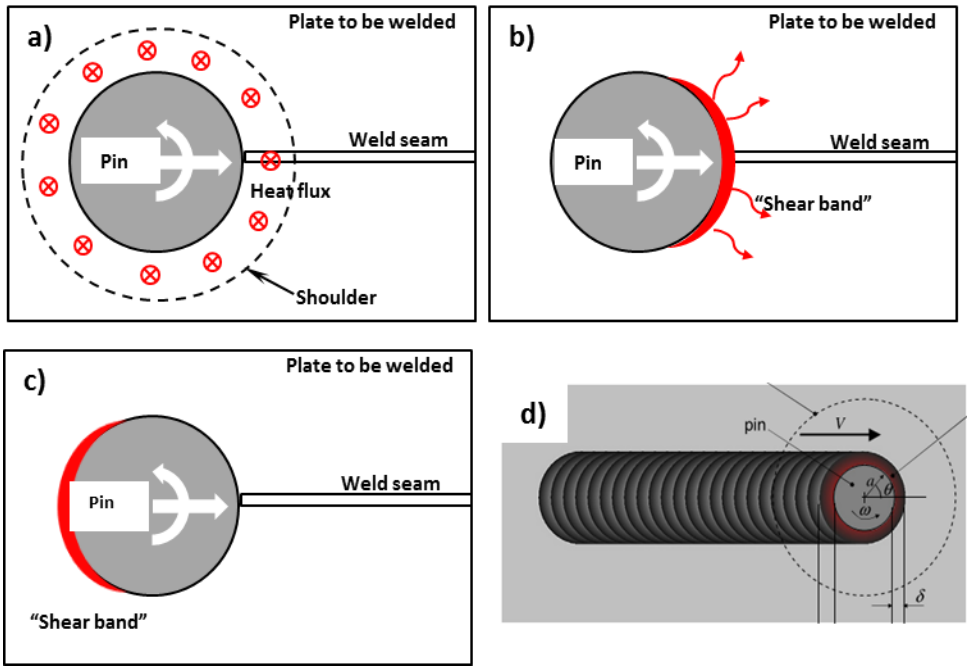

Figure 5.2: Four stages to form a FSW joint: (a) Shoulder/workpiecel interface heating and 3D heat conduction; (b) Pin/workpiece interface sliding and sticking – shear localization; (c) In-plane (2D) Shear flow and band rotation; (d) Formation of banded structure through consecutive shear bands of δ in width

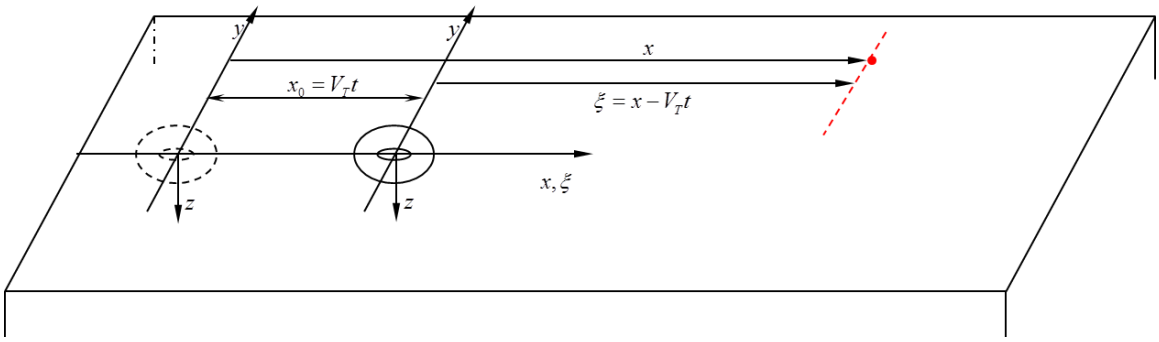

Figure 5.3: Definition of 3D transient heating conduction problem with shoulder/material interface friction heating

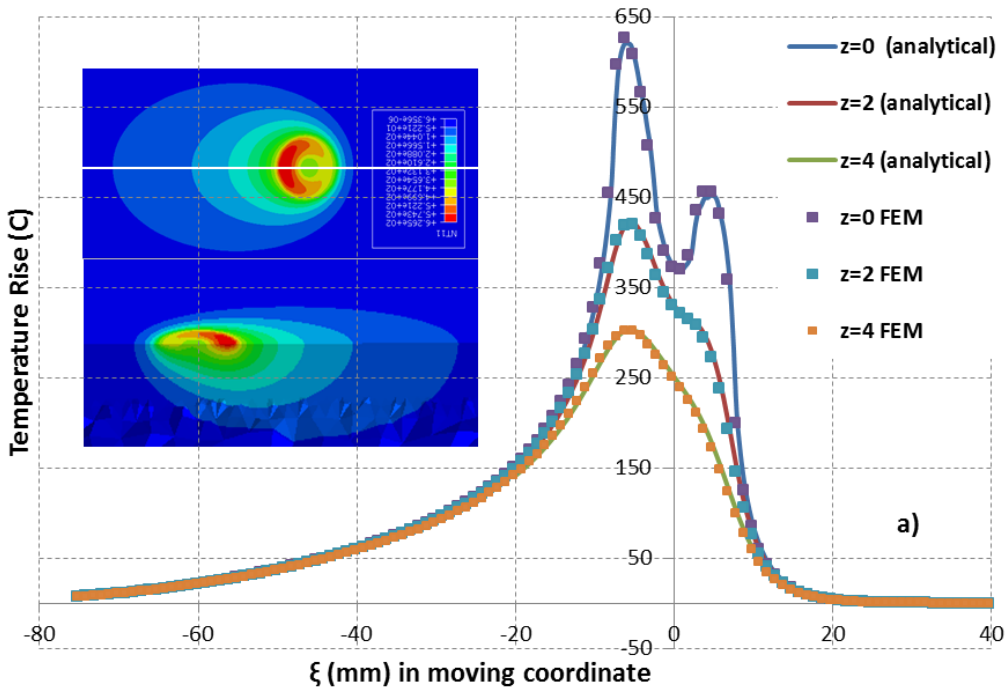

Figure 5.4: Comparison of transient temperature distributions along x-axis at three depths between analytical (Eq. (5.5)) and 3D finite element solutions for a plate of 50mm in thickness

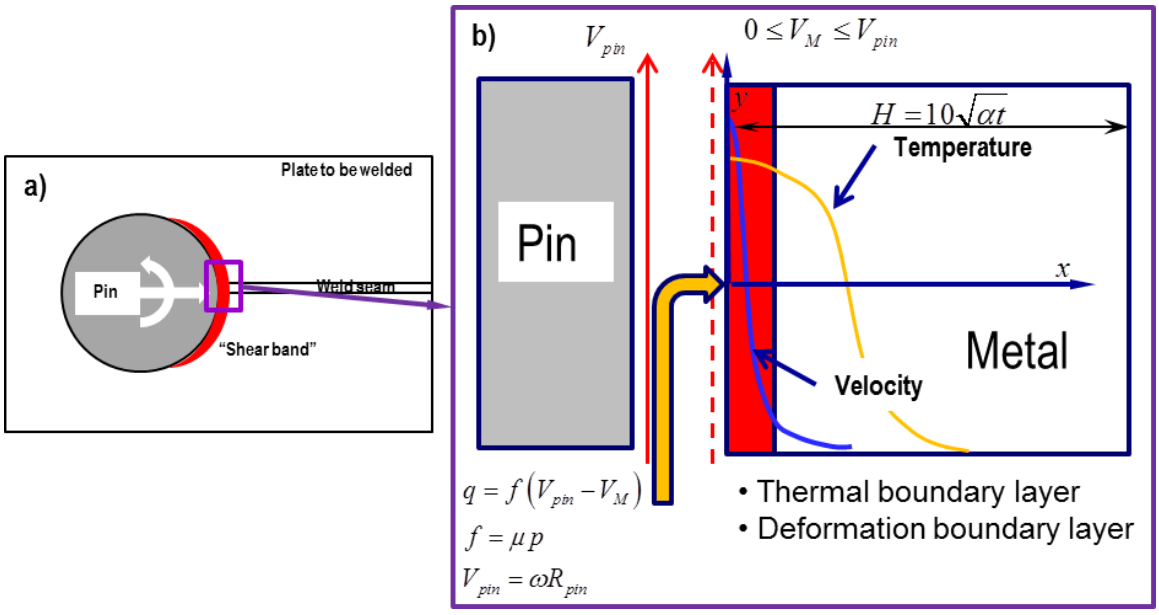

Figure 5.5: Problem definition for pin/workpiece interaction and shear localization: (a) Interaction between the pin and workpiece; (b) 1D thermal and deformation boundary layer problem definition

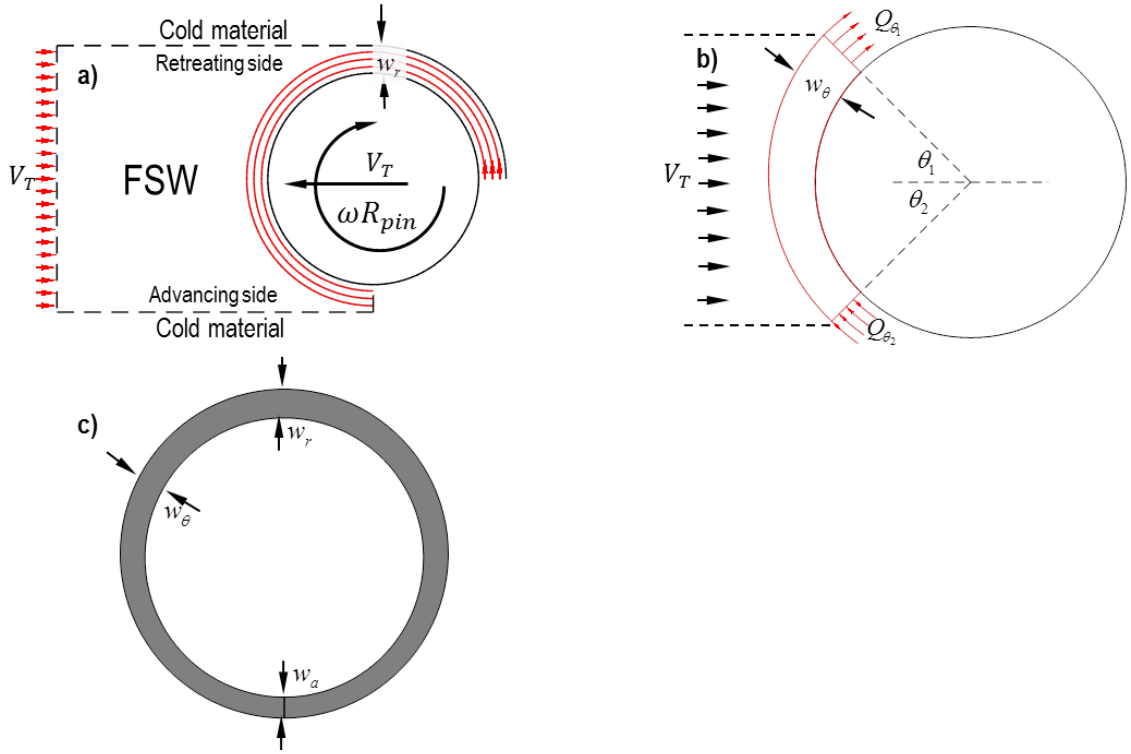

Figure 5.6: Definition of an in-plane (2D) shear material flow problem: (a) Analogy to extrusion process by a rotating pin; (b) Mass conservation and flow continuity conditions during shear band rotation; (c) Well-formed shear band after one pin revolution

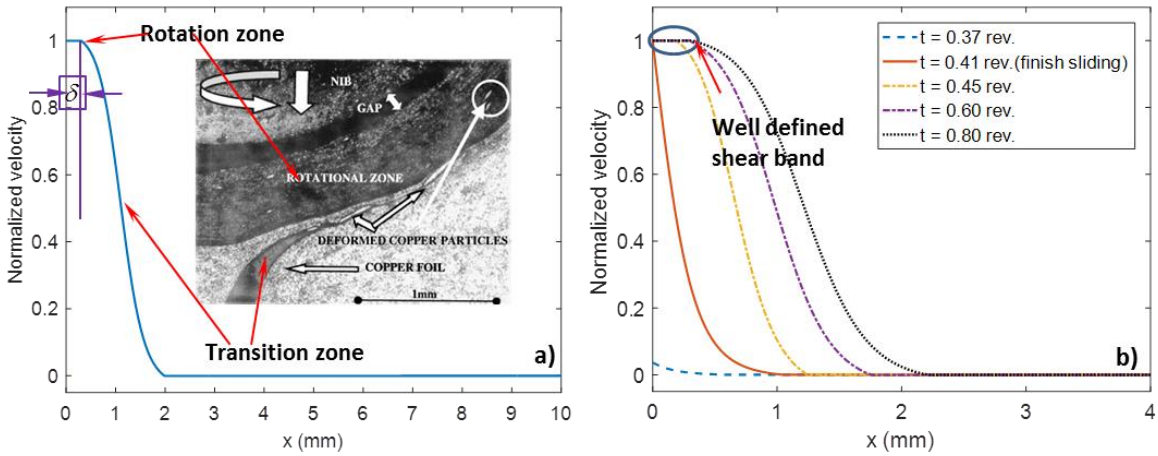

Figure 5.7: Velocity field profile in FSW: a) comparison between velocity distribution in sticking stage and experimental observation by Guerra et al. [32]. b) velocity distribution at different time intervals

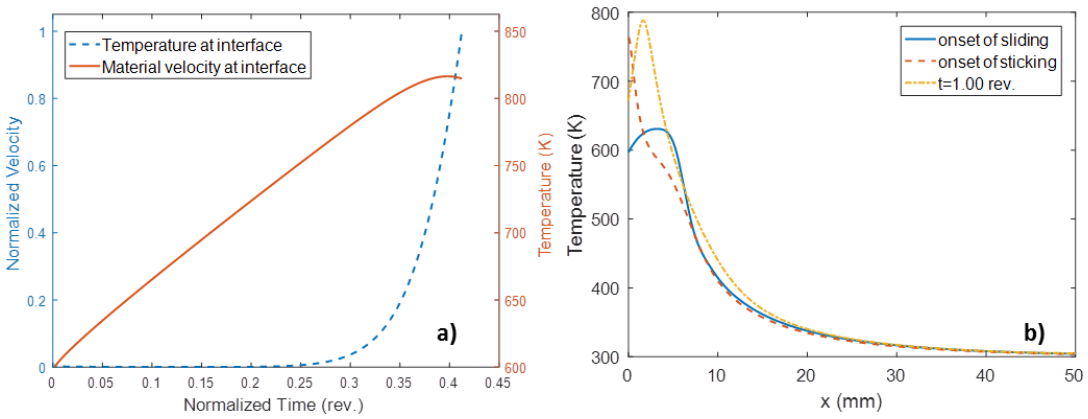

Figure 5.8: Pin/material interface temperature evolution and velocity distribution during FSW. a) Material velocity and temperature evolution at pin/workpiece interface. b) Temperature distributions after shoulder preheating stage and sliding stage.

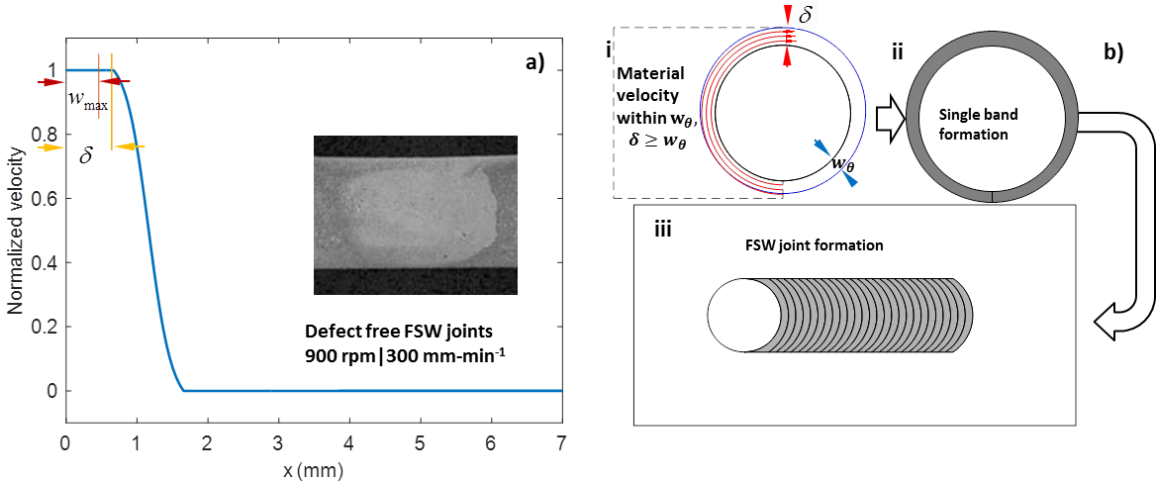

Figure 5.9: Shear localization modeling results indicating $\delta > w_{max}$: (a) Velocity distribution in front of pin and the corresponding macrostructure observed [38]; (b) Schematic illustration of formation of well-defined banded structure leading to quality weld

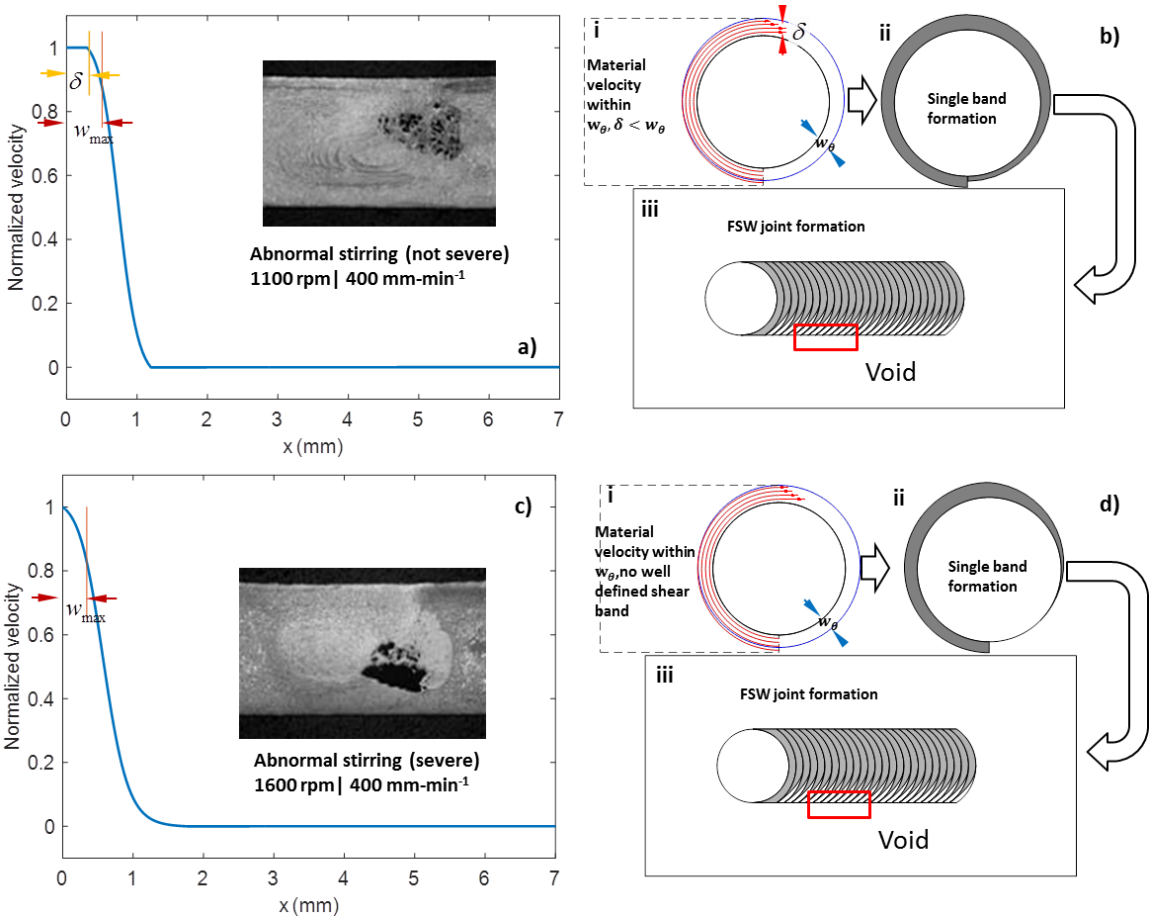

Figure 5.10: Shear localization modeling results indicating $\delta < w_{max}$ and interpretations on subsequent material flow characteristics around stir pin at travel speeds of 400 mm-min-1 : (a) Predicted velocity distribution in front of pin and the corresponding macrostructure observed [38] at 1100RPM; (b) Interpretation of subsequent shear flow; (c) Predicted velocity distribution in front of pin and the corresponding macrostructure observed [38] at 1600RPM; (d) Interpretation of subsequent shear flow

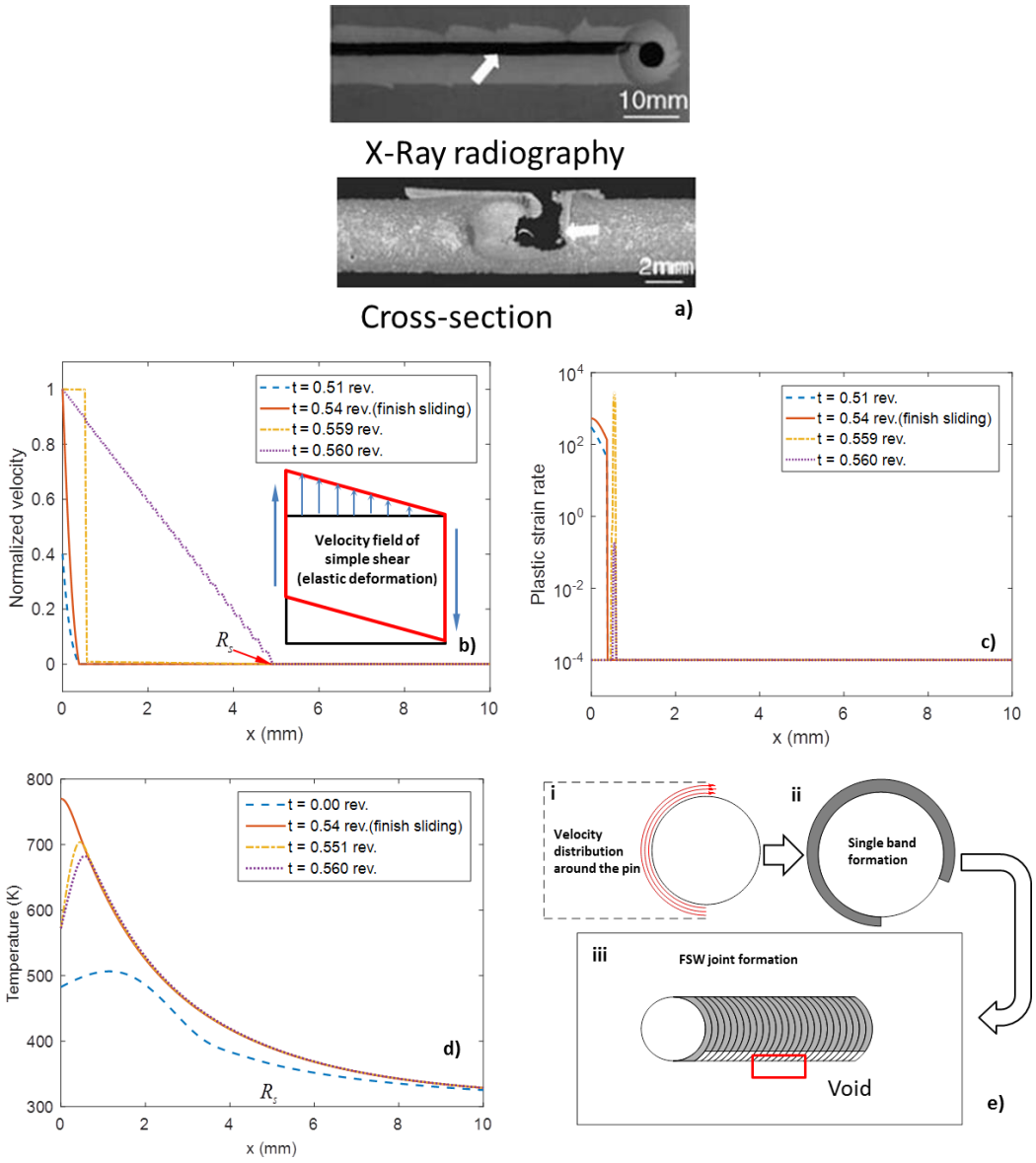

Figure 5.11: Schematics of welds formation with lack of fill defects. a) X-Ray radiography and Cross-section of a weld with lack of fill defect [38] b) Velocity distribution in front of pin at different time. c) Plastic strain rate distribution in front of pin at different time. d) Temperature distribution in front of pin at different time. e) Illustration of weld formation with abnormal stirring defects.

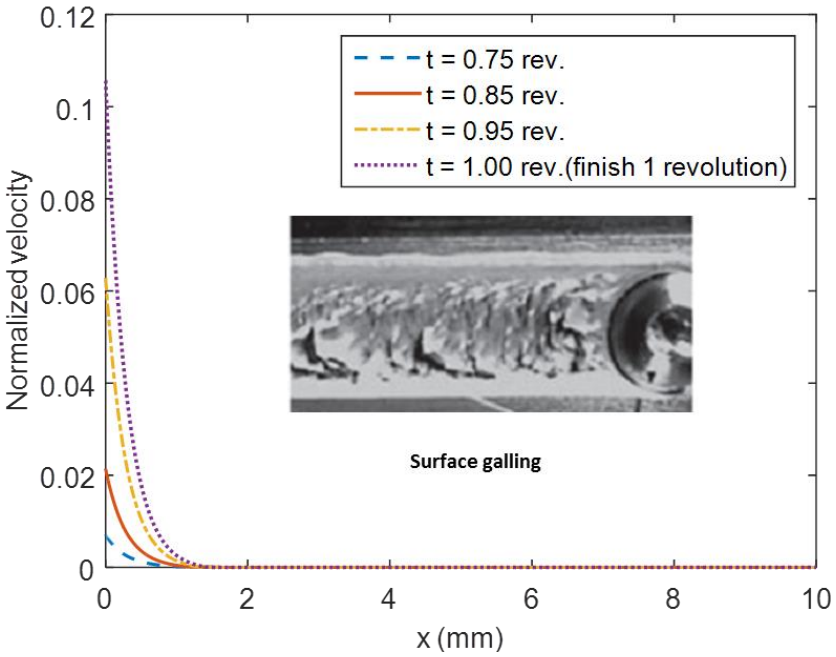

Figure 5.12: Velocity distributions at different times during one pin revolution for surface galling conditions (picture taken from [21])

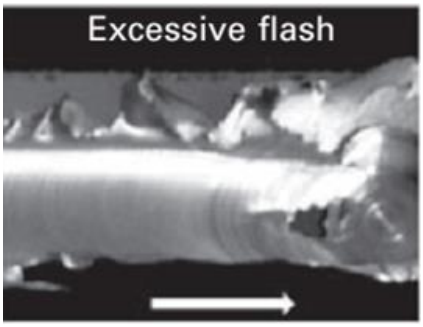

Figure 5.13: Excessive flash defect in FSW (picture from [21])

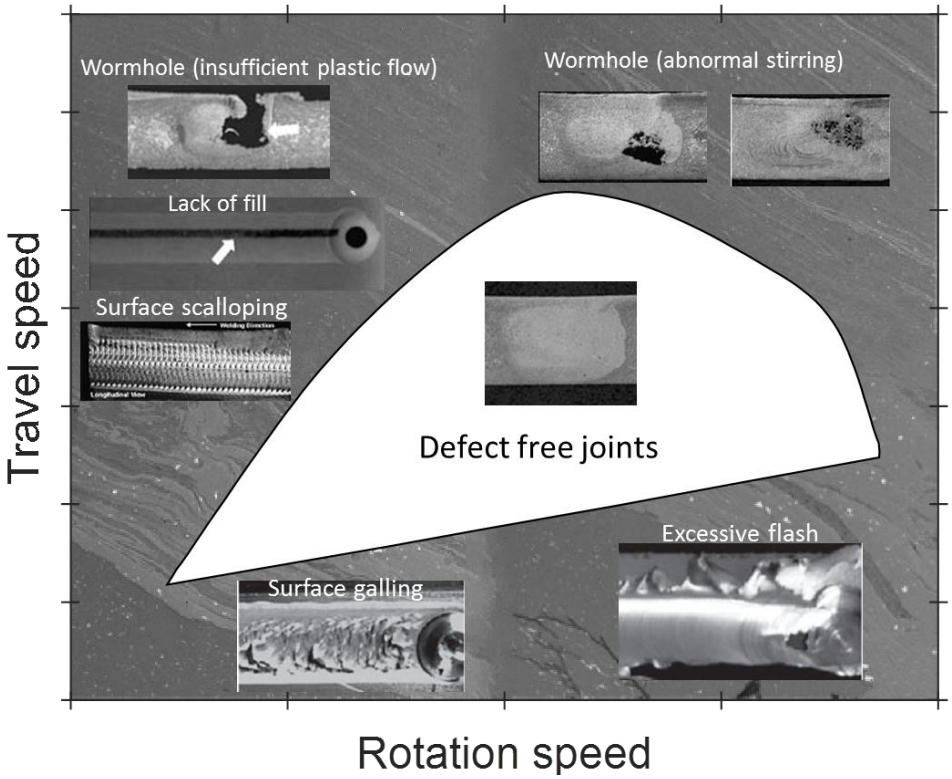

Figure 5.14: Illustration of typical FSW process window [38] and corresponding weld defects.

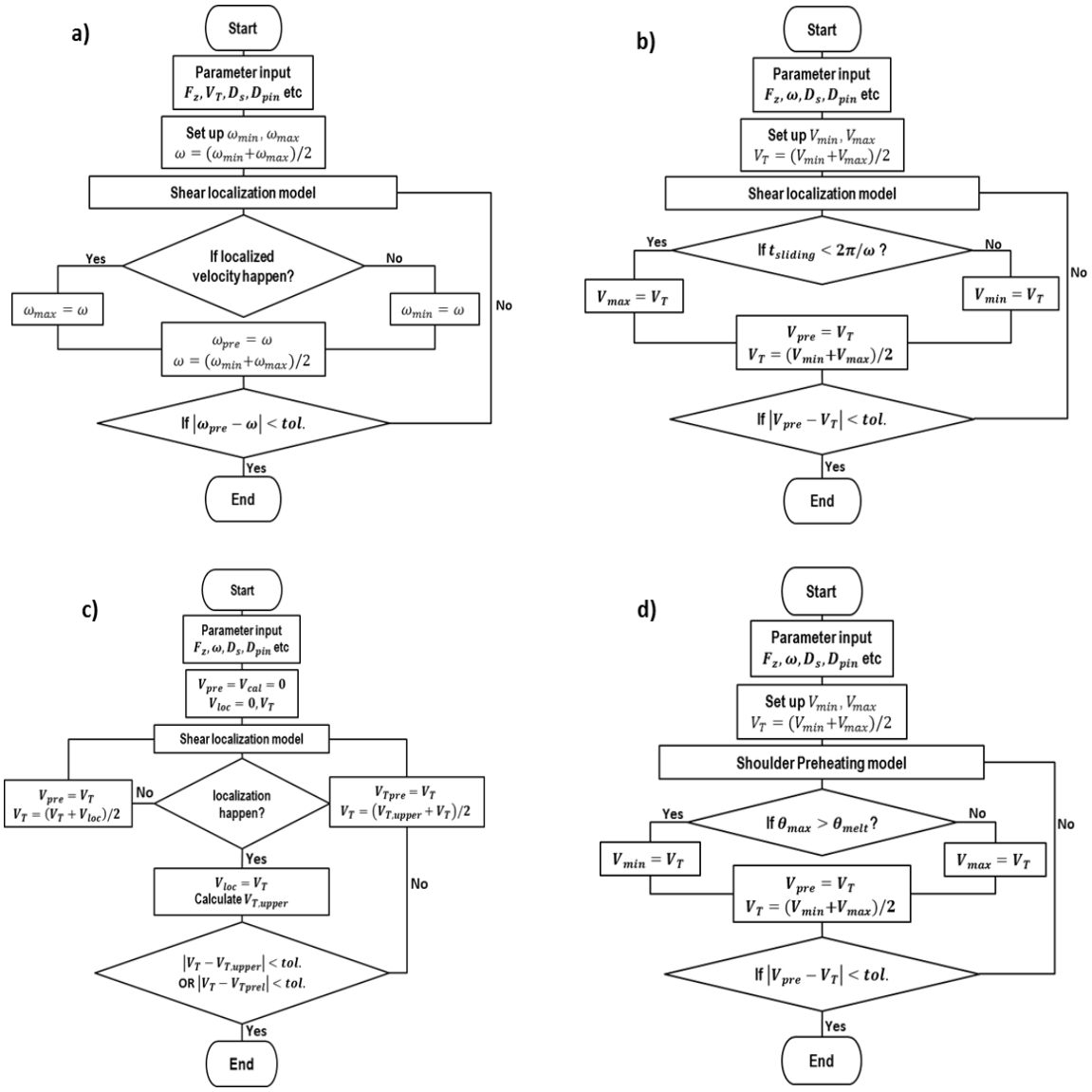

Figure 5.15: Algorithms for determining process window: a) Algorithm to determine minimum rotation speed. b) Algorithm to determine lower bound of travel speed based on surface galling defect criterion. c) Algorithm to determine upper bound 1 of travel speed based on too cold weld and abnormal stirring defects criteria. d) Algorithm to determine lower bound 2 of travel speed based on excessive flash defect criterion.

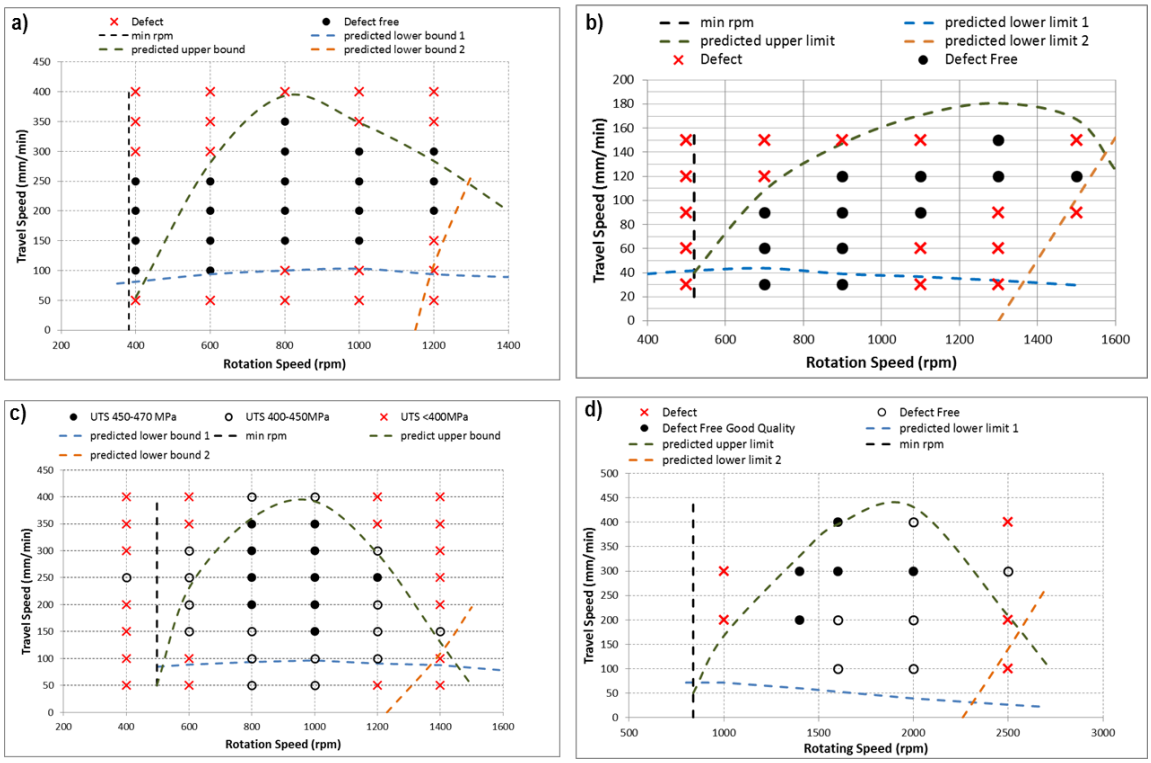

Figure 5.16: Comparison of predicted process window with experimental data: a) AA 2024 in [41] b) AA 2219 in [43]. c) AA 2024 in [42] d) AA 6061 in [44]

References

[1] Thomas, W. M., and E. D. Nicholas. "Friction stir welding for the transportation industries." *Materials & Design* 18.4 (1997): 269-273.

[2] C. Dawes and W. Thomas: 'Friction stir joining of aluminum alloys', TWI Bulletin (6), Cambridge, UK, November/December 1995.

[3] Nandan, R., T. DebRoy, and H. K. D. H. Bhadeshia. "Recent advances in friction-stir welding–process, weldment structure and properties." *Progress in Materials Science* 53.6 (2008): 980-1023.

[4] Qian, Jinwen, et al. "An analytical model to optimize rotation speed and travel speed of friction stir welding for defect-free joints." Scripta Materialia 68.3 (2013): 175-178.

[5] He, Xiaocong, Fengshou Gu, and Andrew Ball. "A review of numerical analysis of friction stir welding." Progress in Materials Science 65 (2014): 1-66.

[6] Gould, Jerry E., and Zhili Feng. "Heat flow model for friction stir welding of aluminum alloys." Journal of Materials Processing and Manufacturing Science 7 (1998): 185-194.

[7] Vilaça, Pedro, Luísa Quintino, and Jorge F. dos Santos. "iSTIR—analytical thermal model for friction stir welding." *Journal of Materials Processing Technology* 169.3 (2005): 452-465.

[8] Chao, Yuh J., X. Qi, and W. Tang. "Heat transfer in friction stir welding-experimental and numerical studies." Transactions-American Society of Mechanical Engineers Journal of Manufacturing Science and Engineering 125.1 (2003): 138-145.

[9] Schmidt, H., Jesper Hattel, and John Wert. "An analytical model for the heat generation in friction stir welding." Modelling and Simulation in Materials Science and Engineering 12.1 (2003): 143.

[10] Schmidt, Henrik B., and Jesper H. Hattel. "Thermal modelling of friction stir welding." *Scripta Materialia* 58.5 (2008): 332-337.

[11] Colligan, K. "Material flow behavior during friction welding of aluminum." Weld J 75.7 (1999): 229s-237s.

[12] Schmidt, Henrik Nikolaj Blicher, T. L. Dickerson, and Jesper Henri Hattel. "Material flow in butt friction stir welds in AA2024-T3." Acta Materialia 54.4 (2006): 1199-1209.

[13] Schmidt, Henrik Nikolaj Blich, and Jesper Hattel. "An analytical model for prescribing the flow around the tool probe in friction stir welding." Friction Stir Welding and Processing (2005).

[14] Seidel, T. U., and Anthony P. Reynolds. "Two-dimensional friction stir welding process model based on fluid mechanics." Science and technology of welding and joining 8.3 (2003): 175-183.

[15] Colegrove, Paul A., and Hugh R. Shercliff. "3-Dimensional CFD modelling of flow round a threaded friction stir welding tool profile." *Journal of Materials Processing Technology* 169.2 (2005): 320-327.

[16] Arbegast, William J. "Modeling friction stir joining as a metalworking process." Proceedings of Hot Deformation of Aluminum Alloys III (2003): 313-327.

[17] Arbegast, William J. "A flow-partitioned deformation zone model for defect formation during friction stir welding." Scripta materialia 58.5 (2008): 372-376.

[18] A. C. Nunes: 'Prolegomena to the study of friction stir welding', Proc. Materials Science

& Technology 2010 – Joining of Advanced and Specialty Materials XII, Houston, TX, USA, October 2010, Paper 14, pp. 2651–2664.
[19] Nunes Jr, Arthur C. "Metal flow in friction stir welding." (2006)
[20] Nandan, R., et al. "Three-dimensional heat and material flow during friction stir welding of mild steel." Acta Materialia 55.3 (2007): 883-895.
[21] Nandan, R., et al. "Numerical modelling of 3D plastic flow and heat transfer during friction stir welding of stainless steel." Science and Technology of Welding & Joining (2013).
[22] Schmidt, Hattel, and Jesper Hattel. "A local model for the thermomechanical conditions in friction stir welding." *Modelling and simulation in materials science and engineering* 13.1 (2004): 77.
[23] Khandkar, M. Z. H., Jamil A. Khan, and Anthony P. Reynolds. "Prediction of temperature distribution and thermal history during friction stir welding: input torque based model." Science and Technology of Welding & Joining (2013).
[24] Frigaard, Øyvind, Øystein Grong, and O. T. Midling. "A process model for friction stir welding of age hardening aluminum alloys." Metallurgical and materials transactions A 32.5 (2001): 1189-1200.
[25] Ulysse, Patrick. "Three-dimensional modeling of the friction stir-welding process." International Journal of Machine Tools and Manufacture 42.14 (2002): 1549-1557.
[26] Cho, Jae-Hyung, Donald E. Boyce, and Paul R. Dawson. "Modeling strain hardening and texture evolution in friction stir welding of stainless steel." Materials Science and Engineering: A 398.1 (2005): 146-163.
[27] Nandan, R., G. G. Roy, and T. Debroy. "Numerical simulation of three-dimensional heat transfer and plastic flow during friction stir welding." Metallurgical and materials transactions A 37.4 (2006): 1247-1259.
[28] Dong, P., et al. "Coupled thermomechanical analysis of friction stir welding process using simplified models." Science and Technology of Welding & Joining (2013).
[29] Song, M., and R. Kovacevic. "Thermal modeling of friction stir welding in a moving coordinate system and its validation." International Journal of Machine Tools and Manufacture 43.6 (2003): 605-615.
[30] Mendez, Patricio F., Karem E. Tello, and Thomas J. Lienert. "Scaling of coupled heat transfer and plastic deformation around the pin in friction stir welding." Acta Materialia 58.18 (2010): 6012-6026.
[31] Pei, X. J., and P. S. Dong. "Shear localisation modelling of friction stir weld formation process." Science and Technology of Welding and Joining 19.5 (2014): 416-426
[32] Pei, Xianjun, and Pingsha Dong. "Modeling of banded structure in friction stir weld in strain rate–hardening materials of Zener–Hollomon type." The Journal of Strain Analysis for Engineering Design (2015): 0309324714563199.
[33] Fonda, R. W., J. F. Bingert, and K. J. Colligan. "Development of grain structure during friction stir welding." Scripta Materialia 51.3 (2004): 243-248.
[34] Guerra, M., et al. "Flow patterns during friction stir welding." Materials characterization 49.2 (2002): 95-101.
[35] Chen, Z. W., T. Pasang, and Y. Qi. "Shear flow and formation of Nugget zone during friction stir welding of aluminium alloy 5083-O." Materials Science and Engineering: A 474.1 (2008): 312-316.

[36] J. A. Schneider and A. C. Nunes Jr: ‘Characterization of plastic flow and resulting microtextures in a friction stir weld’, Metall. Mater. Trans. B, 2004, 35B, (4), 777–783
[37] B. Yang, J. Yan, M. A. Sutton and A. P. Reynolds: ‘Banded microstructure in AA2024-T351 and A2524-T351 aluminum friction stir welds, Part I. metallurgical studies’, Mater. Sci. Eng. A-Struct., 2004, A364, 55–65
[38] K. E. Knipling and R. W. Fonda: ‘Texture development in the stir zone of near-a titanium friction stir welds’, Scr. Mater., 2009, 60,1097–1100
[39] A. L. Pilchak, W. Tang, H. Sahiner, A. P. Reynolds and J. C. Williams: ‘Microstructure evolution during friction stir welding of mill-annealed Ti-6Al-4V’, Metall. Mater. Trans. A, 2011, 42A, (3), 745–762.
[40] Krishnan, K. N. "On the formation of onion rings in friction stir welds." Materials science and engineering: A 327.2 (2002): 246-251.
[41] Guerra, M., et al. "Flow patterns during friction stir welding." Materials characterization 49.2 (2002): 95-101.
[42] Chen, Z. W., and S. Cui. "On the forming mechanism of banded structures in aluminium alloy friction stir welds." Scripta Materialia 58.5 (2008): 417-420.
[43] Xu, Shaowen, and Xiaomin Deng. "A study of texture patterns in friction stir welds." Acta Materialia 56.6 (2008): 1326-1341.
[44] Zhang, Z. H., et al. "Effective predictions of ultimate tensile strength, peak temperature and grain size of friction stir welded AA2024 alloy joints." The International Journal of Advanced Manufacturing Technology 73.9-12 (2014): 1213-1218.
[45] Lakshminarayanan, A. K., S. Malarvizhi, and V. Balasubramanian. "Developing friction stir welding window for AA2219 aluminium alloy." Transactions of Nonferrous Metals Society of China 21.11 (2011): 2339-2347.
[46] Lim, Sunggon, et al. "Tensile behavior of friction-stri-welded Al 6061-T651." Metallurgical and Materials Transactions A 35.9 (2004): 2829-2835.
[47] Carslaw, Horatio Scott, and John Conrad Jaeger. "Conduction of heat in solids." Oxford: Clarendon Press, 1959, 2nd ed. (1959).
[48] Pei, X. J., and P. S. Dong. " A coupled friction stir shear localization model incorporating tool contact and 3D transient friction heating " submitted to Science and Technology of Welding and Joining
[49] Hibbit Karlson and Sorensen Inc 2003 ABAQUS Version 6.12
[50] Batra, R. C., and Z. G. Wei. "Shear bands due to heat flux prescribed at boundaries." International journal of plasticity 22.1 (2006): 1-15.
[51] Wei, Zhigang, and R. C. Batra. "Modeling and simulation of high speed sliding." International Journal of Impact Engineering 37.12 (2010): 1197-1206.
[52] Sellars, C. M., and WJ McG Tegart. "Hot workability." *International Metallurgical Reviews* 17.1 (1972): 1-24.
[53] Kuykendall, Katherine, Tracy Nelson, and Carl Sorensen. "On the selection of constitutive laws used in modeling friction stir welding." International Journal of Machine Tools and Manufacture 74 (2013): 74-85.
[54] Johnson, Kenneth Langstreth, and Kenneth Langstreth Johnson. Contact mechanics. Cambridge university press, 1987.
[55] Guide, MATLAB User’S. "The mathworks." Inc., Natick, MA 5 (1998): 333.
[56] Skeel, Robert D., and Martin Berzins. "A method for the spatial discretization of

parabolic equations in one space variable." SIAM journal on scientific and statistical computing 11.1 (1990): 1-32.
[57] Reynolds, Anthony P. "Flow visualization and simulation in FSW." Scripta materialia 58.5 (2008): 338-342.
[58] Kim, Y. G., et al. "Three defect types in friction stir welding of aluminum die casting alloy." Materials Science and Engineering: A 415.1 (2006): 250-254.

Chapter 6

Conclusions and Recommendations for Future Work

Conclusion

In this dissertation, a shear localization model is presented to study the joint formation mechanism during FSW by focusing the band structure development which is the unique feature associated with FSW process. The model is further coupled with 3D analytical heat transport model and a 2D material flow model to explain the defect generation mechanism of FSW. A set of algorithms are also developed to theoretical estimate process window of FSW based on the proposed model. Major achievements are summarized as follows:

(1) A shear localization model is presented in this work, which focuses on shear band (SB) formation phenomena associated with friction stir welding process. With this model, shear band width, shear band formation time, and shear band propagation speed can be theoretically estimated. The shear band propagation speed serves a direct estimate of the maximum welding speed for a given material to be welded under a set of specified stir pin rotational and translational speeds.

(2) Different constitutive model are compared and material behavior of Sellars Tegart are identified to be more suitable in conducting the presented shear

localization model.

(3) Parametric analyses on three different alloys, i.e., aluminum alloy AA2024, HSLA steel 4340, titanium alloy Ti-6Al-4V have been performed to examine how shear localization parameters introduced here can be used to quantitatively rank material friction stir weldability. Some of key findings are: a)The predicted shear localization parameters clearly indicate that titanium alloy such as Ti-6Al-4V is most difficult to weld due to its narrowest shear band width among all three materials considered. b)Although with its slightly lower shear band propagation speed than Ti-6Al-4V, HSLA 4340 exhibits a significantly wider shear band width, and therefore, implying a much better friction stir weldability than Ti-6Al-4V. c) Aluminum alloys such as AA2024 possesses the best friction stir weldability because of its widest shear band width and shortest shear band formation time among the three alloys studied

(4) Potential means of improving their weldablity, (e.g. significantly improving welding speed), are also examined such as local auxiliary heating and uniform pre-heating. The conclusion is although both local auxiliary heating and uniform pre-heating methods increase the shear band propagation speed (i.e., maximum possible welding speed), a method that provides a more uniform pre-heating in weld area is shown to be potentially much more effective than a localized heating for improving friction stir weldability for difficult-to-weld alloys such as Ti-6Al-4V because pre-heating cannot only reduce shear localization time but also increase shear band width.

(5) A new analytical based 3D transient heat flow solution is developed that

captures detailed spatial resolution of friction heat generation as stir tool shoulder rotates in angular direction and translate welding direction. The resulting temperature distribution clearly indicates temperature differences between advancing and retreating sides. This model can be used to provide the thermal environment in which shear localization happens.

(6) A contact mechanics model is introduced to capture detailed interactions between pin and workpiece at interface, which enables a direct estimation of welding torque required under a given set of welding parameters. As a result, the refined shear localization model is capable of estimating temperature profile in workpiece in front of pin and resulting welding torque, in addition to providing detailed information how shear localization develops and shear band size, which allows an improved understanding on weld formation mechanisms in FSW.

(7) Some of the major weld defect formation mechanisms have been elucidated in details based on the refined shear localization model which combines the 3D heat transport model and contact mechanics model, by further enforcing both mass conservation and plastic flow continuity conditions. These are: a)In order to form continuous banded structure per pin revolution in a consecutive manner, shear band width (δ) formed within one revolution must be equal or larger than the maximum plastic flow band width (w_{max}); b) If shear band width (δ) is less than plastic flow band width (w_{max}) , the defect type of "abnormal stirring" tends to develop; c)If not enough plastic flow is generated during one revolution, the defect type of "cold welds" tends to develop; d) If

sticking condition is not attained within one revolution, the defect of "surface galling" may occur; e) If maximum temperature generated from friction heating between shoulder and workpiece approaches solidus temperature of workpiece, the defect type of "excessive flash" tends to develop.

(8) A set of algorithms is developed to provide a theoretical means for FSW process window estimation and has been demonstrated on three aluminum alloys on which experimentally determined process windows were published by a number of researchers recently. A good agreement has been achieved between the model-based estimations and experimentally determined process windows for all three types of aluminum alloys.

Recommendations for Future Work

6.1.1 Base metal comparison

In this thesis, the shear localization model is implemented to study FSW process of different base metals. However the process window estimation algorithm proposed in Chapter 5 is only applied to aluminum alloys. Some other base metals such as steel and titanium should be further studied not only for process window estimation but also to gain some insight on identifying the key difference for their friction stir weldability. Potential means for mitigating some of the difficulties in friction stir welding of some of the alloys should be also examined to provide guidance for cost-effective development of welding process parameters for new applications.

6.1.2 Extension to a higher dimension model

In this thesis, although three dimensional heat transport model is used, the shear localization model is still one dimensional. Due to this limitation, FSW of dissimilar metal cannot be studied using the proposed model. Furthermore, the presented model is not able to capture three dimensional material flow nature introduced by detail pin feature such as thread of the pin. Along this line, Garikipati's work [e.g. 1-3] is very insightful. Their work presents an analysis of strong discontinuities in inelastic solids at finite strains by introducing a softening modulus in a classical multiplicative plasticity continuum model. Solutions exhibiting this type of discontinuities, characterized by a discontinuous displacement field, are shown to make physical and mathematical sense in a classical multiplicative plasticity continuum model and may be implanted to study the shear localization phenomenon in FSW.

6.1.3 Further simplification for engineering application

In engineering application, a closed-form expression for estimating of process window is highly desired. However the proposed model also need numerical implementation, and is not convenient for direct engineer application. Mendez et al. [e.g. 4,5] developed an "order of magnitude scaling" technique which can obtain approximate closed-form solution for differential equation. This technique permits a simple computer implementation to overcome the limitations of the current scaling approach, in which dominant terms are manually selected and tested for consistency. Thus this method is suitable for getting approximately closed-form solution of many coupled differential equations, as presented in the shear localization problem. Thus it may be possible to gain

closed-form expression for FSW process window estimation based on the differential equation provided in this work using Mendez's technique.

Reference

[1] Armero, Francisco, and Krishna Garikipati. "An analysis of strong discontinuities in multiplicative finite strain plasticity and their relation with the numerical simulation of strain localization in solids." *International Journal of Solids and Structures* 33.20-22 (1996): 2863-2885.

[2] Garikipati, Krishna, and Thomas JR Hughes. "A study of strain localization in a multiple scale framework—the one-dimensional problem." *Computer Methods in Applied Mechanics and Engineering* 159.3-4 (1998): 193-222.

[3] Garikipati, Krishnakumar R. *On strong discontinuities in inelastic solids and their numerical simulation*. Diss. Stanford University, 1996.

[4] Mendez, Patricio F., and Thomas W. Eagar. "Order of magnitude scaling: a systematic approach to approximation and asymptotic scaling of equations in engineering." *Journal of Applied Mechanics* 80.1 (2013): 011009.

[5] Mendez, Patricio F. "Characteristic values in the scaling of differential equations in engineering." *Journal of Applied Mechanics* 77.6 (2010): 061017.